UFRRJ

INSTITUTO DE AGRONOMIA

PROGRAMA DE PÓS-GRADUAÇÃO EM MODELAGEM E EVOLUÇÃO GEOLÓGICA

DISSERTAÇÃO

Arquitetura de Fácies Vulcânicas do Campo de Badejo, Bacia de Campos

Dandara David Braga

2022

UNIVERSIDADE FEDERAL RURAL DO RIO DE JANEIRO
INSTITUTO DE AGRONOMIA
PROGRAMA DE PÓS-GRADUAÇÃO EM MODELAGEM E EVOLUÇÃO GEOLÓGICA

Arquitetura de Fácies Vulcânicas do Campo de Badejo, Bacia de Campos

DANDARA DAVID BRAGA

Sob a Orientação do Professor
Sérgio de Castro Valente

Dissertação submetida como requisito parcial para obtenção do grau de **Mestre em Geociências**, no Programa de Pós-Graduação em Modelagem e Evolução Geológica, Área de Concentração em Modelagem de Processos Geológicos e Geodinâmicos

Seropédica, RJ

Fevereiro de 2022

FICHA CATALOGRÁFICA

B813a

Braga, Dandara David, 15/03/1988-
Arquitetura de Fácies Vulcânicas do Campo de Badejo, Bacia de Campos / Dandara David Braga. - Rio de Janeiro, 2022.
94 f.

Orientador: Sérgio de Castro Valente.
Dissertação(Mestrado). -- Universidade Federal Rural do Rio de Janeiro, Programa de Pós-Graduação em Modelagem e Evolução Geológica/ Área de Concentração em Modelagem de Processos Geológicos e Geodinâmicos, 2022.

1. derrames basálticos subaéreos. 2. vulcanologia física. 3. Bacia de Campos. 4. Campo de Badejo. 5. reservatórios não convencionais. I. Valente, Sérgio de Castro , 31/07/1962-, orient. II Universidade Federal Rural do Rio de Janeiro. Programa de Pós-Graduação em Modelagem e Evolução Geológica/ Área de Concentração em Modelagem de Processos Geológicos e Geodinâmicos III. Título.

MINISTÉRIO DA EDUCAÇÃO
UNIVERSIDADE FEDERAL RURAL DO RIO DE JANEIRO
DEPARTAMENTO DE PETROLOGIA E GEOTECTÔNICA

TERMO Nº 1276 / 2022 - DPETRO (11.39.40)

Nº do Protocolo: 23083.075408/2022-81

Seropédica-RJ, 12 de dezembro de 2022.

UNIVERSIDADE FEDERAL RURAL DO RIO DE JANEIRO
INSTITUTO DE AGRONOMIA
CURSO DE PÓS-GRADUAÇÃO EM MODELAGEM E EVOLUÇÃO GEOLÓGICA

NOME DO(A) PÓS-GRADUANDO(A): **DANDARA DAVI BRAGA**

Dissertação de mestrado submetida como requisito parcial para obtenção do grau de Mestre em Geociências no Curso de Pós-Graduação em Modelagem e Evolução Geológica, área de Concentração em Modelagem de Processos Geológicos e Geodinâmicos.

DISSERTAÇÃO APROVADA EM 23/02/2022

Conforme deliberação número 001/2020 da PROPPG, de 30/06/2020, tendo em vista a implementação de trabalho remoto e durante a vigência do período de suspensão das atividades acadêmicas presenciais, em virtude das medidas adotadas para reduzir a propagação da pandemia de Covid-19, nas versões finais das teses e dissertações as assinaturas originais dos membros da banca examinadora poderão ser substituídas por documento(s) com assinaturas eletrônicas. Estas devem ser feitas na própria folha de assinaturas, através do SIPAC, ou do Sistema Eletrônico de Informações (SEI) e neste caso a folha com a assinatura deve constar como anexo ao final da tese / dissertação.

BANCA EXAMINADORA:

Dr. Sérgio de Castro Valente (presidente da banca; DPG-UFRRJ)
Dr. Artur Corval Vieira (membro titular interno; DPG-UFRRJ)
Dra. Natália Famelli Pereira (membro titular externo, CENPES/PETROBRAS)

(Assinado digitalmente em 13/12/2022 09:00)
ARTUR CORVAL VIEIRA
PROFESSOR DO MAGISTERIO SUPERIOR
DPETRO (11.39.40)
Matrícula: 1648928

(Assinado digitalmente em 12/12/2022 11:05)
SERGIO DE CASTRO VALENTE
PROFESSOR DO MAGISTERIO SUPERIOR
DPETRO (11.39.40)
Matrícula: 387109

(Assinado digitalmente em 12/12/2022 11:10)
NATÁLIA FAMELLI PEREIRA
ASSINANTE EXTERNO
CPF: 102.704.287-20

Visualize o documento original em **https://sipac.ufrrj.br/public/documentos/index.jsp** informando seu número: **1276**, ano: **2022**, tipo: **TERMO**, data de emissão: **12/12/2022** e o código de verificação: **09e0dbd842**

UNIVERSIDADE FEDERAL RURAL DO RIO DE JANEIRO

INSTITUTO DE AGRONOMIA

PROGRAMA DE PÓS-GRADUAÇÃO EM MODELAGEM E EVOLUÇÃO GEOLÓGICA

DANDARA DAVID BRAGA

Dissertação submetida como requisito parcial para obtenção do grau de Mestre em Geociências, no Programa de Pós-Graduação em Modelagem e Evolução Geológica, Área de Concentração em Modelagem de Processos Geológicos e Geodinâmicos.

DISSERTAÇÃO APROVADA EM 23/02/2022

____

Sérgio de Castro Valente (*Ph.D.*) UFRRJ
(Orientador e presidente da banca)

____

Natália Famelli (Dra) PETROBRAS
(Integrante externo da banca)

____

Artur Corval (Dr) UFRRJ
(Integrante interno da banca)

AGRADECIMENTOS

Agradeço em primeiro lugar a **DEUS** por ter me capacitado e permitido concluir este mestrado.

Ao meu orientador **prof. PhD. Sérgio de Castro Valente** pela presença em todas as fases deste projeto. Não poderia ter escolhido um orientador melhor.

Aos meus coorientadores informais, os geólogos **Gabriel Medeiros Marins** e **Yaro Moises Parizek Silva**, que foram os grandes incentivadores para a realização deste mestrado e que me deram todo o suporte através do Projeto de Pesquisas em Rochas Ígneas como Reservatório com dicas e conselhos valiosos em todos os momentos.

Ao geólogo **Filipe Vidal** pela ajuda na parte relacionada aos perfis elétricos.

Aos geólogos **Adriana Pereira da Silva**, **Natasha Pereira Rocha**, **Leandro Arrais Bevilaqua**, **Mariana Meirelles Lima da Silva**, **Grace Kelly Millanao Malo**, **Polianna do Nascimento Costa**, **Paula Gomes de Carvalho** que me ajudaram em fases diferentes, desde a escolha do tema e apoio para fazer uma pós-graduação até a ajuda em laboratório.

Aos gerentes **Ricardo Lykawka**, **Rita Parisi Conde Pozzi** e **Fagner Oliveira de Almeida** pela liberação parcial para o mestrado e toda a paciência para conciliar com as demandas internas, sempre me dando o suporte necessário.

Ao meus pais, **Vera Lucia David** e **Luiz Eduardo Evaristo Braga**, que sempre me incentivaram a estudar e me apoiam em qualquer novo desafio.

A todos os alunos da primeira turma do Programa de Pós-Graduação em Modelagem e Evolução Geológica da Rural (**Carolina de Lucena Sagrillo**, **Maristela Almada Gomes de Oliveira**, **Amanda Ribeiro de Souza**, **Fábio Vladimir dos Santos**, **Graciano Carlos de Freitas**, **Priscilla Azevedo dos Santos**, **Priscila Castro de Brito**) que me ajudaram dando carona, compartilhando conhecimento e pelos momentos de descontração no cafezinho e almoço na Rural, necessários depois da enxurrada de informação das matérias condensadas.

Aos **profissionais da PETROBRAS** que, mesmo fazendo o seu trabalho, se empenharam ao máximo quando as demandas eram urgentes, em especial **Michele Santiago Merces**.

À **PETROBRAS** e ao **projeto de pesquisa Magmatismo máfico alcalino e toleítico do Cretáceo e Paleógeno no Estado do Rio de Janeiro na área continental adjacente às bacias de Santos e Campos** pelo patrocínio do estudo e à **ANP** pela disponibilização dos dados.

Ao Universidade Federal Rural do Rio de Janeiro (**UFRRJ**) e ao Programa de Pós-graduação em Modelagem e Evolução Geológica (**PPGMEG-UFRRJ**) pela oportunidade de desenvolver esta pesquisa, infraestrutura, recursos. A todos os **professores da UERJ, UFRGS e UFSC** que me possibilitaram aprender um pouco mais sobre rochas vulcânicas, um desafio para mim.

O presente trabalho foi realizado com apoio da Coordenação de Aperfeiçoamento de Pessoal de Nível Superior - Brasil (**CAPES)** - Código de Financiamento 001.

RESUMO GERAL

BRAGA, Dandara David. Arquitetura de Fácies Vulcânicas do Campo de Badejo, Bacia de Campos. 2022. 93p Dissertação (Mestrado em Modelagem e Evolução Geológica, Geociências). Instituto de Geociências, Departamento de Petrologia e Geotectônica, Universidade Federal Rural do Rio de Janeiro, Seropédica, RJ, 2022.

A Bacia de Campos está localizada no SE do Brasil e está entre as maiores bacias sedimentares produtoras de hidrocarbonetos do país. A produção de hidrocarbonetos a partir de rochas magmáticas ainda é rara no Brasil mas foi bem sucedida no campo de Badejo, na Bacia de Campos. O campo de Badejo está situado na porção central da Bacia de Campos, a 75 km a sudeste do Cabo de São Tomé e sob lâmina d´água de 85 metros. As rochas vulcânicas da Formação Cabiúnas são basaltos toleíticos relacionados com os volumosos derrames que extravasaram antes e durante a fragmentação do Gondwana no Cretáceo Inferior. Apesar de sua ampla distribuição na Bacia de Campos, estudos de vulcanologia física e arquitetura de fácies vulcânicas nos basaltos Cabiúnas ainda são escassos. A área de estudo desta dissertação tem aproximadamente 12 km² e inclui a Formação Cabiúnas com espessura máxima perfurada de 650 metros. O objetivo principal da dissertação foi compreender e identificar sequências vulcano-sedimentares em detalhe na área de estudo selecionada na Bacia de Campos, e representar a sua distribuição em um modelo de arquitetura de fácies conceitual usando, para isso, conceitos da vulcanologia física. Os métodos de estudo incluíram procedimentos usualmente adotados em estudos petrológicos e de correlações estratigráficas, tais como descrição macroscópica de testemunhos, estudo petrográfico sob microscópio óptico de luz transmitida, análise litogeoquímica e correlação entre os poços utilizando perfis elétricos. Os testemunhos recuperados dos poços BD-02, BD-04 e BD-08, furados no campo de Badejo, foram o material estudado para reconstruir as geometrias 3D dos derrames vulcânicos na área. Dois fluxos Compostos-entrelaçados (Sequência 1 e Sequência 3) e um fluxo Tabular-clássico (Sequência 2) foram identificados a partir deste estudo. Morfologias ou associações de litofácies incluem lavas do tipo clássico, *hummocky*, tabular e *rubbly pahoehoe*. Foram reconhecidas litofácies coerentes, brechados e peperitos e intertrapas. Taxas de efusão, estimadas a partir da espessura dos lóbulos, indicaram que inflação por pulsos foi o processo predominante na

Sequência 3. A duração mínima de colocação dos fluxos foi estimada em 3 meses e 7 meses para os poços BD-02 e BD-04, respectivamente. Estimativas de valores D para as lavas *hummocky* são maiores que para as lavas *pahohoe* clássicas, indicando porosidades e permeabilidades potencialmente boas para *plays* exploratórios. Os dados litogeoquímicos mostraram boa correlação na parte superior da Sequência 3, indicativo de emissão a partir do mesmo conduto. A Sequência 2, do tipo composto entrelaçado, pode ter alcançado até 89,5 m, sendo bem mais espessa que os 40 m estimados para as lavas tabulares clássicas na Sequência 3. O paleoambiente vulcânico era predominantemente subaéreo e úmido em todas as sequências. Os resultados do estudo destes três poços poderão servir à caracterização de reservatórios vulcânicos potenciais em outras partes da Bacia de Campos e em bacias sedimentares do SE do Brasil associadas à fragmentação do Gondwana.

ABSTRACT

Campos Basin is located in SE Brazil, being among the most productive sedimentary basins regarding hydrocarbons in the country. Hydrocarbon production from volcanic reservoir rocks in Brazil is rare but it was succesfully achievied in the Badejo field, Campos Basin. The Badejo field is located southern Campos, about 75 km offshore SE the São Tomé Cape, in the continent, under 85 m of sea water. The volcanic rocks are basalts of the Cabiúnas Formation, related with the voluminous flows that erupted prior and during the Gondwana breakup in the Early Cretaceous. Despite their widespread distribution in Campos Basin, volcanic facies architectures and studies of physical volcanology regarding the Cabiúnas basalts are still scarce. The study area is 12 km^2 and includes about 650 m of magmatic rocks of the Cabiúnas Formation. The aims of the study was to discriminate volcanosedimentary sequences in detail and to represent their distribution using concepts of physical volcanology and architecture of volcanic facies. The methods applied included usual systematics in petrological research as well as volcanic stratigraphy, with macroscopic description of well cores, optical microscopy and lithogeochemical analysis. The cores recovered from wells BD-02, BD-04 and BD-08, drilled in the Badejo field, provided an excelent material to reconstruct the 3D geometries of the volcanic flows in the area. Two Compound-braided flows (Sequence 1 and 3) and a Tabular-classic flow Sequence (Sequence 2) were identified in the studied wells. Morphologies or lithofacies associations include classical, hummocky, sheet and rubbly pahoehoe lavas. Coherent, brecciated, peperites and intertraps lithofacies were also described in the well cores. Effusion rates, based on the thickness of the lobes, indicated that pulsed inflation was the major process in Sequence 3. Minimum emplacement duration is estimated in 3 and 7 months for wells BD-2 and BD-04, respectively. Estimated D values for hummocky lavas are higher than those for classical pahoehoe lavas, pointing to porosities and permeabilities adequate to potential plays. Lithogeochemical data revealed a good correlation in the upper part of Sequence 3 indicating eruption from the same emission center. The compound-braided Sequence 2 may have reach 89.5 m, much thicker than the 40 m thick tabular-classical lavas in Sequence 3. The volcanic paleoenvironment

corresponds to subaerial lava flows with humidity in all sequence. This information can be of great importance for better characterization of potential offshore volcanic reservoirs within Campos and other sedimentary basins associated with the Gondwana breakup in SE Brazil.

LISTA DE ILUSTRAÇÕES

LISTA DE TABELAS

Sumário

1. INTRODUÇÃO GERAL

1.1 Apresentação

O estudo da arquitetura de fácies vulcânicas visa compreender o arranjo tridimensional das lavas e as suas relações em diferentes escalas reconstruindo, assim, o ambiente vulcano-sedimentar em questão. A relevância deste tipo de estudo está em poder individualizar as facies, servindo como análogo para outras áreas, como por exemplo, a extrapolação para áreas sem dados de rocha ou com apenas dados sísmicos.

Este projeto tem como foco a Formação Cabiúnas (Figura 1) que é composta por derrames ígneos, subalcalinos, subaéreos e subaquosos, com espessura máxima perfurada de 650 metros (Winter *et al*, 2007). Basaltos e diabásios são os principais litologias desta unidade, podendo ocorrer localmente intratrapas de rochas sedimentares. Temporalmente, os eventos ígneos Cabiúnas e Serra Geral, da Bacia do Paraná, são correlacionáveis (Winter *et al*, 2007).

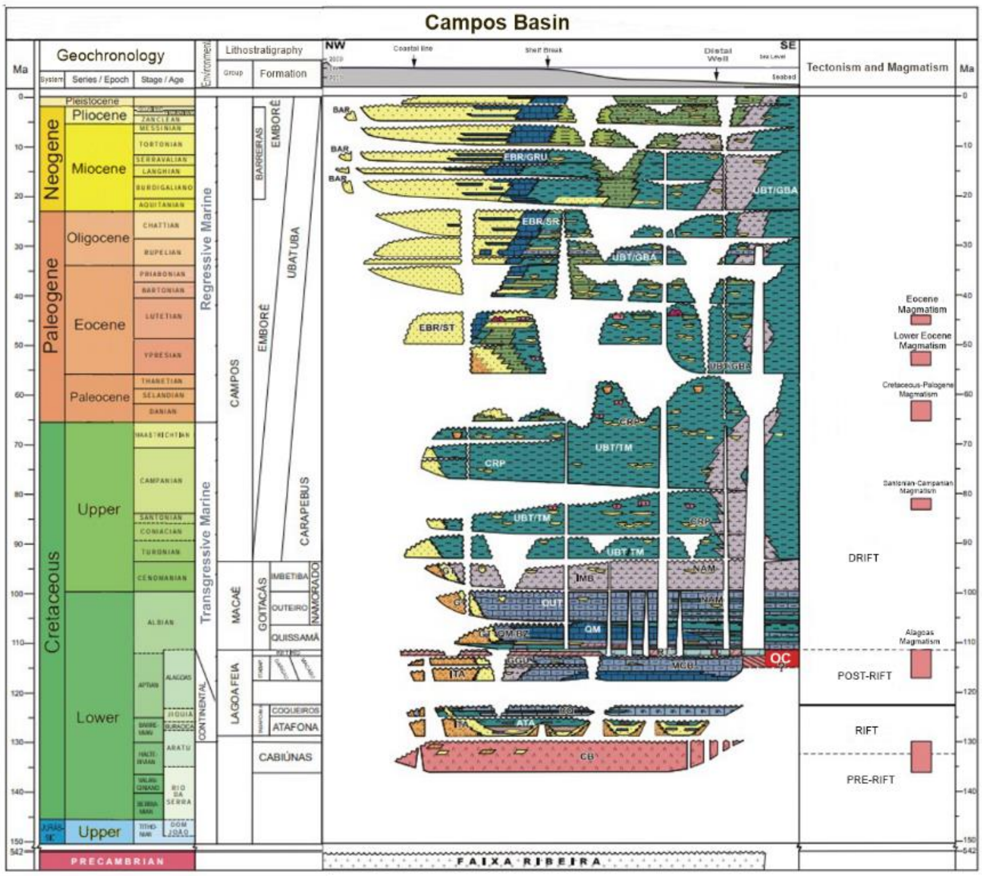

Figura 1: Carta estratigráfica da bacia de Campos (Winter et al., 2007)

As rochas vulcânicas do campo de Badejo produziram óleo de 31° API e representam uma das poucas acumulações comerciais de óleo no Brasil tendo rochas ígneas como reservatório. Na década de 1980, estes poços foram fruto de estudo da dissertação de mestrado de Mizusaki (1986) que propôs um modelo vulcano-sedimentar para a área de Badejo, Pampo e Linguado, onde a região de Badejo seria predominantemente associada a vulcanismo subaéreo. As análises geoquímicas indicaram que os basaltos estudados fazem parte de uma associação vulcânica pouco diferenciada e de natureza transicional a subalcalina de origem continental (Misuzaki, 1986). A datação radiométrica, pelo método K-Ar, chegou a valores entre 120 Ma e 130 Ma (Thomaz, 1981, 1984). Os poços BD-02, BD-04 e BD-08, investigados no presente estudo, não foram comerciais devido à baixa permeabilidade das rochas ígneas que, no entanto, apresentaram indícios da presença de óleo.

Mizusaki (1986) inseriu os basaltos e rochas vulcanoclásticas dos campos estudados em 4 grandes sequências estratigráficas: A) Basaltos e brechas de fricção, B) Basalto e arenitos vulcânicos, C) Basaltos e tufos e D) Basaltos, brechas vulcânicas, sedimentos e brechas hidrovulcânicas. A Sequência A estaria associada a condições subaéreas sendo a mais frequente nos testemunhos analisados. Ela é caracterizada por basaltos intercalados com brechas de fricção centimétricas de cor avermelhada. A sequência B é individualizada devido a maior proporção de arenitos vulcânicos. Ela foi caracterizada no poço BD-03 e interpretada nos outros poços por meio de perfis elétricos. A sequência C apresenta basaltos muito alterados e oxidados tornando-se de difícil reconhecimento. A Sequência D presente, principalmente, no campo de Linguado, tem como principal fácies as brechas hidrovulcânicas e pode apresentar-se incompleta. As fácies hidrovulcâncias foram reconhecidas devido às bordas de reação, caracterizando uma interação entre os sedimentos e lava. Esta sequência foi interpretada como de ambiente subaquoso (Figura 2).

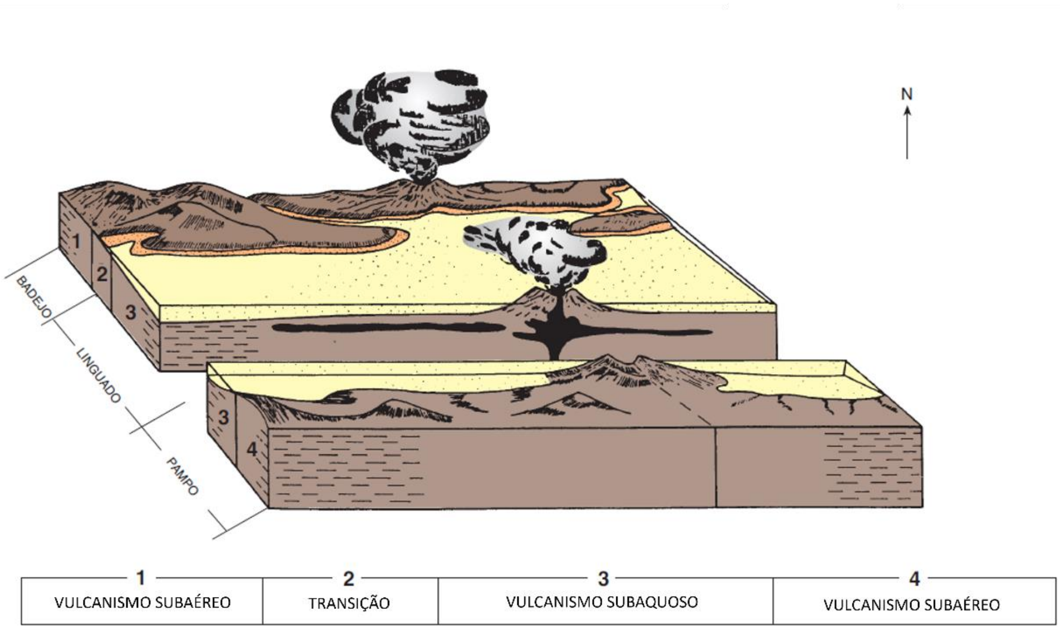

Figura 2: Modelo vulcano-sedimentar para área de Badejo- Pampo e Liguado (Mizusaki, 1986).

1.2 Objetivos

O objetivo principal do trabalho é compreender e identificar sequências vulcano-sedimentares em detalhe, numa área selecionada da Bacia de Campos, e representar a sua distribuição em um modelo de arquitetura de fácies conceitual usando, para isso, conceitos da vulcanologia física. As sucessões vulcânicas definidas servirão como base para a reconstrução do ambiente vulcano-sedimentar da região do campo de Badejo utilizando os testemunhos dos poços BD-08, BD-04 e BD-02 além de perfis elétricos.

Objetivos específicos incluem a compreensão do ambiente deposicional e dos mecanismos de colocação da lava (estimativa da taxa da efusão magmática, periodicidade e tempo, viscosidade, topografia, temperatura, distância e espessura dos pulsos de lava).

1.3 Justificativa

A utilização de parâmetros físicos para a descrição e reconstituição do empilhamento das sequências vulcano-sedimentares foi proposta inicialmente por Walker (1971), que individualizou as sequências de lavas efusivas em unidades de fluxo. Posteriormente, diversos trabalhos têm se dedicado a este tema como Self (1998), Jerram (2002), Waichel *et. al*. (2006) e Duraiswami *et. al.* (2013), com a discriminação de diversos tipos de fluxos de lava e processos vulcânicos associados (Figura 3). A caracterização de sequências vulcânicas nas bacias costeiras brasileiras ainda é muito escassa devido à ausência de poços com amostragem desse tipo de rocha e também devido à histórica baixa relevância desta informação para indústria do petróleo. Com o avanço da fronteira exploratória, a amostragem de rochas vulcânicas vem se tornando cada vez mais abundante. Por exemplo, Marins *et al.* (2018) apresentaram uma nova interpretação para as sucessões vulcânicas de um poço no Campo de Badejo. Os autores propuseram uma revisão das sequências estratigráficas considerando as novas metodologias de empilhamento de sequências.

Esta dissertação de mestrado visa contribuir para estudos de vulcanologia física com aplicação de modernas técnicas descritivas de arquitetura de fácies vulcânicas com vistas a ampliar o conhecimento dos processos magmáticos no âmbito da indústria do petróleo.

Tipo de derrame	Definição	Descrição	Esboço gráfico
***Pahoehoe* composta**	Superfícies lisas, onduladas ou em corda. Composta por várias unidades chamadas de lobos.	Formam-se com baixas taxas de efusão do magma em regime intermitente de fluxo.	
***Pahoehoe* simples/ inflada**	Lobos inflados e coalescentes com estruturas semelhantes a *pahoehoe* composta. O seu empilhamento forma uma geometria tabular.	Formam-se com baixas taxas de efusão do magma. Exibem o empilhamento das 3 estruturas internas típicas de *pahoehoe* (crosta superior, núcleo denso e crosta inferior).	
Slabby pahoehoe	Placas do topo de *pahoehoe* quebradas pelo movimento de lava abaixo da crosta superior.	Tipo de derrame transicional entre *pahoehoe* e *'a'a*. Ocorrem com o aumento da taxa de efusão do magma.	
Rubbly pahoehoe	Topos autobrechados como dos derrames tipo 'a'a e base preservada como das demais *pahoehoes*.	Tipo de derrame transicional entre pahoehoe e 'a 'a. A taxa de efusão do magma é maior que das outras *pahoehoes*.	
'A'a	Possuem topo e base autobrechados, escoriáceos. Vesículas esparsas e estiradas nas reentrâncias das zonas brechadas e núcleo denso.	Formam-se com altas taxas de efusão em lavas mais viscosas que avançam mais lentamente do que os derrames do tipo *pahoehoe*, considerando a mesma declividade.	

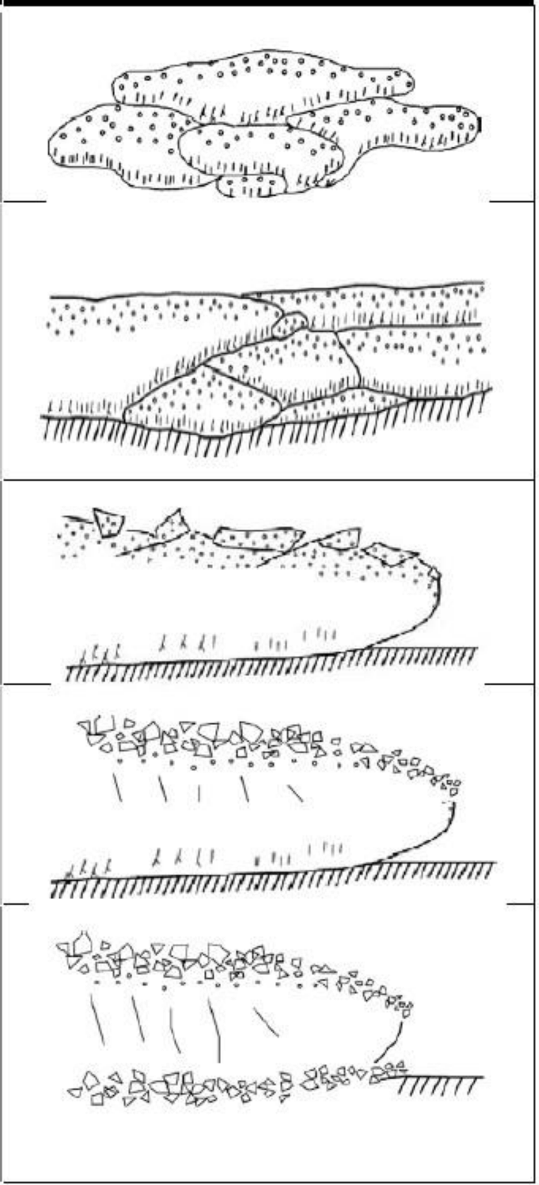

Figura 3:Tipos morfológicos de lava pahoehoe (Fornero, 2018).

1.4 Área de estudo

O campo de Badejo está localizado na porção sudoeste da bacia de Campos, em águas rasas com profundidade 85 metros e a cerca de 115 km da cidade de Campos (Mizusaki, 1986) (Figura 4). O campo está sobre a elevação do embasamento chamado Alto de Badejo, de direção NW-SE, que faz parte de uma serie de horsts e grabens formados durante a fase rifte da bacia (Scalvi, 2009).

A área de estudo (Figura 5) tem aproximadamente 12 Km² e compreende a área dos poços BD-02, BD-04 e BD-08 inserido nos *ring-fence* dos campos de Badejo e Linguado. Nesta mesma área, encontra-se o poço BD-01, que testou e confirmou a produtividade de óleo a partir de rochas magmáticas.

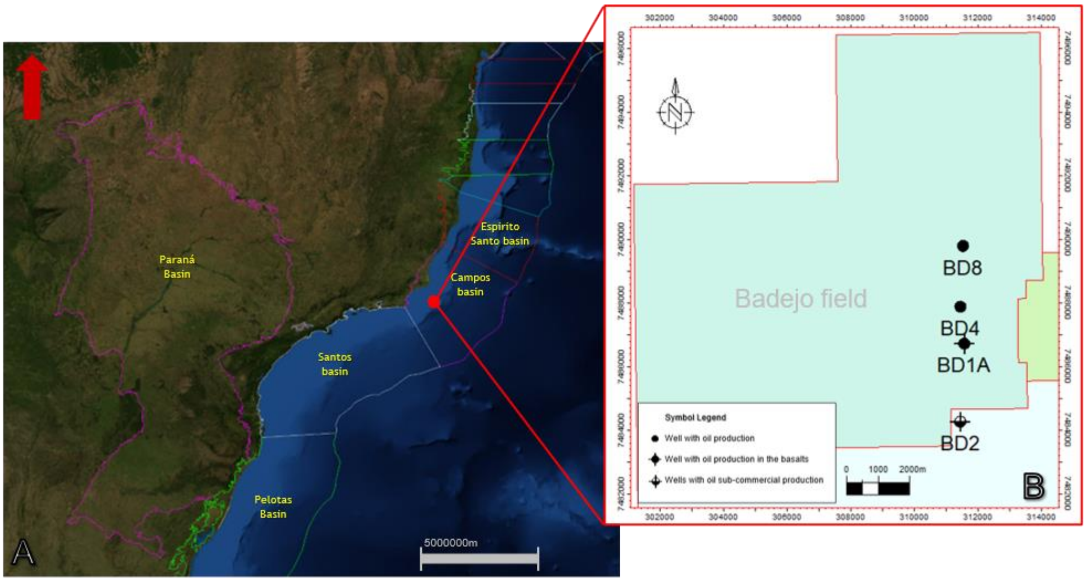

Figura 4: Mapa de localização do campo de Badejo. A) Imagem de satélite com a delimitação das bacias brasileiras. B) *ring-fance* de Badejo (em azul) incluindo os poços BD-08, BD-04 e BD-01 e de Linguado (em verde) com o poço BD-02.

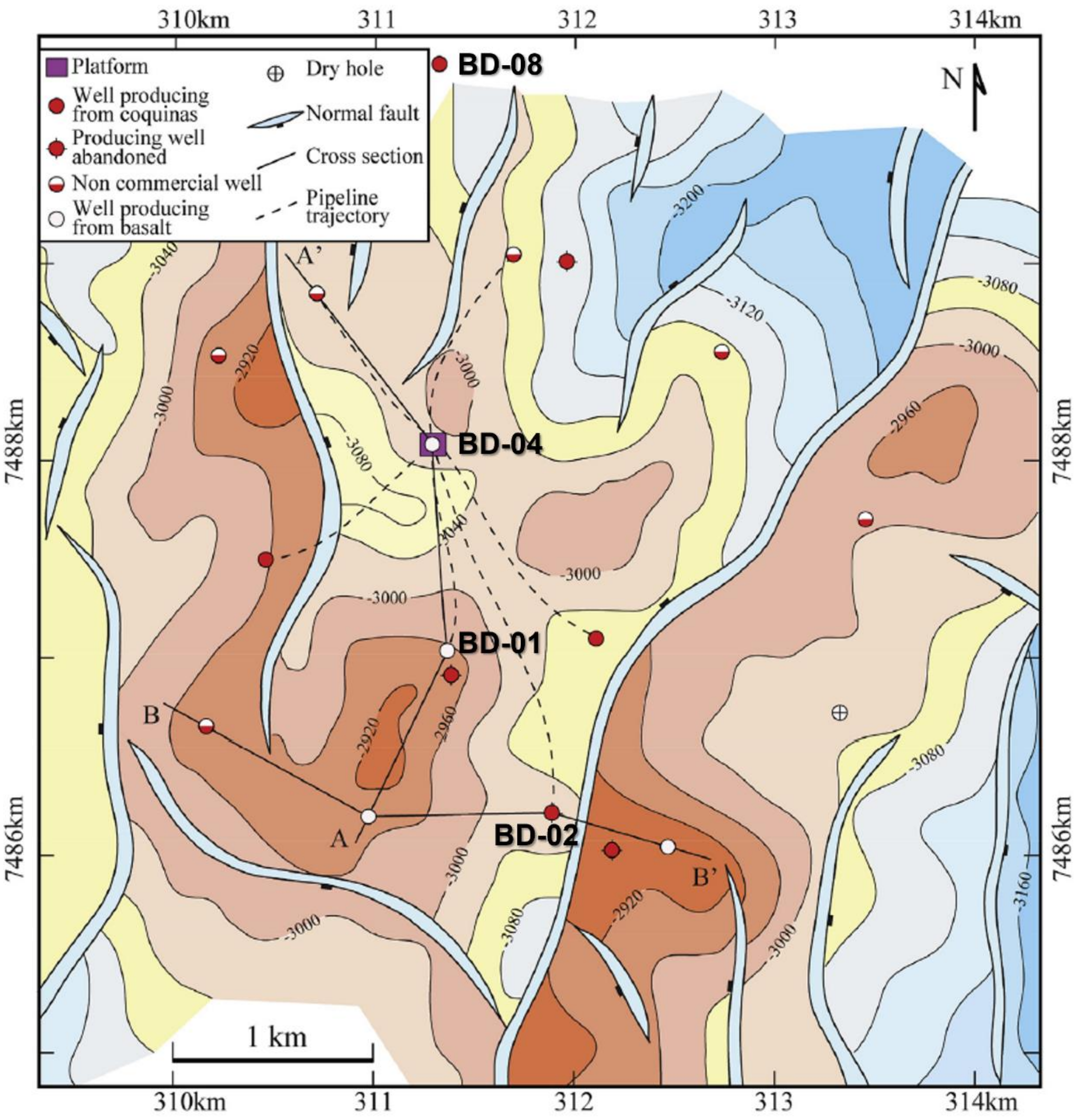

Figura 5: Mapa estrutural do topo das ígneas incluindo os poços BD-01, BD-02, BD-04 e BD-08 (Ren *et. al*., 2020).

2. REVISÃO TEMÁTICA

2.1 O magmatismo no contexto de abertura do Atlântico Sul

Processos magmáticos relevantes acompanharam o processo de fragmentação do Gondwana, no Cretáceo Inferior, e posterior abertura do Atlântico Sul, contribuindo para as configurações atuais da costa da América do Sul. A evolução da quebra do supercontinente Godwana, no Cretáceo Inferior, ocorreu em contexto geodinâmico extensional (Castro, 2015) e influenciou a deposição das rochas sedimentares.

Na margem equatorial, a separação entre os continentes teria se iniciado há aproximadamente 210 Ma com sentido de propagação de NW para SE (da Guiana Francesa para as bacias de Foz do Amazonas e Marajó). A evolução da abertura teria sido impedida devido a uma forte resistência impostas pelos crátons São Luiz e Oeste Africano, impossibilitando a sua migração para sul, causando um intenso vulcanismo nas bacias do Amazonas, Solimões e Acre no período Triássico. De forma concomitante, na margem sudeste, os primeiros vestígios da abertura estão relacionados a bacias argentinas (San Julian e Norte Malvinas no Triássico, San Jorge e Valdez/Rawson no Jurássico). A abertura evolui para norte, no Neocominiano, com a deposição de espessos derrames de lava basáltica nas bacias argentinas de Salado e Colorado e nas bacias brasileiras de Pelotas, Santos, Campos e Espírito Santo. Do mesmo modo que a margem equatorial, os extensos derrames de lava da formação Serra Geral, na bacia do Paraná, seriam relacionados à resistência provocada pelas regiões cratônicas (Thomaz Filho et al., 2000). Os basaltos neocomianos encontrados nas bacias marginais podem também ser interpretados como uma extensão do magmatismo que gerou os basaltos da Formação Serra Geral na Bacia do Paraná. A colocação das lavas da Formação Serra Geral teria ocorrido alguns milhões de anos antes que as lavas das bacias marginais, já que dados paleomagnéticos indicam que o vulcanismo na Bacia do Paraná migrou de oeste para leste (Mizusaki et al, 1992). Independentemente do modelo, a Formação Serra Geral apresenta inúmeros e excelentes afloramentos que o caracteriza como um ótimo análogo para o magmatismo das bacias marginais (Reis, 2013).

De formal geral, as bacias inseridas no contexto da formação da margem continental passiva do Atlântico Sul passaram por três estágios geotectônicos: pré-rifte/rifte (fase relacionada a elevação da atenosfera e afinamento crustal, com grande atividade tectônica gerando falhas normais de grande rejeito), pós-rifte (fase com relativa diminuição da atividade tectônica) e drite (desenvolvimento das cadeias meso-oceânicas dominando os processos relacionados ao espalhamento da litosfera oceânico) (Mohriak et al., 2008a;

Mohriak et al., 2002). As bacias da margem sudeste, ao sul do zona de fraturas Florianópolis/Rio Grande e de idade de abertura mais antiga do Triássico (*i.e.,* Bacia de Pelotas), são caracterizadas por de grandes volumes *seaward dipping reflectors* (SDRs), o que indica a presença de intenso vulcanismo durante a gênese da margem (Moulin et al., 2010; Blaich et al., 2013). Na Bacia de Pelotas é possível observar sequências vulcânicas bem desenvolvidas com presença de campos de lava da Formação Serra Geral na fase pré-rifte e SDRs nas fases rifte e pós-rifte (Bueno et al., 2007; Stica et al., 2014). A pluma Tristão da Cunha, localizada abaixo do segmento das bacias de Pelotas e da Cadeia de Walvis, desde 145 Ma (Heine, 2013), pode ter influenciado no volume do magmatismo, sendo observado a diminuição da intesidade de fusão para direção sul (Blaich et al., 2013).

Nas bacias de Santos, Campos e Espírito Santo, a fase pré-rifte/rifte se desenvolveu de forma similar às bacias ao sul da zona de fraturas Florianópolis/Rio Grande, e são marcadas por expressivo vulcanismo com a formação dos derrames de lava, constituindo as formações Camboriú, em Santos, Cabiúnas, em Campos e, já intercalado com sedimento e em menor proporção, da também Formação Cabiúnas, no Espírito Santo. Estes basaltos são cortados pelas falhas relacionadas à fase de intenso tectonismo e o seu principal episódio de vulcanismo basáltico (datações K/Ar com idades entre 122 ± 5 Ma e 134 ± 4 Ma; Mizusaki et al., 1989) precede ligeiramente a fase rifte podendo ser interpretados como embasamento vulcânico ou sequência pré-rifte (Mohriak et al., 2002).

O progresso do processo extensivo (fase rifte genuína) gerou uma série de feições alongadas paralelas à costa e lagos profundos preenchidos por rochas vulcânicas e siliciclásticas. Na Bacia de Campos este processo é representado pelas rochas sedimentares do Grupo Lagoa Feia, associadas à fan deltas, rios entrelaçados e lagoas (Winter et al., 2007; Castro et al., 2014). O ambiente lacustre, com águas salobras a hipersalinas, é formado por folhelhos laminados intercalados com carbonatos que representam a principal rocha fonte dos hidrocarbonetos da bacia (Guardado et al., 2000).

Na fase pós-rifte, prevaleceu, na porção proximal, a sedimentação continental e nas porções ditais sedimentação em ambiente marinho raso em um mar epicontinental (Dias et al., 2005). Destacam-se a Formação Macabu, em Campos, e Formação Barra Velha, em Santos, constituídas, majoritariamente, por rochas carbonáticas (laminitos microbiais e estromatólitos) que constituem o principal reservatório do pré-sal brasileiro (p.ex.: Winter et al., 2007; Rangel el al., 1994; Castro et. al., 2014). Na Bacia do Espírito Santo desenvolveram-se sistemas deposicionais dominados por leques aluviais e canais fluviais na parte proximal e na parte distal uma passagem gradativa do ambiente continental para transicional com intercalações de folhelhos esverdeados, calcilutitos e arenitos finos (França et al., 2007). Na porção inferior do pós-rifte da Bacia de Santos ocorre um evento magmático, 118 Ma que se forma concomitante à deposição de carbonatos e com a mesma idade da discordância intra-alagoas (Moreira *et. al.* 2007). Em Campos, o segundo pulso magmático (Magmatismo Alagoas – mais novo que o evento da Bacia de Santos) é associado a ruptura definitiva dos continentes (Dani et al., 2017). Nas regiões mais distais, são interpretados SDRs que representam o estágio de transição para a crosta oceânica (Winter et al., 2007). Já na Bacia de Espírito Santo, esse segundo pulso magmático não ocorre (França et al., 2007). No final da fase pós-rifte uma anomalia térmica formou a dorsal de São Paulo impedindo a livre circulação das águas marinhas propiciando, assim, deposição de espessas camadas de sal. Esses depósitos de sal margeiam a primeira crosta oceânica formada ao sul da zona de fraturas de Florianópolis/Rio Grande (Amorim, 2013; Moulin et al., 2010; Dias et al., 2005).

A fase difte vai do Albiano ao Recente e representa um progressivo aumento na batimetria com a transição carbonática de águas rasas para fácies de águas mais profundas (Mohriak et al., 2008). Esta fase apresenta dois grandes eventos magmáticos, do Santoniano-Turoniano e do Eoceno-Oligoceno, com vulcanismo com caráter mais alcalino e tendência à linearidade (possível *hotspot*) (Thomaz filho et al., 2008; Thomaz Filho et al., 2000)

2.2 Magmatismo Cabiúnas na Bacia de Campos

A Bacia de Campos localiza-se no litoral norte do estado do Rio de Janeiro e a sul do Estado do Espírito Santo, sendo limitada ao norte pelo Arco de Vitória e a sul pelo Arco de Cabo Frio (Winter, 2007). Ela cobre uma área de mais de 100.000 km² com preenchimento sedimentar chegando a 9 km. Os primeiros registros de magmatismo na Bacia de Campos, associados à Formação Cabiúnas, vêm sendo foco de estudo de diversos pesquisadores desde a década de 1980 onde destacam-se diversos trabalhos. Em Fodor (1983), os dados composicionais dos basaltos dos poços RJS-92 e BD-03 (com datações entre 116 a 124 Ma) foram importantes para concluir que a crosta continental se estende a dezenas de quilômetros *offshore* na Bacia de Campos. Uma das evidências da presença de crosta continental é grande quantidade de elementos terras raras leves enriquecidos e as razões de La/Yb (cerca de 4.5). Usando dado sísmico, magmático e dados de gravidade, Kowsmann et al. (1982), também propõem uma crosta continental para o embasamento desta região. As idades desses basaltos estão na faixa mais recente do intervalo entre 147-120 Ma reconhecida para os basaltos da Formação Serra Geral na Bacia do Paraná. Isto sugere que os basaltos Cabiúnas foram extravasados sobre crosta estirada e atenuada.

Mizusaki et al. (1992) propõem uma datação entre 134 a 122 Ma para os basaltos toleíticos do Cretáceo Inferior, semelhantemente ao proposto por outros autores (Thomaz 1981,1984; Mizusaki, 1987; Mizusaki e Saracchini, 1991). As idades mais novas encontradas (111 a 116 Ma) possivelmente estão relacionadas à perda de Ar, pois os basaltos estão abaixo de sedimentos barremianos do intervalo de 124-119 Ma. De forma geral, os basaltos apresentam-se intensamente alterados devido à interação com água do mar, o que leva a um enriquecimento MgO, FeO total, K_2O, Rb e Ba e empobrecimento em SiO_2 e CaO. Não há alterações significativas dos teores de Zr, Nb, Y e elementos terras raras (ETR) quando associados à perda ao fogo abaixo de 4%. Os basaltos Cabiúnas apresentam similaridades composicionais com os basaltos toleíticos do Paraná, datados entre 140 a 130 Ma, aproximadamente, como a baixa concentração de elementos incompatíveis e TiO_2 abaixo de 2%. Baseado nas datações e dados paleomagnéticos, o magmatismo Cabiúnas do Cretáceo Inferior é interpretado como uma extensão a leste e mais nova do magmatismo da Bacia do Paraná. A formação destes basaltos teria ocorrido em um contexto de crosta continental fina, devido ao processo de rifteamento na fase inicial de abertura do Atlântico Sul, e suas fontes foram relacionadas a um o manto litosférico subcontinental e a uma pluma-OIB do tipo Dupal (Tristão da Cunha) (Mizusaki *et al*., 1992).

3 MATERIAIS E MÉTODOS

Os testemunhos dos poços BD-08 e BD-04 e BD-02 do campo de Badejo, na Bacia de Campos, foram estudados nesta dissertação. Os métodos incluíram procedimentos usualmente adotados em estudos petrológicos e de correlações estratigráficas, com base na seguinte sistemática:

- Descrição detalhada dos testemunhos com registro fotográfico;
- Estudos petrográficos sob microscópio óptico de amostras representativas das seções discriminadas em testemunhos;
- Análise litogeoquímica de litotipos discriminados nas etapas anteriores;
- Interpretação de dados e redação de relatórios e trabalho científico em revista ou periódico de categoria B1 ou superior da área de geociências do qualis capes.
- Os métodos utilizados para obtenção dos dados litogeoquímicos estão detalhados no Capítulo 4 desta dissertação

3.1 Descrição dos testemunhos

A descrição dos testemunhos contou com apoio da infraestrutura do Centro de Pesquisa da Petrobras (CENPES) onde foram descritos 29 metros de rochas basálticas do poço BD-08, 83 metros do poço BD-04 e 22 metros do poço BD-02. A seleção levou em consideração a distribuição espacial dos poços e correlação lateral, com base nos dados de Misusaki (1986), evitando também as falhas de grande rejeito. As descrições foram feitas na escala 1:50 com o objetivo de caracterizar os atributos internos ao lobo como, por exemplo, topos brechados, núcleo maciços e vesículas (formato, proporção e tamanho). As porosidades totais também foram estimadas a partir de dois perfis levando em consideração a porosidade relativa às vesículas/amigdalas e a porosidade relativa às fraturas naturais. As descrições foram sintetizadas em perfis de 1:100 para melhor representar visualmente as sequências/geometrias 3D identificadas. Foram selecionadas áreas de interesse para fotografia representantes das litofacies e contatos, além das fotos de conjuntos dos testemunhos. Os termos utilizados para descrição dos aspectos texturais, composicionais e de litofacies são de Mcphie et al. (1993).

3.2 Confecção de lâminas petrográficas

Foram confeccionadas 192 lâminas petrográficas com o objetivo de detalhar áreas de difícil interpretação sob análise macroscópica, auxiliar na interpretação das amostras selecionadas para análise litogeoquímica e caracterizar na escala microscópica as litofacies. As lâminas foram descritas no microscópio óptico da *Zeiss*, tendo sido tomadas fotos em diversas escalas a partir da câmera acoplada ao microscópio e editadas no software *Zen.3.0* da mesma marca. Para a descrição das lâminas foi utilizado a terminologia de Mckenzie et al. (1982).

4 ARTIGO CIENTÍFICO: *Facies architecture of lava flows of the Cabiúnas Formation in Campos basin, SE Brazil*

Este capítulo apresenta o artigo científico submetido ao *Journal of South American Earth Sciences*

AUTHORS:

Dandara David Braga (PETROBRAS; PPGMEG-UFRRJ)

Sérgio de Castro Valente (PPGMEG-UFRRJ)

Gabriel Medeiros Marins (PETROBRAS)

Yaro M. Parisek-Silva (PETROBRAS)

4.1 Abstract

Hydrocarbon production from volcanic reservoir rocks in Brazil is rare but it was successfully achieved in the Badejo field, Campos Basin. The volcanic rocks are basalts of the Cabiúnas Formation, related with the voluminous lava flows that erupted prior and during the Gondwana breakup in the Early Cretaceous. Despite their widespread distribution in Campos Basin, volcanic facies architectures and studies of physical volcanology regarding the Cabiúnas basalts are still scarce. The cores recovered from wells BD-02, BD-04 and BD-08, drilled in the Badejo field, provided an excellent material to reconstruct the 3D geometries of the volcanic lava flows in the area. Two Compound-braided flows (Sequence 1 and 3) and a Tabular-classic flow sequence (Sequence 2) were identified in the studied wells. Lithofacies associations or morphologies include classical, hummocky, sheet and rubbly pahoehoe lavas. Coherent, brecciated, peperites and intertraps lithofacies were also described in the well cores. Effusion rates, based on the thickness of the lobes, indicated that oscillation of supply rates or pulsed inflation was the major process in Sequence 3. Minimum emplacement duration is estimated in 3 and 7 months for wells BD-2 and BD-04, respectively. Estimated D values for hummocky lavas are higher than those for classical pahoehoe lavas, pointing to porosities and permeabilities adequate to the best potential plays in Sequence 3. Lithogeochemical data revealed a possible correlation between BD-04 and BD-02 wells in the upper part of Sequence 3 indicating eruption from the same emission center. The Compound-braided Sequence 3 may have reach 89.5 m, much thicker than the 40 m thick Tabular-classical lavas in Sequence 2. The volcanic paleoenvironment corresponds to subaerial lava flows with humidity in all sequences. This information can be of great importance for better characterization of potential offshore volcanic reservoirs within Campos and other sedimentary basins associated with the Gondwana breakup in SE Brazil.

4.2 Introduction

The discrimination of volcanic facies architectures is fundamental to understand the 3D arrangement of lava flows. The methodology has been applied to the study of physical processes related with thick and complex sequences of lava flows in Continental Flood Basalt Provinces (CFB), including the Deccan traps, Columbia River and Paraná-Etendeka (Waichel *et al.*, 2012; Vye-Brown *et al.,* 2013; Barreto *et al.* 2014; Rosseti *et al.*, 2014, Svensen *et al.*, 2018; Rossetti *et al.*, 2018; Duraiswami *et al.*, 2014, Famelli *et al.*, 2021a). The discrimination of volcanic facies architectures in continental areas also provides analogues for paleoenvironment reconstructions in offshore areas (e.g. Jerram *et al.*, 2009; Reis, 2013).

Composed lava facies and its internal subdivisions and simple lava facies with a single unit were firstly described in Hawaii (Walker, 1971). The recognition of volcanic facies and association of facies based on geometric parameters, as well as seismic volcanic facies, are now part of current work on physical volcanology and is approached at different scales (*e.g.* Single and Jerram, 2004). For instance, lobes and toes (< 0.5 m) can be discriminated in lava flows under detailed scales (Rossetti *et al.*, 2014). The internal attributes of lobes are pipe vesicles, massive cores and vesicles with different sizes and shapes that help to derive parameters related with topography and distance from the vents (Wilmoth & Walker, 1993; Single and Jerram, 2004). It is known that A´a and classical pahoehoe lavas (Dutton, 1884), that may be considered end-members of possible lava types, are formed as a result of different viscosity and turbulence conditions (Macdonald, 1953). However, emplacement mechanisms, topography and depositional environments may lead to transitional lava types that can comprise even a single lava flow (Lockwood & Hazlett, 2010; Duraiswami *et al.*, 2014). In addition, the process of inflation can transform cm-thick lava lobes in m-thick lava piles in a matter of few weeks (Self *et al.*, 1998; Hon *et al.*, 1994). Under a less detailed scale, facies types and facies association have been used to discriminate stacking lava piles in CFB worldwide and in sedimentary basins. As a result, the 3D arrangements of lava flows can now be related with basin evolution associated with volcanic rift margins (Jerram *et al.*, 2009; Jerram, 2012; Svensen *et al.*, 2018). In addition, seismic volcanic facies can also be distinguished on seismic due to the internal characteristics of the reflectors (e.g. Mohriak *et al.*, 2002; Franke, 2013; Stica *et al.*, 2014) allowing the investigation of relevant variations in magmatic features along and between different rifted margins (Planke *et al.* 2000).

Igneous rocks can occur as reservoirs, seals and traps in petroleum systems in many sedimentary basins in Brazil (Ren *et al*., 2020). However, the study of volcanic facies in hydrocarbon exploratory projects are still scarce although it has been increasing in the last decade (Nelson *et al.*, 2009a; Fornero *et al.*, 2019; Jerram *et al.*, 2009). The giant oil and gas fields in Santos and Campos sedimentary basins, located offshore the southeastern continental margin in Brazil, are among the largest in the world (Bruhn *et al.* 2003; Zhang *et al.* 2019). These basins were originated during the rifting process associated with the Gondwana breakup at Early Cretaceous and evolved to passive margin basins during the opening of the South Atlantic Ocean (Chang *et al.*, 1992; Cainelli & Mohriak, 1999; Heilbron *et al.* 2000, Heine *et al.*, 2013). The pre-rift, rift, post-rift and drift sedimentary sequences in those two basins are associated with magmatic processes (Caddah *et al.*, 1994;1998; Thomaz Filho *et al.*, 2000; Alves, 2005; Rangel, 2005; Moreira *et al.*, 2005; Winter *et al.*, 2007; Thomaz Filho *et al.*, 2008; Dani *et al.*, 2017; Ren *et al.*, 2020, Almeida *et al.* 2021). In particular, the Early Cretaceous, pre-rift/rift-related magmatism in Campos Basin comprises the tholeiitic basalts of the Cabiúnas Formation, being coeval with the Paraná-Etendeka CFB (Fodor *et al.*, 1983; Fodor & Vetter, 1984; Mizusaki *et al.*, 1992; Lobo *et al.*, 2007). A stratigraphic approach has been applied to the study of the basaltic volcanism in Paraná-Etendeka allowing the recognition of lava flow morphologies and interaction processes with sediments (Waichel, *et al.* 2006, Barreto *et al.* 2014; Waichel *et al.* 2012; Rossetti *et al.*, 2018; Moraes & Seer, 2018; Famelli *et al.*, 2021b). However, this approach has only rarely been applied to the study of the Cabiúnas volcanism in Campos basin (Mizusaki *et al.*, 1988; Marins & Parizek-Silva *et al.*, 2018).

The aim of the present work is to discriminate volcanic facies associated with the Cabiúnas basalts in Campos Basin. Both stratigraphic and petrological approaches, using cores and well logs, were applied in this study. The discrimination of different volcanic sequences with distinctive interactions between lavas and sediments allowed the proposition of possible volcano-sedimentary paleoenvironments that prevail in the study area within Campos Basin in the Early Cretaceous. It is also expected that the results of this work will demonstrate the usefulness of integrating the proposed approach to prospective models associated with the pre-salt hydrocarbon plays in Campos and other sedimentary basins in Brazil.

4.3 Geological setting

The Campos Basin is located offshore the northern part of Rio de Janeiro, SE Brazil (Figure 6 and 7). The basin comprises up to 9 km of sedimentary rocks and covers an area over 100,000 km² (Winter *et al.*, 2007). The studied wells (BD-02, BD-04 and BD-08) are located in the Badejo oil and gas field under water depths of 85 m (Mizusaki, 1986).

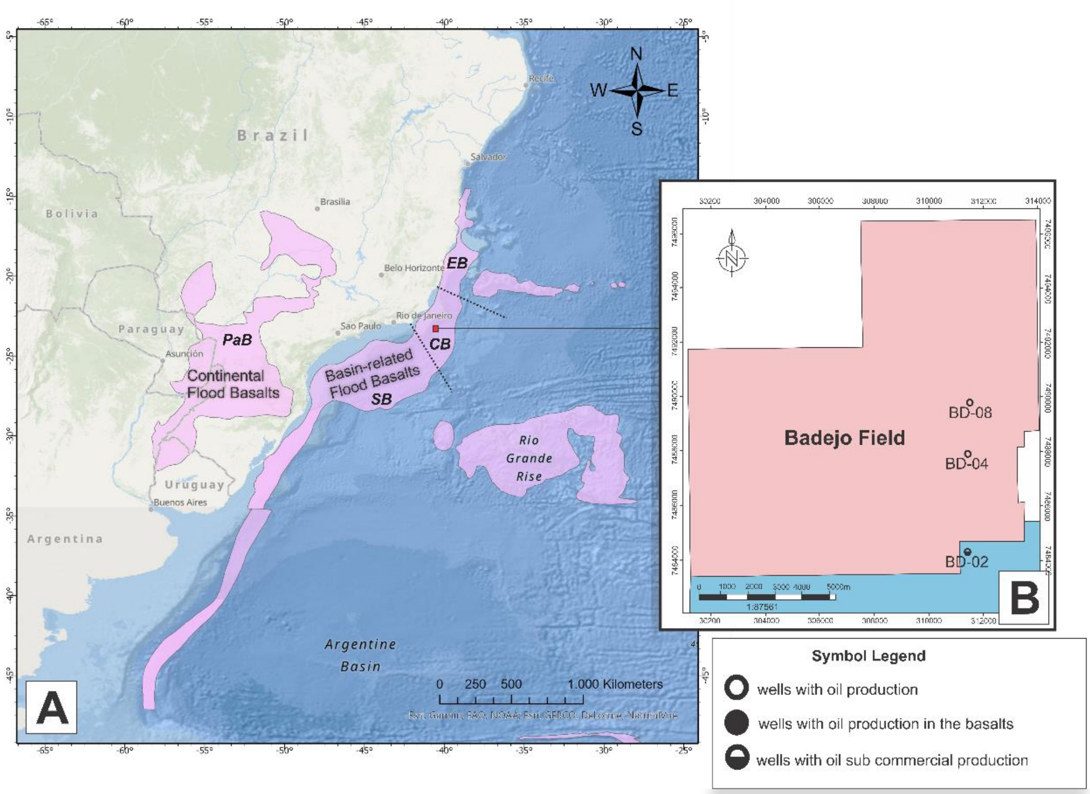

Figure 6: Location map of the Badejo field in Campos basin. (A) Regional topographic-bathymetric map of the western portion of the South Atlantic Ocean with the location of the Paraná (PaB), Santos (SB), Campos (CB) and Espírito Santo basins (EB). Dotted lines: approximate delimitation of Campos basin. (B) Detailed location of the Badejo (pink) and Linguado (blue) fields with the locations of wells BD-01A, BD-02, BD-04 and BD-08.

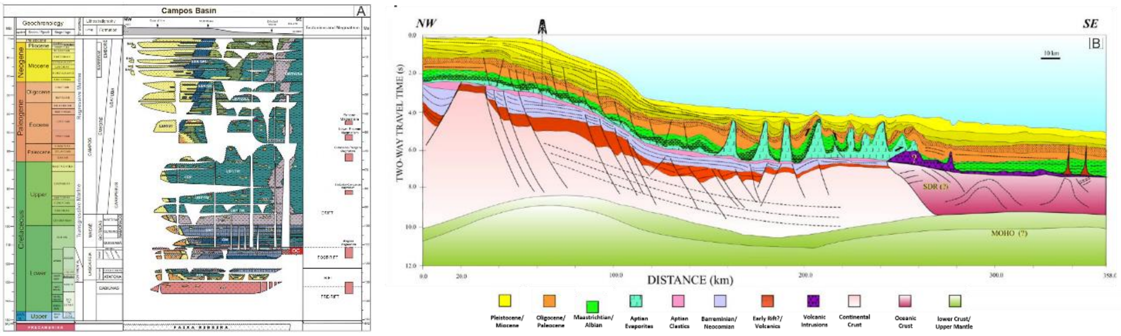

Figure 7: Stratigraphic data and schematic geological section of Campos Basin. (A) - Chronostratigraphic chart of Campos Basin (modified from Winter et al., 2007). (B) - Geological (time-related) section of Campos Basin. The local continental crust is represented by the NeoProterozoic-Cambrian Ribeira Orogen (modified from Mohriak *et al.*, 1998, 2004).

Campos is a passive margin, sedimentary basin whose origins date back to the Early Cretaceous due to the Gondwana rifting process. The tectonic evolution of the basin is recorded in three main sedimentary sequences. The pre-rift/rift sedimentary sequence is marked by Early Cretaceous (*ca.* 134 ± 4 Ma; whole-rock K-Ar age, Mizusaki *et al.*, 1992), extensive basalt lava flows that comprise the Cabiúnas Formation (Figure 7A). The basaltic lava flows have been associated with a pre-rift stage of basin evolution since they are cut by syn-rift faults (Mohriak *et al.*, 2002). They were erupted over the Neo-Proterozoic/Cambrian granitic gneiss basement of the Ribeira Orogen (Figure 7B). The time-related shales and interbedded limestones of the Atafona Formation represent lacustrine sedimentation that took place in deep, enlongated, hypersaline alkaline lakes (Winter *et al.*, 2007; Castro *et al.*, 2014). The black, talc-stenvisite shales of the Atafona Formation are the main hydrocarbon source rocks in Campos basin (Guardado *et al.*, 2000) and may have formed in alkaline lakes associated with volcanic, hydrothermal processes (Mohriak *et al.*, 2008). The post-rift sedimentary sequence in Campos is associated with the sag tectonic stage of basin evolution and is represented by continental-derived, proximal siliciclastic sedimentation and shallow, epicontinental sea, distal sedimentation (Dias *et al.* 2005). The microbial limestones and stromatolites of the Macabu Formation constitute the main reservoir rocks in the pre-salt petroleum system of Campos basin (Rangel *et al.*, 1994; Winter *et al.* 2007; Castro et. al. 2014). The final stages of the post-rift sequence are characterized by thick salt (mainly halite and anhydrite) layers formed due the restricted sea water circulation imposed by the São Paulo Ridge combined with an arid climate (Dias *et al.*, 2005; Moulin *et al.* 2010; Amorim, 2013). The salt layers of the Retiro Formation represent the main seal rocks in Campos basin. Finally, the drift sedimentary sequence extends from the Albian to Recent and represents a progressive increase in the bathymetry and the transition from shallow, marine limestones to deep sea, turbiditic siliciclastic rocks (Mohriak *et al.*, 2008). The latter are the main reservoir rocks in the post-salt plays in Campos basin.

4.4 The Cabiúnas magmatism

The Cabiúnas Formation is mostly represented by basalt lava flows that erupted on the Neo-Proterozoic to Cambrian gneisses of the continental crust basement of Campos basin (Kowsmann *et al.*, 1982; Fodor *et al.*, 1983). The continental basalts of the Cabiúnas Formation display the typical Nb negative anomaly and high La/Yb_n ratios of CFB worldwide. They comprise a low-Ti, tholeiitic basalt series of predominantly subaerial basaltic lava flows (Fodor *et al.*, 1983/1984; Fodor & Vetter, 1984; Mizusaki *et al.*, 1992; Lobo *et al.*, 2007). Whole-rock K-Ar ages are rather variable (*ca.* 134 - 116 Ma) but the youngest ages were attributed to Ar loss since the basalts are located under the Barremian rocks dated at 124-119 Ma (Mizusaki *et al.*, 1992). The Cabiúnas basalts evolved by assimilation and fractional crystallization and were originated by 9-25% partial melting from a garnet peridotite mantle source involving mixing of DUPAL-like components and the subcontinental lithospheric mantle (SCLM) (Mizusaki *et al.*, 1992; Lobo *et al.*, 2007).

The Cabiúnas basalts in the area of the Badejo, Linguado and Pampo hydrocarbon fields (Figure 1) were related with a volcano-sedimentary sequence that includes subaerial (Badejo and Pampo) and subaquous (lacustrine, Linguado) lava flows, pyroclastic tuffs, hydrovolcanic pyroclastic breccia and epiclastic rocks (Mizusaki *et al.*, 1988; Mizusaki *et al.*, 1992). The basalts were described as grey to reddish, fractured, aphanitic to microgranular rocks with vesicles and amygdales. They are interbedded with autoclastic, pyroclastic and epiclastic rocks as well as siltstone and fine-grained sandstone. The autoclastic rocks are friction breccia with rounded, carbonate- and silica-cemented clasts of basalt due to the fragmentation of lava. The pyroclastic rocks are clay mineral-rich tuff and hydrovolcanic breccia. The epiclastic rocks are volcanic breccia and volcanic sandstones with subangular to subrounded, reworked clasts of magmatic rocks. The volcanic breccia are silt-rich and quartz-feldspathic rocks whereas the volcanic sandstones are fine-grained rocks with up to 20%vol. of basaltic clasts. Tuffs and breccia predominate in the Badejo field, the former being reddish in color and showing incipient pedogenesis that indicate a subaerial environment. The volcanic sandstones display good selection and high primary porosity that may be related to a near shore depositional environment. The hydrovolcanic breccia are taken as products of subaqueous volcanism and predominate in the Linguado field and southern Badejo field. Overall, the rock associations may be related to a transitional subaerial to subaqueous (shallow lacustrine) volcano-sedimentary environment, the former predominating over the latter and prevailing in Badejo field (Mizusaki, 1986).

Four volcanic units were identified in a 90 m-long core recovered from well BD-11 in the Badejo field. These units represent distinctive eruptive events that formed amygdaloidal and vesicular basalt, massive basalts, autoclastic breccia, volcanic sandstone, conglomerate and peperite. Composed pahoehoe lava, volcanic conglomerate and volcanic red sandstone were formed during inicial eruptive stages under low effusive rates. Subsequently, higher eruptive rates gave rise to a 35 m-thick, simple, rubbly pahoehoe lava. Intermittent to low rate eruptions formed composed pahoehoe lava flows interbedded with peperites that were covered by basaltic volcanoclastic rocks. Further higher eruptive rates generated the simple, rubbly basaltic lava associated with peperites. In general, the distinctive eruptive episodes were taken as subaerial lava flows that locally interacted with water-saturated sediments in shallow lakes with water/lava ratios lower than 3 (Marins & Parizek-Silva *et al.*, 2018).

On seismic, similarly to other landward flows (*eg.* Planke *et al.* 2000), the Cabiúnas basalts, that consisting of flood basalts in a predominantly subaerial environment, display sheet shapes and internally parallel to subparallel, high amplitude and disrupted reflectors in seismic profiles (Stica *et al.*, 2014).

4.5 Material and methods

Core samples from three wells (BD-02, BD-04 and BD-08) drilled in the Badejo field, Campos basin were studied in this work. Samples were studied under different scales of observation, as suggested by other authors (e. g. Németh & Palmer, 2019; Bischoff *et al.* 2017). Lithofacies were discriminated under both macroscopic and microscopic scales throughout petrographic descriptions (Barreto *et al.*, 2014; Costa, 2015; Famelli *et al.*, 2021a). Furtherly, lithofacies were grouped in lithofacies associations that in turn were related with different volcanic sequences (Waichel *et al.*, 2012; Jerram, 2012; Duraiswami *et al*., 2014; Rossetti et al, 2018). This methodology was generally based on, althought slightly modified from, previous works on lava facies architectures related with continental flood basalt provinces (Single & Jerram, 2004; Nelson *et al*., 2009a).

Cores were firstly described under macroscopic scale throughout sketchs, sections and photos. Thin sections of 192 selected samples were described under the optical microscope (68 from BD-02, 92 from BD-04 and 32 from BD-08). Textural parameters such as crystalinity, granularity and crystal shapes, as well as intergranular relationships and structures (*e.g.* flowage and cavities) were discriminated following the nomenclature of MacKenzie *et al.* (1991). Rock classifications used the terminology proposed by McPhie *et al.* (1993) and LeMaitre *et al.* (2002). The shape of the vesicles and amygdales were described in five categories as shown in the picture bellow (Figure 8) and correlated with the D parameter and strain rate (Duraiswami *et al.*, 2003; 2014).

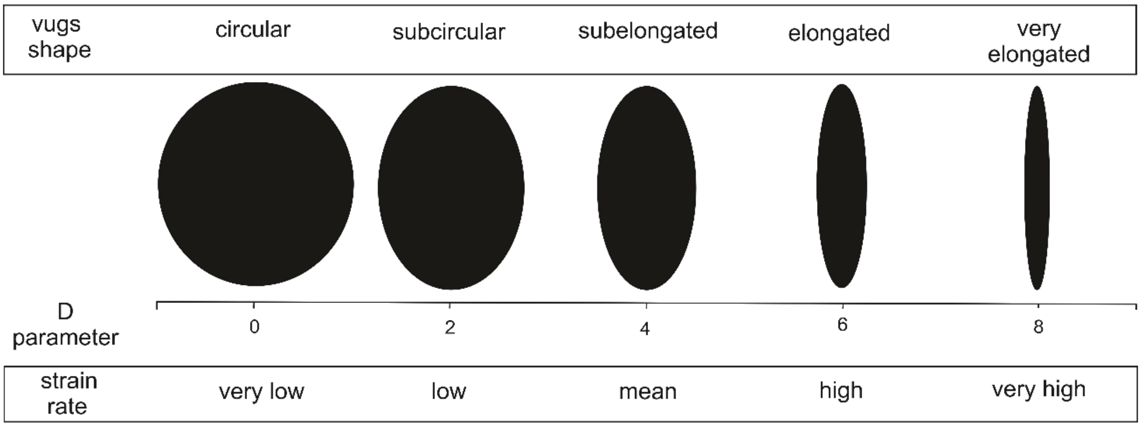

Figure 8: Vug shape classification and the correlated values for D parameter and strain rates.

A subset of 20 samples was selected to be crushed and milled for geochemical analysis (major and trace elements, including the rare earth elements; REE). Whole-rock geochemical analyses were done at Activation Laboratories Ltd. (Actlabs, Canada) on fused samples. Major elements were performed by inductively coupled plasma optical emission spectrometry (ICP-OES) in a Thermo Jarrell Ash ENVIRO II equipament. Calibrations were performed using seven prepared USGS and CANMET certified reference materials. The rare earth elements (REE) and selected trace elements were determined by inductively coupled plasma mass spectrometry (ICP-MS) in a Perkin Elmer Sciex ELAN 9000 equipment. Calibrations were performed using ten synthetic calibration standards. A set of ten certified reference material runned before and after every batch of samples.

The petrographic and lithogeochemical data were interpreted to propose a simple 3D characterization of the volcanic environment. Finally, well log data (density and sonic) of the three studied wells were tentatively associated with the discriminated lithofacies associations.

4.6 Lithofacies Association Discrimination

Four lithofacies associations of typical subaerial lava flows were identified in the studied well cores (Figure 9 and 10). Classical pahoehoe lavas and the transitional types Hummocky, Sheet and Rubbly pahoehoe lithofacies association.

Classical pahoehoe (Duraiswami *et al.*, 2014 and Self *et al.*, 1998) lavas are reddish in color with lobes average thickness of 37 cm, displaying 7 cm-thick toes and 1.5 m-thick lobes formed by amygdaloidal/vesicular basalts lithofacies (amB/vsB) (Figure 9B). A glassy crust is clearly seen with spherical vesicles up to 5mm in diameter and may also be partially filled by carbonate and clay material forming the lithofacies amygdaloidal basalts within glassy crust (amB_g) (Figure 9A). Lobes are stacked giving rise to compound pahoehoes frequently interbedded with lenses of sedimentary rocks bearing basalt clasts with fluidal-like margins similar to peperites.

Hummocky pahoehoe lavas (Duraiswami *et al.,* 2014; Bondre *et al.*, 2004; Self *et al.*, 1998) are compound, predominate greyish in color with lobes average thickness of 71 cm (0.25 - 4.5 m). The same facies occur as in the classical pahoehoe (Figure 9C,D), but differently they present a glassy crust with 7 mm long vesicles that tend to be strongly elongated topwards (Basalts with elongated amygdala lithofacies - amB_e) (Figure 9E). In the inner part of the lobes, the vugs tend to be more twisted forming the lithofacies basalts with interconnected vesicles (amB_i) (Figure 9F). Highly vesicular crust is one of the characteristics of *Hummocky pahoehoe lavas e*lsewhere (Duraiswami, 2009).

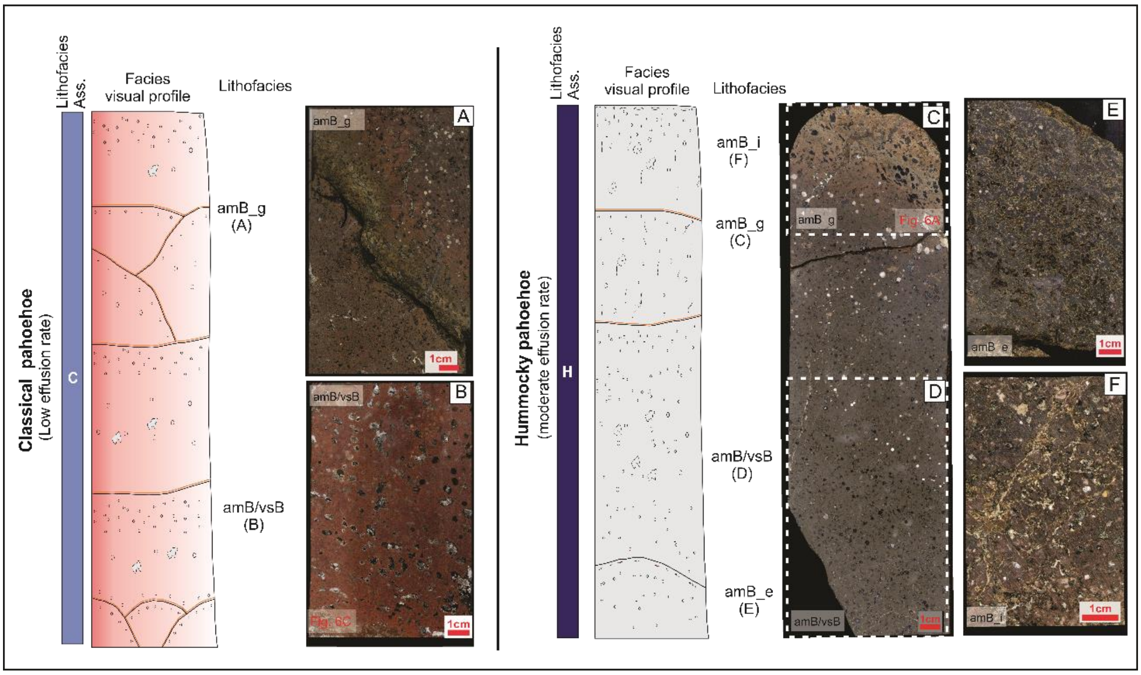

Figure 9: Classical and Hummocky pahoehoe lithofacies association and the correlated coherent basaltic lithofacies discriminated in BD-02, BD-04 and BD-08 wells, Badejo field. A) Amigdaloidal basalt within glassy crust (amB_g) from depth 3118,80, BD-04 well B) Amygdaloidal/vesicular basalt lithofacies (amB/vsB) from depth 3167.37, BD-08 well. C) Amigdaloidal basalt within glassy crust (amB_g) from depth 3156.79, BD-02 well. D) Amygdaloidal/vesicular basalt lithofacies (amB/vsB) from depth 3156.79, BD-02 well. E) Basalt with enlongated amygdales within glassy crust (amB_e) from depth 3101.55, BD-04 well. F) Amygdaloidal basalt with interconnecting vesicles lithofacies (amB_i) from depth 3194.91, BD-02 well.

Sheet pahoehoe lavas *(*Duraiswami *et al.*, 2014; Hon *et. al*., 1994; Self *et al.*, 1998) have an average thickness of 4.3 m (1.3 - 9.4 m) and have typical top-bottom vesicular layers and massive Basalts (mB) in the core (Figure 10A), forming simple flow units. The glassy crust can occur as basalts with elongated amygdales (amB_e) and amygdaloidal basalts within glass crust (amB_g) lithofacies. Top lobe is formed of amygdaloidal/vesicular basalts lithofacies (amB/vsB) and amygdaloidal basalts with interconnecting vesicles (amB_i), but the base are formed solely of amB/vsB showing circular to subcircular vugs (Figure 10B).

Rubbly pahoehoe lavas (Marins *et al.*, 2022 submitted; Sheth *et al.*, 2017; Duraiswami *et al.*, 2014; Keszthelyi, 2002) are up to 20 m in thickness display autoclastic breccia lithofacies (autBr) (Figure 10C, D) in the top and the core are formed with very fine-grained massive basalt (mB) (Figure 10F). Autoclastic breccias with jigsaw-fit texture (autBr_j) can also occur in the cores (Figure 10E). Bottom layers display structures indicating interaction with sediments, giving rise to peperites.

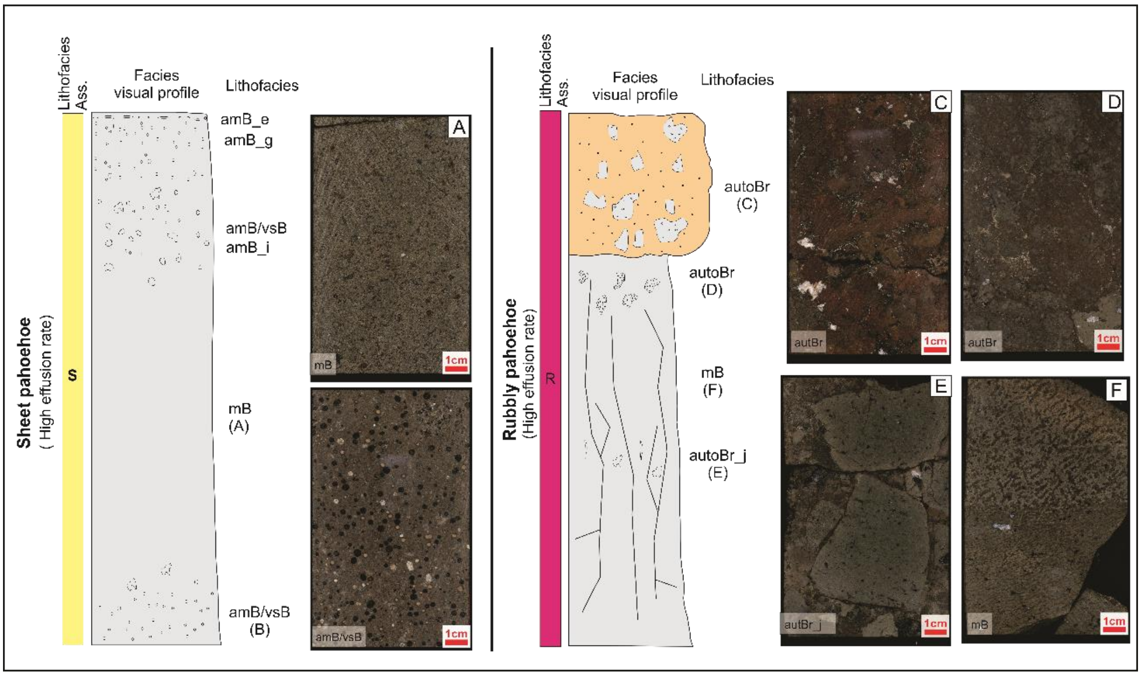

Figure 10: Sheet and Rubbly pahoehoe lithofacies association and the correlated coherent basaltic lithofacies discriminated in BD-02, BD-04 and BD-08 wells, Badejo field. A) Massive basalt (mB) from depth 3083.73, BD-04 well. B) Basal amygdaloidal/vesicular basalt lithofacies (amB/vsB) from depth 3086.63, BD-04 well. C) Autoclastic breccia lithofacies (autBr) with siltitic matriz from depth 3121.33, BD-04 well. D) Autoclastic breccia lithofacies (autBr) with basaltic matriz from depth 3128.74, BD-04 well. E) Autoclastic breccia with jagsaw-fit texture lithofacies (autBr_j) from depth 3156.68, BD-08 well. F) Massive basalt (mB) from depth 3156.15, BD-08 well.

4.7 Lithofacies Discrimination

Eleven lithofacies were described in the studied wells (Table 1). Thin sections of 192 selected samples were described under the optical microscope (68 from BD-02, 92 from BD-04 and 32 from BD-08). These samples represent the lithofacies described previously and modal composition of the basalt lithofacies are shown in Table 2.

The amygdaloidal/vesicular basalt lithofacies (amB/vsB) is reddish (Figure 9B) in classical pahoehoe to predominant greyish in hummocky and lobe top and base from sheet pahoehoes (Figure 9D; 10B). Presents isolated or agglutinated, circular to subelongated vug up to 0.5 cm in diameter with the naked eye. Amygdales are more frequent than vesicles, the latter being open to semi-open and restricted to a few depth intervals in the well cores. The amount of glass increases towards the top crust. Under microscope, most of these basalts are plagioclase- and pyroxene-phyric rocks with phenocrysts immersed in a microcrystalline, hypohyaline matrix (Table 2). In the classical pahoehoe comprises porphyritic and glomeroporphyritic rocks with a microcrystalline, hypohyaline matrix. The volume of crystals (90%) prevails over glass (10%) in the matrix and near-crust samples tend to be hypocrystalline. Anhedral to subhedral clinopyroxene and plagioclase phenocrysts are corroded, zoned and display sieve texture attesting to disequilibrium processes, being isolated or in clots (Figure 11C). The larger plagioclase phenocrysts comprise 10 - 25 vol% of the rock. Amygdales (0.5 - 7 mm) prevail over vesicles, being subcircular to circular and filled with silica-rich phase, as well as carbonate and clay minerals (Figure 11D). Diktaxitic texture can be observed (Figure 11C) and the amygdaloidal basalts lack fractures. In the hummocky pahoehoe and lobe top and base in the sheet pahoehoes rocks are plagioclase-phyric with a microcrystalline, hypohyaline matrix, with higher proportions of glass when compared with the classical pahoehoe (Table 2). Matrix crystal are often finer in the hummocky pahoehoe, with microlites smaller than 0.05 mm (Figure 11E). Anhedral to subhedral plagioclase phenocrystals isolated and clots displays disequilibrium textures. Amygdales and vesicles (1 - 9 mm) are circular to subenlongated and filled with carbonate and clay minerals (Figure 11E). Diktaxitic texture can be observed, rare open fractures surround the amygdales.

The rocks of the amygdaloidal basalt within glassy crust facies (amB_g) in the crust of hummocky, classical and sheet pahoehoe are an altered glass-rich lithofacies being typically light brown in color. They are porphyritic with a microcrystalline, holohyaline to hypocrystalline matrix where glass prevails over crystals (Table 1). Plagioclase and clinopyroxene phenocrysts are zoned and display sieve texture, sometimes oriented, attesting to disequilibrium processes. The greater the amounts of glass, the lower the volume of phenocryst. Vesicles are rare or absent, amygdales (0.5 - 5mm) are subcircular to elongated, less often subcircular in shape, and filled with calcite, glass, and clay minerals (Figure 11A e 9C).

The basalt with elongated amygdales within glassy crust lithofacies (amB_e) is found in the crust of the lobes in hummocky and sheet pahoehoes. Similar to the lithofacies described previously but vesicles are amalgamated as linear films that give the basalt crust a greyish color (Figure 9E). This crust is often fragmented due to the discontinuities generated by the aligned, amalgamated amygdales. Plagioclase microphenocrysts prevail over clinopyroxene ones surrounded by hypocrystalline to holohyaline matrix (Table 1). The amount of glass in the amB_e is lower than in the amB_g and the amygdales (0.7 – 7 mm) in the former are elongated to very elongated and filled with calcite, dolomite and clay minerals that may have been partially dissolved leaving vesicles behind. Both open and filled microfractures are either connected are surrounding the amygdales (Figure 11B). Fractures are more abundant in the glassy matrix.

The amygdaloidal basalt with interconnecting vesicles lithofacies (amB_i) is greyish, and, sometimes reddish in color and are present in the hummocky pahoehoe and sheet pahoehoe´s lobe top. The main distinctive feature is the connection of subcircular to elongated amygdales by submillimeter fractures (Figure 9F). In the macroscopic scale, vary from 0.5 to 6 mm in diameter, but can reach 1-5 cm if amalgamated. Very fine-grained plagioclase phenocrysts are immersed in hypohyaline matrix and have amount of glass similar to amB/vsB in classical pahoehoe (Table 2). In the microscopic scale, vugs vary from 0.5 - 10 mm, are filled with carbonate and clay minerals and are connected by microfractures filled by clay minerals (Figure 11F). The filled microfractures are cut by open fractures. Diktaxitic texture can be observed.

Table 1: Main characteristics of discriminated lithofacies in the Badejo field.

#	Lithofacies	Code	Color	Petrography	Vugs	Others
1	Amygdaloidal/vesicular basalt.	amB/vsB	Reddish or greyish.	Pg- and Py-phyric. hypohyaline matrix.	Isolated or agglutinated. Circular to subelongated. Macroscopic (0.5 cm in diameter) and microscopic (1-	% of glass increases towards the top crust.

					7 mm).	
2	Amygdaloidal basalt with glassy crust.	amB_g	Light brown.	Aphyric or Pg-phyric. Glassy (hypocrystalline to hypohialline) matrix.	Enlongated to subenlongated. 1-10 mm long.	Altered, glass-rich lithofacies
3	Basalt with enlongated amygdales within glassy crust	amB_e	Greyish.	Pg > Px-phyric. Glassy (hypocrystalline to hypohialline) matrix.	Enlongated; rarely subcircular. Amalgamated as linear films. 0.5 - 7 mm long.	Fragmented crust.
4	Amygdaloidal basalt with interconnecting vesicles.	amB_i	Greyish and sometimes reddish.	Pg-phyric. Hypohialine matrix.	Subcircular to enlongated. Interconnected by submilimetric fractures. 0.5 - 6 mm in diameter; 1-5 cm when amalgamated.	-
5	Massive basalt.	mB	Greyish.	Aphyric and Pg-phyric. Hypohyaline to holocrystalline matrix.	Vug-free.	Densely fractured. Incipient foliation.
6	Autoclastic breccia.	autBr	Greyish to reddish.	Oligomythic. Siltic matrix-supported or basalt matrix-supported Subangular clasts (0.5 - 2.0 cm) of massive basalt and amygdaloidal/vesicular basalt.	Vug-free.	-
7	Autobreccia.	aBr	Greyish.	Oligomythic. Basalt clast-supported with angular fragments cemented by carbonate and clay-like material. .	Vug-free.	Jig-saw arrangement.
8	Volcanic breccia	vBr	-	Polimythic. Clast- to matrix-spported. Subangular to subcircular clasts (0.25 - 80.0 mm) of massive basalt, amygdaloidal basalt and autoclastic breccia. Brownish, fine to medium-grained sandstone matrix.	Vug-free.	-

9	Peperite	P	Greyish, greenish and reddish.	Greyish to reddish basalt (irregular, block, fluidal and scoriaceous) fragments. Sandy to silty, greenish to greyish matrix. Closed-packed and dispersed internal structures.	Locally vesiculated.	mm-to-m thick layers
	Volcanic Green Siltstone	gS	Greenish	massive	Vug-free.	Can occur as peperites matrix
10	Volcanic sandstone	vS	yellowish and reddish.	Moderately sorted. Greyish to reddish basalt clasts, altered plagioclase and opaque minerals fragments.	Vug-free.	-

Table 2: Modal compositions of the basalt lithofacies described in wells BD-02, BD-04 and BD-08. Breccias not included. Gls = glass. Min = minerals. Mtx = matrix. Ph = phenocrysts. Pg = plagioclase. Cpx = clinopyroxene. Opq = opaque minerals. Codes of lithofacies as in Table 1. Lava morphologies are indicated.

Lithofacies	Gls:Min	MtxPg	MtxCpx	MtxOpq	MtxGls	PhPg	PhCpx
amB/vsB (classical)	10:90	60	20	10	10	x	x
amB/vsB (hummocky and sheet)	25:75	48	25	2	25	x	
amB_g	84:16	10	5	1	84	x	x
amB_e	35:65	20	10	35	35	x	x
amB_i	10:90	50	34	1	10	x	
mB (rubbly)	2:98	50	40	8	2	x	
mB (sheet)	10:90	50	35	5	10	x	

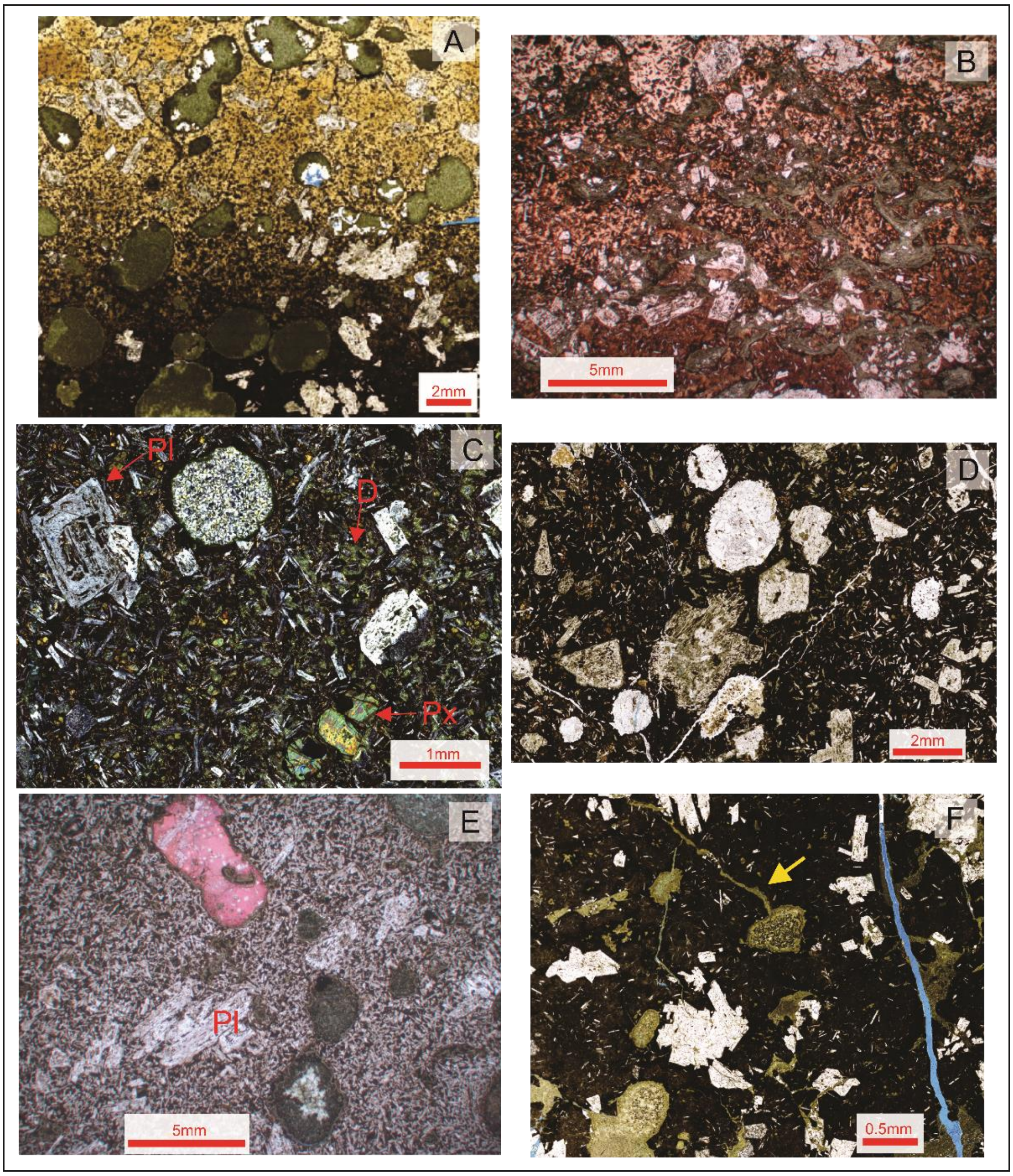

Figure 11: Photomicrographs from coherent basaltic lithofacies discriminated in wells BD-02, BD-04 and BD-08 in the Badejo field. A) Amygdaloidal basalt within glassy crust facies (amB_g), well BD-02. B) Basalt with elongated amygdales within glassy crust facies (amB_g), well BD-02. B) Basalt with elongated amygdales within glassy crust facies (amB_e), well BD-04. C) Amygdaloidal basalt/vesicular basalt lithofacies (amB/vsB) from classical pahoehoe, well BD-08. D) Amygdaloidal basalt/vesicular basalt lithofacies (amB/vsB) from classical pahoehoe, well BD-08. Pl – zonated plagioclase with sieve texture. E) Amygdaloidal basalt/vesicular basalt lithofacies (amB/vsB) from hummocky pahoehoe, well BD-04. F) Amygdaloidal basalt with interconnecting vesicles facies (amB_i), well BD-02. Yellow arrow – microfracture interconnecting amygdales. (A, B, D, E, F - // polarizers; C – X polarizers)

Vug-free basalts are included in the massive basalt lithofacies (mB), being greyish and densely fractured rocks (Figure 10A, F). They are founded in the rubbly and sheet pahoehoe cores. The highly fractured portions of the massive basalts are poorly recovered from the well cores. The massive basalts are aphyric to poor porphyritic and can display plagioclase phenocrysts within a very fine-grained, hypohyaline to holocrystalline, microcrystalline matrix being hypohyaline to holocrystalline in the rubbly pahoehoe (Figure 12B) and hypohyaline in the sheet pahoehoe (Figure 12C). Microlites in the rubbly pahoehoe are much finer than in sheet pahoehoes (Figure 12B). The proportion of plagioclase phenocrysts change in the rubbly and sheet pahoehoe, comprising rocks with relatively less and more amounts, respectively (Table 2). Disequilibrium textures in plagioclase phenocrysts are a common feature in both lithofacies association, but they are predominantly anhedral in the rubbly pahoehoe. Diktaxitic texture is more common in sheet pahoehoe (Figure 12C). A distinctive structural feature is the foliation in this lithofacies in the rubbly pahoehoe, given by layers of microlites with different sizes (Figure 10F, 12A).

There are three brecciated lithofacies in the studied wells (Table 1). Rocks in the autoclastic breccia with sedimentary matrix (autBr), in the rubbly pahoehoe crust, is oligomythic, matrix-supported, greyish-to-reddish rocks with clasts of massive basalt and amygdaloidal/vesicular basalt varying in size from 0.5 cm to 2.0 cm. The matrix is siltitic and reddish in color (Figure 10C). Additionally, autoclastic breccia can also occur as clast/matrix-supported rocks with subangular basalt fragments immersed in a basaltic matrix (Figure 10D). The fragments are very difficult to distinguish with the necked eyes and looks like a lot with massive basalts lithofacies. Under microscope, autoclastic breccia with sedimentary matrix (autBr) comprise fragments of fine-grained, aphyric, massive basalt. The groundmass is formed by volcanic sandstone with fragments of basalt, plagioclase (0.1 mm) and clay mineral (Figure 12F). The autoclastic Breccia with basaltic matrix (autBr) is formed by rocks with fragments of amygdaloidal, porphyritic basalt and porphyritic massive basalt displaying irregular rims. Fragments are surrounded by a microcrystalline hypohialline matrix and clay mineral (Figure 12E). Rims of fragments become nearly indistinguishable closer to the massive basalts (mB) lithofacies.

Autoclastic breccia with jigsaw-fit texture (autoBr_j) are associated with the inner and more fragmented parts of rubbly pahoehoes. They are oligomythic and displays a clear brecciated structure that can locally acquire a jigsaw fit texture (Figure 10E). The rock is clast-supported, greyish in color and the angular fragments are cemented by carbonate/clay-like material. They are formed of angular fragments of aphyric massive basalt (60% plagioclase, 30% glass, 10% pyroxene) with variable sizes (0.2 to 18 mm), all cemented by calcite and clay minerals (Figure 12D).

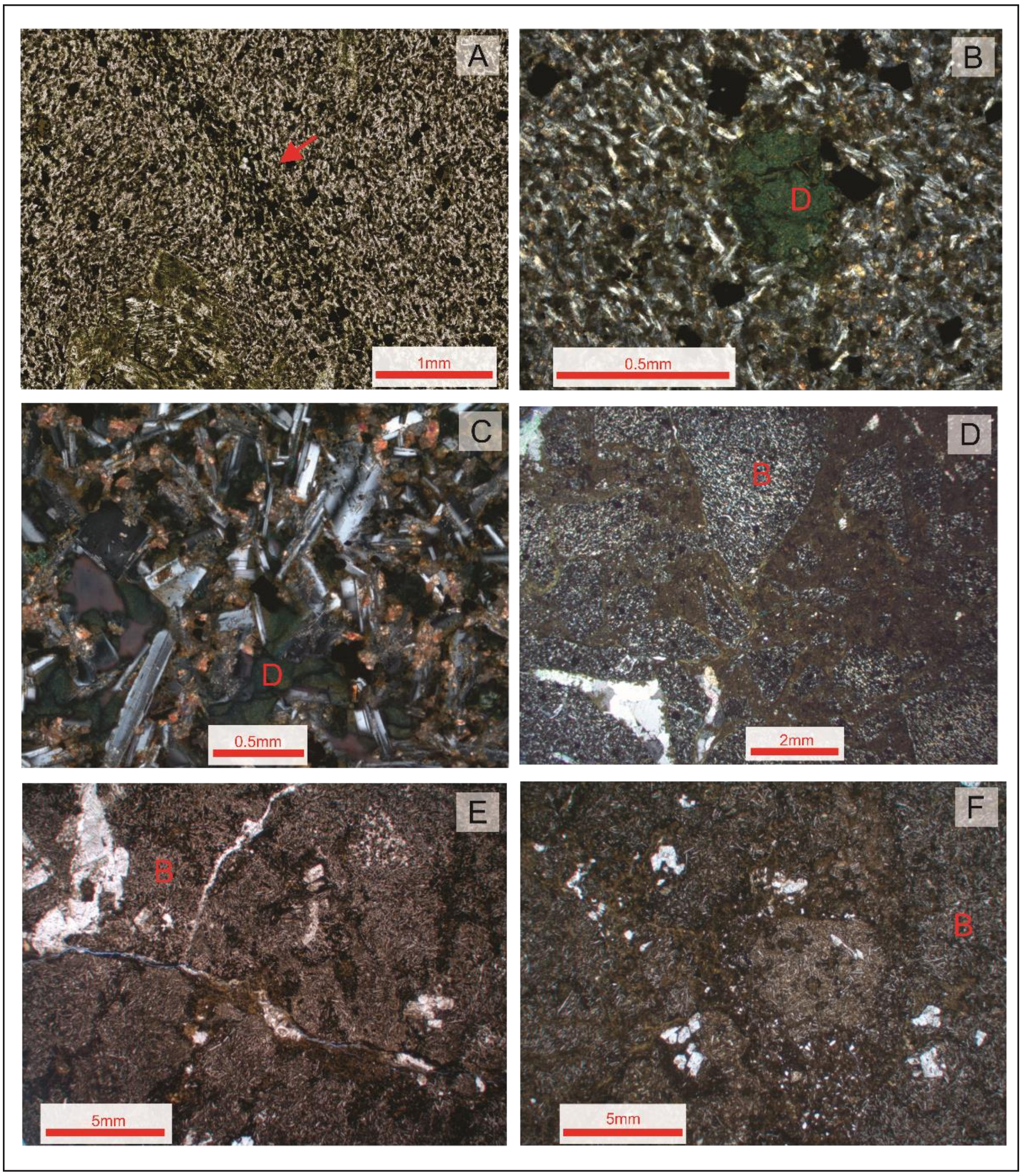

Figure 12: Photomicrographs from coherent and brecciated basaltic lithofacies discriminated in wells BD-02, BD-04 and BD-08 in the Badejo field. A) Massive

basalt lithofacies (mB) from rubbly pahoehoe, well BD-08. Red arrow – microlites foliation. B) Massive basalt lithofacies (mB) from rubbly pahoehoe, well BD-08. C) Massive basalt lithofacies (mB) from sheet pahoehoe, well BD-04. D) Autoclastic beccia with jagsaw-fit texture (autBr_j), well BD-08. E) Autoclastic Breccia with basaltic matrix (autBr), well BD-04. F) Autoclastic breccia with sedimentary matrix (autBr), well BD-04. Pl – Plagioclase, Px - Piroxene, D – Dicktitaxitic cavity, B – Basalt. (A, D, E, F - // polarizers; B, C – X polarizers).

Different structures were discriminated in the peperite lithofacies (P). Peperites can be fluidal (Figure 13A, D, I, J) or blocky (Figure 13E, F, G, H), having greyish to reddish basalt fragments that can be irregular, blocky, fluidal and scoriaceous in shape and immersed in sandy to silty, greenish to greyish, locally vesiculated, matrix. Peperites are interbedded with pahoehoe lobes as mm-to-m thick layers (Figure 13I). They present closed-packed and disperse internal structures and are associated with the bottom parts of the rubbly pahoehoes (Figure 13A, B) as well as between lobes of the hummocky and classical pahoehoes.

The fluidal peperite (Figure 13A) that occurs as intertraps between lobes in the classical and hummocky pahoehoe are a mixture of siltose to sandstone material with an amygdaloidal basalt, porphyritic with microcrystalline, hypocrystalline matrix. Basaltic fragments are fluidal to irregular, sometimes with no clear boundary, with circular and subangular shape. The rock is strongly fractured with joints filled by clay and silica-rich material. A close-packed peperite (Figure 13A, D and 14B) also occurs at the top of the hummocky and classical morphologies. It comprises a mixture of fragments (1-15 mm) of porphyritic massive basalt with clear borders but more irregular than those in the fluidal peperite. Fragments are surrounded by medium- to fine-grained altered immature sandstone with angular to sub-angular feldspar. Aligned microfractures filled with calcite may be related with fluidization of the sandstone. A blocky peperite does also occur in the hummocky pahoehoe (Figure 13E and 14F), being formed by fine-grained volcanic sandstone with sub-angular fragments of basalt, plagioclase and glass highly mixed with porphyritic massive basalt with hypohialline matrix. The basalt could present fluidal borders rather indistinctive from those of the surrounding sandstone. The disperse peperite in the bottom of the rubbly pahoehoe is matrix-supported, comprising clasts of scoria with 1.5 to >10 mm in size with open vugs and a very fine-grained siltose matrix (Figure 13A and 14D). Peperites become closed-packed and clast-supported towards the top with scoriaceous fragments with 1.0 to 14 mm in a highly fractured, microcrystalline hypocrystalline basalts and low content of the siltose matrix (Figure 13A, B and 14C). Some scoriaceus fragments are filled with carbonate.

The poorly sorted volcanic breccia lithofacies (vBr) is polimythic, clast- to matrix-supported rocks with subangular to subcircular fragments, 0.25 to 80.0 mm in size, of massive, grey basalt (mB), reddish to greyish amygdaloidal basalt (amB) and autoclastic breccia (autBr). The matrix is composed by a fine to medium-grained, brownish volcanic sandstone with crystaloclasts of plagioclase, clinopyroxene and opaque minerals (Figure 13N, 14E). The volcanic breccia occurs at the top of BD-02 and BD-04 wells and eventually interbedded with sheet pahoehoe lobes.

The volcanic sandstone (vS) lithofacies occur as intertraps between lobes in the hummocky pahoehoe. It is yellowish and reddish, moderately sorted, volcaniclastic rocks with greyish and reddish basalt clasts, altered plagioclase and opaque mineral grains (Figure 13C, L). Fragments are sub-angular, fine- to very fine-grained surrounded by a clay-like matrix (Figure 13A, C, L and 14G) with no clear evidence of interaction with basaltic lavas.

The volcanic green siltstone lithofacies (gS) is massive and very fine-grained similarly to the one shown in Figure 14D. Occurs as intertraps between lobes of hummocky pahoehoe lithofacies association (Figure 13M).

Figure 13: Peperites and sedimentary lithofacies discriminated in wells BD-02, BD-04 and BD-08 in the Badejo field. A) Peperites from Sequence 1 and Sequence 2 of BD-08 well. E) Interval with blocky peperite lithofacies. Details of A: B) Closed-packed peperite depth 3161.05, BD-08 well. C) Volcanic sandstone in contact with Peperite, depth 3163.00, BD-08 well. D) Closed-packed fluidal peperite depth 3163.53, BD-08 well. Details of E: F) blocky peperites, depth 3176.24, BD-0-02 well G) Pore-water steam explosion texture and H) Yellow arrow indicates amygdal inside the sediment I) Fluidal peperites as thin layers between lobs, depth 3164.92, BD-08 well. J) closed-packed fluidal peperites as thin layers between lobs depth 3191.99, BD-02 well. L) yellowish volcanic sandstone lithofacies (vS), depth 3088.85, BD-04 well. M) volcanic

green siltstone depth 3194.53, BD-02 well. N) Volcanic breccia lithofacies (vBr) from depth 3150.27, BD-02 well. cP: Closed-packed peperite. dP: disperse Peperite. bP: blocky Peperite. Seq. 1: Sequence 1. Seq. 2: Sequence 2.

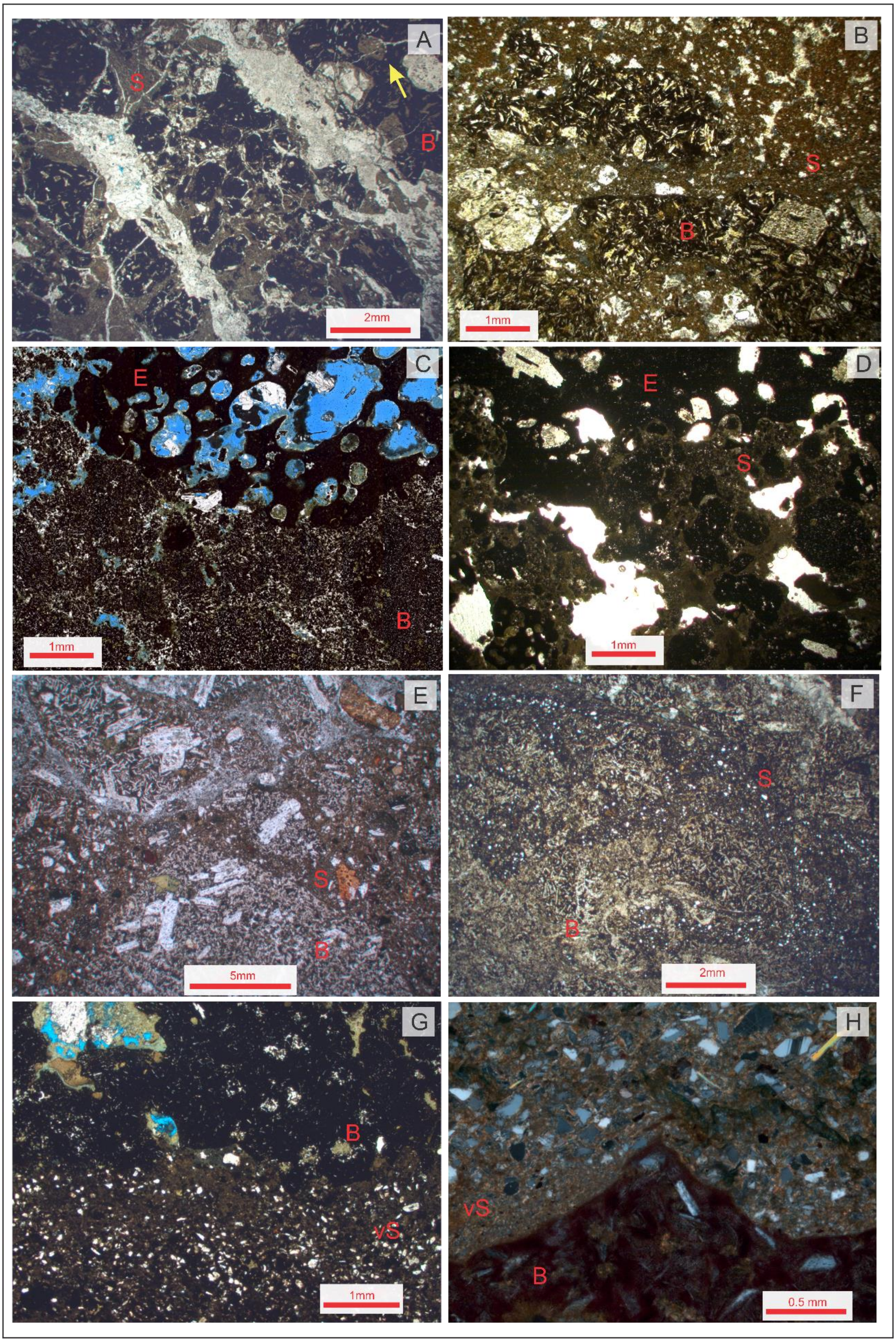

Figure 14: Photomicrographs from peperites and volcanogenic sedimentary lithofacies discriminated in wells BD-02, BD-04 and BD-08 in the Badejo field.

A) Fluidal peperite with irregular clasts, well BD-08. Yellow arrow – sediment inside the basalt. B) Closed-packed peperite with fluidal clasts, well BD-08. C) Closed-packed peperite, BD-08 well. D) Disperse peperite, BD-08 well. E) Volcanic breccia (vBr), BD-04 well. F) Blocky peperite with fluidal clast, BD-02 well. G) Volcanic sandstone (vS) from Sequence 1 in contact basalt from Sequence 2, BD-08 well. H) Volcanic sandstone (vS) in contact with Basalt, BD-04 well. B- Basalt, S- Sediment, E- Scoreaceus fragment. (A, B, D, E, F,G- // polarizers; H– X polarizers).

4.8 3D Geometries Classification

To extrapolate the information found in the wells and characterize correlated sequences within the Badejo field area, we sought to relate the characteristics of lithofacies association, and their thicknesses found in the wells with the 3D basin-scale geometries found in the literature. The classic architectural elements proposed for 3D geometries of subaerial basalt lava flows are tabular-classic flow, compound-braided flow and ponded flow (Nelson *et al.,* 2009a). The interval that comprises the thick of rubbly pahoehoe lithofacies associations, in wells BD-04 and BD-08, was interpreted as one tabular-classic flow (Sequence 2). In general, tabular-classic flows (Sequence 2) comprise tabular, laterally extensive thick flows (Figure 3B). Extensions of the latter can be as long as tens to hundreds of kilometers in basalt lava flows elsewhere (Jerram, 2002). The Classic pahoehoe lithofacies in the base of BD-08 association was interpreted as compound-braided flow (Sequence 1). The interval of Hummocky pahoehoe and low thinness sheet pahoehoe lithofacies association founded in BD-02 and BD-04 wells was interpreted also as compound-braided flow (Sequence 3). Compound-braided flows comprising thin anastamosing pahoehoe sheets and lobes up to several meters in thickness (Jerram, 2002). The summary of observation scales found in the Badejo area are summarized in the Figure 15.

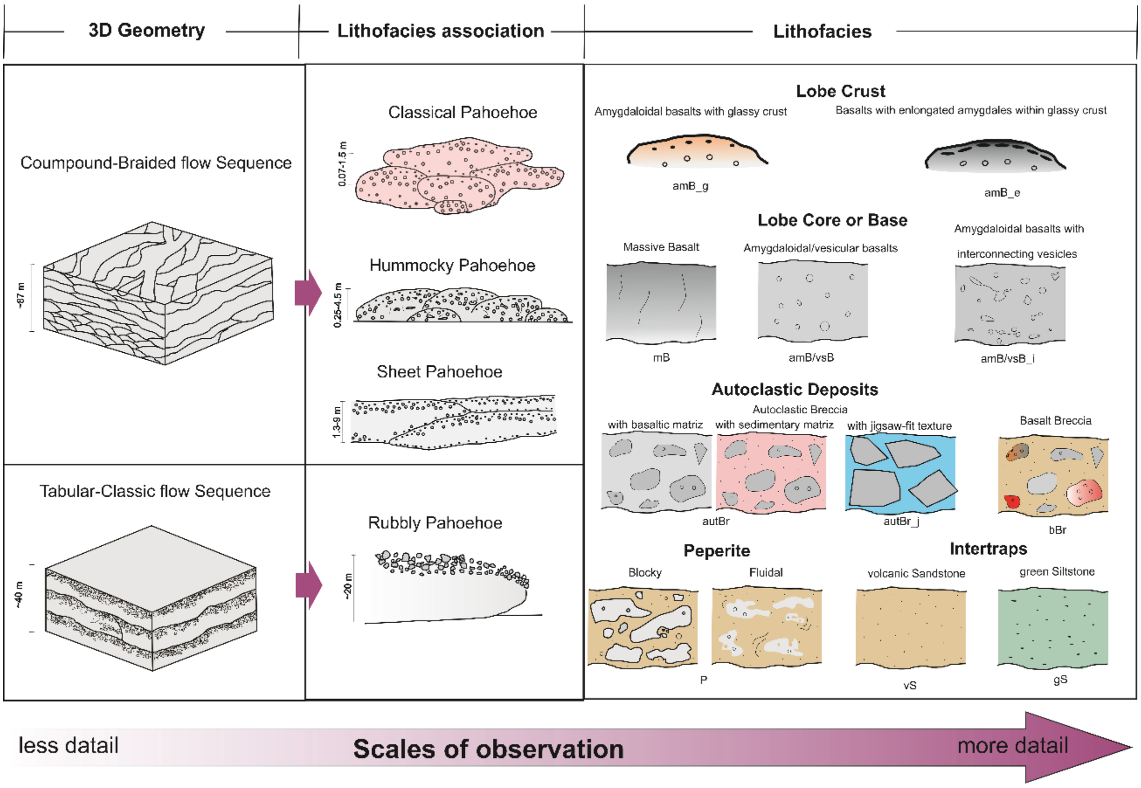

Figure 15: Typical scales of observation of subaerial basaltic lava flows in the Badejo field. A) Seismic facies. B) 3D geometries. C) Lithofacies associations. D) Discriminated lithofacies. Peperite lithofacies are blocky and fluidal.

4.9 Well core and respective facies

4.9.1 Well BD-02

This well is located at the north area of the Linguado field (Figure 6). Core was drilled between 3199.25 m and 3150 m with 22 m of recovered magmatic rocks. Only sequence 3 (compound-braided flow) is represented in this well. It comprises a series of lobes and toes from 0.15 m to 2.5 m in thickness (average 0.5 m) forming typical hummocky pahoehoe, as well as intervals of sheet pahoehoe lithofacies association (Figure 6). A 4 m-thick of blocky peperite (Figure 13E) and a 1 m thick volcanic breccia interbedded with sheet pahoehoe lava were also described (Figure 13N).

The hummocky pahoehoe occurs at different depths in well BD-02. At the bottommost lobes, amygdaloidal basalt/vesicular basalt lithofacies (amB/vsB)

(Figure 9D) and the amygdaloidal basalts with interconnecting vesicles (amB_i) (Figure 11F) displays grey and sometimes reddish color. Lobe crusts are formed by amygdaloidal basalts within glassy crust (amB_g) (Figure 9C and 11A) and basalts with enlongated amygdales within glassy crust (amB_e) lithofacies. The thickest lobes have amalgamated subcircular to elongated vuggy. A close-packed cm-thick peperite (P) lithofacies with fluidal fragments (Figure 13J) occurs at 3191.99 m above a sheet pahoehoe. Also, mm-thick layers of yellowish volcanic sandstone (vS) and volcanic greenish siltstone (gS) (Figure 13M) lithofacies can occur between lobes. Amygdales are strongly deformed, amalgamated and interconnected by vertical microfractures give a brecciated-like aspect at the middle of the core.

The sheet pahoehoe in well BD-02 occurs at 3191.75-3188.50 m, 3172.75-3169.00 m, 3154.75-3152.75 m and 3151.75-3150.25. The sheet pahoehoe at 3191.75-3188.50 m is greyish and comprise the amygdaloidal basalt/vesicular basalt lithofacies (amB/vsB) at the bottom with amygdales increasing in volume and size topwards. This lithofacies is overlain by massive basalt (mB) locally with calcite-infilled fractures. The lobe top and crust could not be observed. At 3172.75-3169.00 m, the distinguish lithofacies are the thick interval of amygdaloidal basalts with interconnecting vesicles (amB_i) lithofacies and the crust formed by amygdaloidal basalts within glassy crust (amB_g). Another two sheet pahoehoes occur at 3154.75-3150 m with interbedded volcanic breccia (vBr) lithofacies with 1 m and 0.25 m in thickness (bottom to top). The uppermost lobe lacks the top crust.

A peperite (P) lithofacies with blocky structure occurs at 3176.75-3172.75 m (Figure 13E, F,G,H and 14F) displaying subangular to angular clasts of greyish massive basalt (mB) with sparse amygdales are 0.1 cm to 50 cm long immersed into a fine-grained, yellowish volcanic sandstone. An evidence of pore-water steam explosions (Figure 13G) is locally seen and peperites present a coarsening upward structure at bottom-middle parts that gives place to fining upward grain size at the top (Figure 13E). Vesiculated sediments also occur in this interval (Figure 13H).

4.9.2 Well BD-04

This well is located at the center area of the Badejo field (Figure 6). Core was drilled between 3144.25 m and 3061 m with 83 m of recovered magmatic rocks. The well includes Sequence 2 (tabular-classic flow) and Sequence 3 (compound-braided flow). Sequence 2 comprises the top of an incomplete rubbly pahoehoe with 20 m in thickness. Sequence 3 consists of (from bottom to top) classical pahoehoe with 3.5 m in thickness of 0.07 m to 1.25 m-thick lobes and toes (average 0.25 m), as well as four intervals of *sheet pahoehoe* with 4 m, 3 m, 10 m and 8 m in thickness from base to top interbedded *with hummocky pahoehoe*. Sequence 3 finishes up with the deposition of 2 m-thick volcanic breccia (Figure 16).

Sequence 2 rubbly pahoehoe started with an autoclastic breccia with basaltic matrix (AutBr) lithofacies with 3 m in thickness occurs at the bottom rubbly pahoehoe in Sequence 2, displaying welded clasts of reddish basalt involved by a reddish basaltic matrix. Clasts become richer in vesicles to the top. A 9 m-thick, grey massive aphanitic basalt (mB) lithofacies covers the underlain autoclastic breccia, being strongly jointed (shorter at the base; longer at the top) and bearing cm-long autholits topwards. A 1 m-thick autoclastic breccia with basaltic matrix (autBr) lithofacies covers the massive basalt. It has a coarsening upward grain size, is grey in color and bears circular to subangular fragments of porphyritic basalt with fluidal terminations immersed in a microcrystalline matrix. Topwards, this autoclastic breccia lithofacies is succeeded by a 1.5 m-thick, massive basalt (mB) lithofacies with autholiths. Two layers of autoclastic breccia with basaltic matrix lithofacies (Figure 10D, 12E) with coarsening upward grain size, 2 m and 3.5 m in thickness, as well as an autoclastic breccia (autBr) lithofacies with a reddish volcanic sandstone matrix at the very top (Figure 10C, 12F), complete Sequence 2 in well BD-04.

The classical pahoehoe in Sequence 3 comprises reddish amygdaloidal basalt (amB) lithofacies with circular to subcircular vesicles with 0.1 to 0.5 cm in size. Toes predominate at the bottom and lobes at the top. Lobes are formed by amygdaloidal basalt with glassy crust (amB g) lithofacies. Yellowish, mm-thick volcanic sandstone (vS) lithofacies occurs between toes but the former shows no interaction with the latter.

The sheet pahoehoe in Sequence 3 occurs at 3117.75-3113.25 m, 3111.5-3108.5 m, 3087-3077,25 m and 3072.5- 3064.5 m. The sheet pahoehoe at 3191.75-3188.50 m is greyish and comprise greyish amygdaloidal basalt/vesicular basalt (amB/vsB) lithofacies with circular to subcircular vesicles at the bottom, massive basalt (mB) lithofacies at the center and amygdaloidal basalt/vesicular basalt (amB/vsB) lithofacies with circular to subcircular amygdales that amalgamate topwards. The crust is formed by amygdaloidal basalt with elongated amygdales within glassy crust (amB_e) lithofacies. The sheet pahoehoe at 3111.5-3108.5 m is similar to the preceding one but with a thinner crust. Greyish amygdaloidal basalt/vesicular basalt (amB/vsB) (Figure 10B), massive basalt (mB) (Figure 10A, 12C) and breccia-like amygdaloidal basalt (amB/vsB) lithofacies form respectively the bottom, center and crust of the sheet pahoehoe at 3087-3077.25 m. Finally, the sheet pahoehoe at 3072.5-3064.5 m comprises amygdaloidal basalt (amB) lithofacies at the bottom, greyish massive basalt (mB) at the center whereas the top portion comprises a transition from amygdaloidal to more vesicular basalts (amB/vsB) and, at the uppermost part, reddish amygdaloidal basalts with interconnecting vesicles (amB_i). The crust is formed by amygdaloidal basalts with glassy crust (amB_g).

The hummocky pahoehoe in Sequence 3 comprises amygdaloidal basalt/vesicular (amB/vsB) and amygdaloidal basalt with interconnecting vesicles (amB_i) lithofacies with a predominated lithofacies crust formed by basalts with elongated amygdales within glassy crust (amB_e) (Figure 12B). Oil occurs in both amygdaloidal basalt/vesicular basalt and basalt with elongated amygdales lithofacies (Figure 9E) around the depth 3108.50 m. The thickest lobes have amalgamated subcircular to elongated vug and seems to be more fractured and with more vesicles than the BD-02 well. A cm-thick, yellowish volcanic sandstone (vS) lithofacies (Figure 13L, 13H) occur right below a reddish amygdaloidal basalt (amB) lithofacies. A mm-thick peperite (P) lithofacies also occurs. At the last hummocky pahoehoe lobes, lithofacies comprehend vesicular basalt (vsB), reddish amygdaloidal basalt with interconnecting vesicles (amB_i) lithofacies and a crust with reddish amygdaloidal basalt with glassy crust (amB_g). Similar to those in well BD-2, a polymitic volcanic breccia (vBr) occurs (Figure 8E) ending the core section.

4.9.3 Well BD-08

This well is located at the north area of the Badejo field (Figure 6). Core was drilled between 3140 m and 3169 m with 29 m of recovered magmatic rocks. Sequence 1 (compound-braided flow) and Sequence 2 (tabular-classic flow) were identified in this well core. Sequence 1 comprises a series of lobes and toes from 0.25 m to 2.5 m in thickness (average 0.5 m) forming classical pahoehoe morphology and Sequence 2 comprises an incomplete sequence of rubbly pahoehoe with 20.75 m in thickness (Figure 16).

A classical pahoehoe lithofacies association with 7 m is formed by amygdaloidal basalt/vesicular basalt (amB/vsB) lithofacies (Figure 9B) with aphanitic, reddish matrix involving moderate amounts of medium-grained plagioclase and pyroxene phenocrysts (Figure 11C, D), as well as thin intervals with massive, porphyritic basalt (mB) lithofacies. The top of the lobes also presents a yellowish color with decreasing size of the amygdales towards the top, indicating the presence of a cooling border (amB_g). Vesicles are circular to subcircular and 0.5 cm to 1 cm in size. Four millimetric to centimetric layers of peperite (P) lithofacies with fluidal structure comprising small (0.2-2 mm) fragments of basalt within a greenish matrix of siltite occur between lobes (Figure 13I, 14A). Sequence 1 ends up with a peperite (P) lithofacies (Figure 13A) with irregular, fluidal-shaped clasts of amygdaloidal reddish basalt from the lower lobe giving rise to a close-packed structure at the base (Figure 13D, 14B), and towards the top, a volcanic reddish sandstone (vS) prevails (Figure 13C, 14G).

A dispersed peperite (P) lithofacies occur at the bottom of a rubbly pahoehoe formed by greenish siltstone matrix with scoreaceus clasts. The siltstone matrix (Figure 14D) becomes less frequent (Figure 14) topwards where the peperite (P) lithofacies acquires a closed-packed structure (Figure 13B). A 20 m-thick, massive, aphanitic gray basalt (mB) covers the underlain peperite, having autholithic scoria basalt clasts at the base. Locally, it has thin, horizontal dark gray foliation (associated with differences in microlites sizes and compositions) (Figure 10F and 12A, B) and becomes strongly fractured in some intervals, being poorly recovered by the well core sampling. Clast-supported, monolithic, autoclastic breccia (autBr_j) lithofacies (Figure 10E) with angular clasts of massive basalt in a jigsaw arrangement is also seen in Sequence 2. The classification as a rubbly pahoehoe is due the microcrystalline fine-grained matrix of the massive basalts, not being possible to identify the typical broken crust. On this basis, it is estimated that the rubbly pahoehoe flow might have been thicker due to the absence of autoclastic breccia lithofacies or even autoliths.

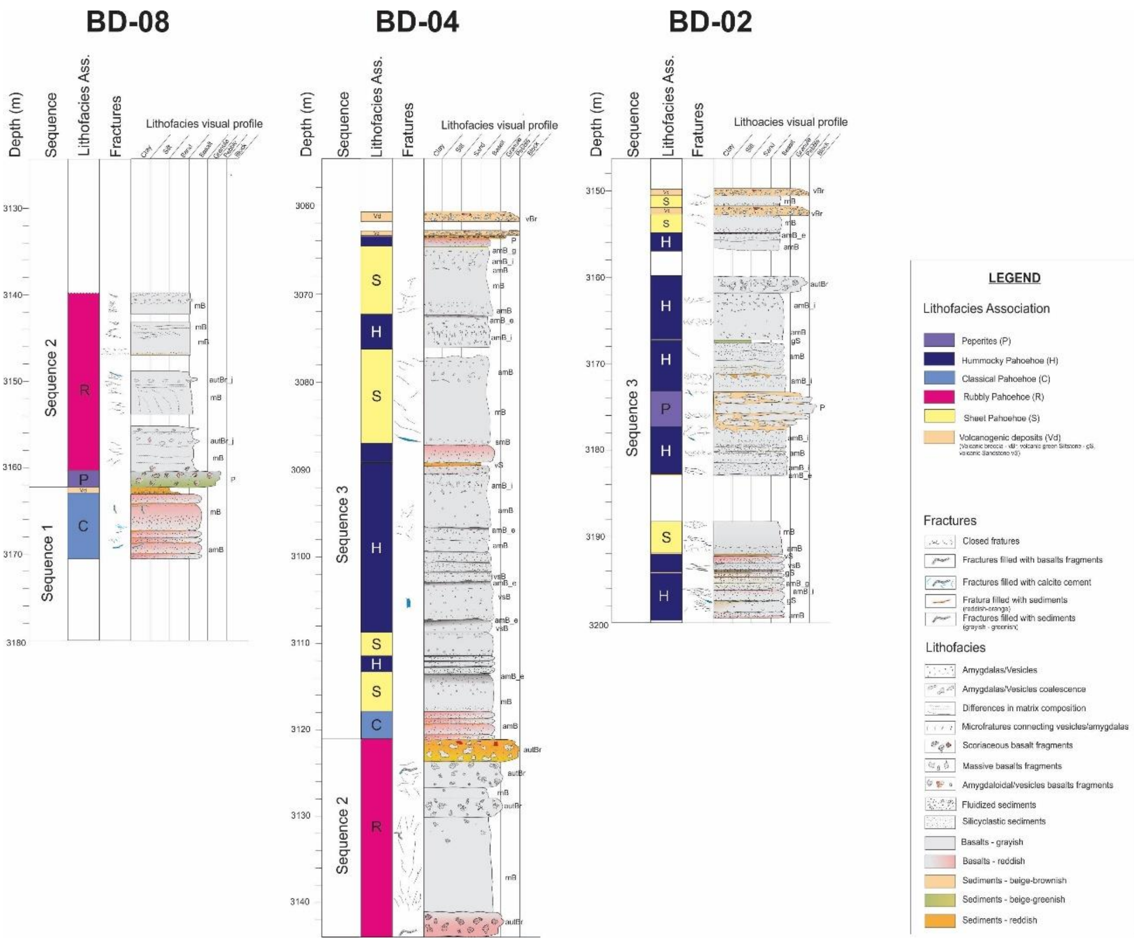

Figure 16: Main stratigraphic features in wells BD-02, BD-04 e BD-08 in the Badejo field.

4.10 Lithogeochemistry

Nine samples were selected from well BD-02 (from 3,153.55 m to 3,198.49 m), seven from well BD-04 (from 3,066.07 m to 3,143.88 m) and four from well BD-08 (from 3,149.48 to 3165.90 m) for lithogeochemical analyses (Table 3). Samples were crushed, cleaned and then reduced to power in a WC mill. The selected samples were analyzed for major and trace elements (including the earth rare elements; REE). Major and trace elements were measured from fused samples by ICP-AES and ICP-MS, respectively. The loss on ignition (LOI) was measured by weight differences after heating at 1,100 - 1,200 °C during 2 hours and total iron was measured as ferric iron ($Fe_2O_3^t$). Detection limits were below 0.01 wt.% for major elements and 2 ppm for trace elements (except Ni and Cr; 20 ppm). Detection limits for the REE were below chondritic values. Accuracy values for major elements varied from 0,6% to 3.3 % (except for P_2O_5; 7%) and were below 9% for the REE and other trace elements (except Th and Zr; 12%). Precision values were below 1% and 3% for major and trace elements, respectively (except for Er (4%) and Hf (6%)). Values obtained for Ta were discharged due to possible contamination during comminution in a WC mill.

Samples represent relatively evolved basalts (4.63 < MgO < 6.56; 5.51 ± 0.44 wt.%; Ni < 110 ppm, Cr < 220 ppm) with LOI values ranging from 2.32 wt.% to 7.02 wt.% (except for sample BD-4-3130,23; 10.16 wt.%), the highest values being attributed to alteration. No coherent variations of major and trace element contents with depth were observed along the three studied wells.

Samples straddle the thermal divide in the total alkalis *versus* silica (TAS) diagram (Figure 17A) but comprise a coherent, subalkaline (Nb/Y < 1; Figure 12B), low-TiO_2 (0.76 < TiO_2 < 1.57 wt.%; average Ti/Y = 290) basaltic suite with tholeiitic affinity (normative hypersthene = 9.5 ± 3.8 wt.% combined with either normative quartz or normative olivine). Sample BD-4-3130,23 displays normative nepheline due to its high LOI content (10.16 wt.%).

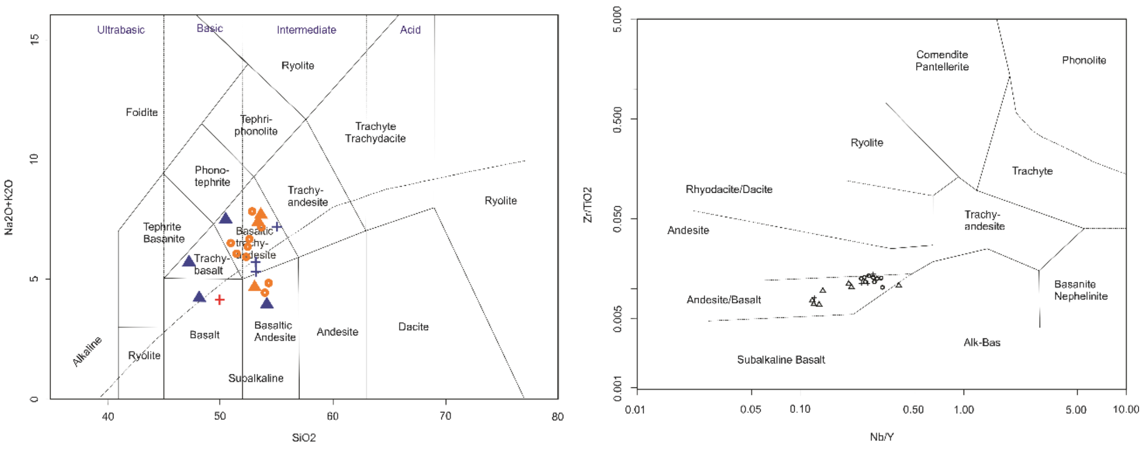

Figure 17: Classification diagrams for selected samples from the studied lithofacies discriminated in wells BD-02 (circles), BD-04 (triangles) and BD-08 (crosses) in the Badejo Field, Campos Basin. Sequence 1 (red), Sequence 2 (blue), Sequence 3 (orange). A) - Samples plotted in the TAS diagram (LeMaitre et al., 2002). Data recalculated to 100% on a volatile-free basis. Oxides in wt.%. Boundary curve between the alkaline and subalkaline fields from Irvine & Baragar (1971). B) - Samples plotted in the classification diagram using immobile trace element ratios (Winchester & Floyd, 1977).

The lithogeochemical data of samples from the three wells are dispersed in variation diagrams for major elements and immobile trace elements (Ti, Y, Nb and Zr) indicating that samples do not represent basaltic magmas cogenetic by differentiation processes. The same applies when samples from individual wells are plotted in variation diagrams. Patterns in the chrondrite-normalized REE diagrams also cannot be explained by differentiation processes as depicted by the La/Yb_n ratios of the least, intermediate and more evolved compositions in wells BD-02, BD-04 and BD-08 (Figure 18 A-C). In addition, the La/Yb_n ratios of the least evolved samples with similar MgO contents in the three wells spread over a wide range, from 1.4 (BD-04), 3.5 (BD-08) to 8.7 (BD-2) with the Nb troughs in normalized-multielement diagrams typical of continental flood basalts (Figure 18D). The different La/Yb_n ratios resulted from either contamination processes in magma chambers located in the upper crust or, more likely, partial melting processes involving different mantle sources and/or components with at least a contribution from the enriched subcontinental lithospheric mantle.

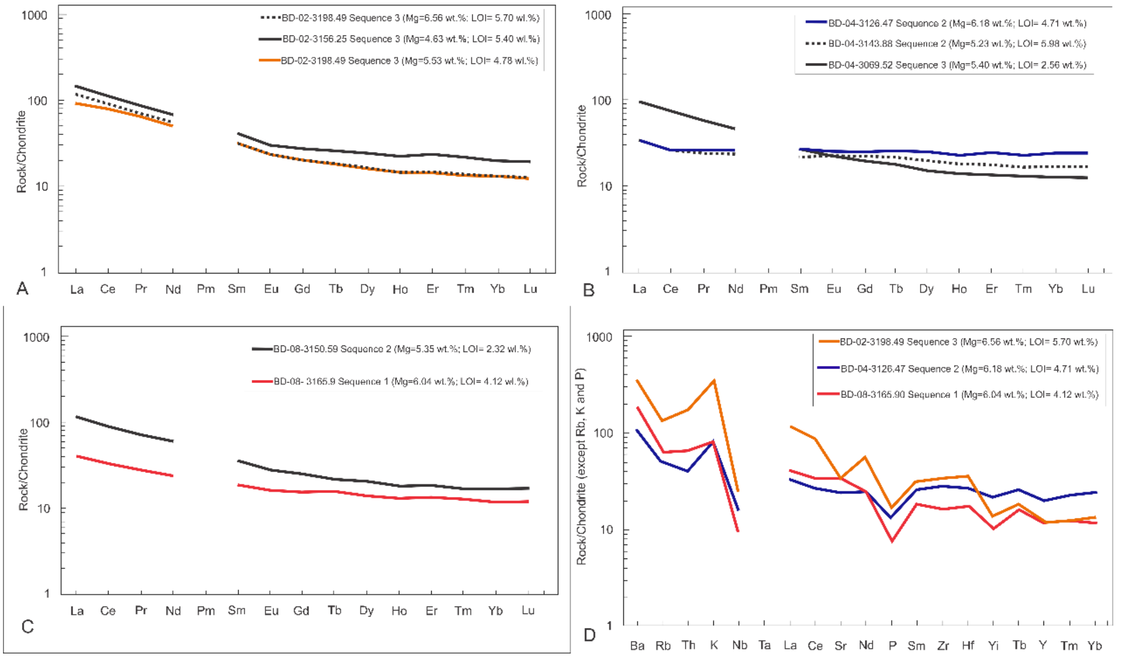

Figure 18: Chrondrite-normalized REE diagrams with samples representing the least, intermediate and more evolved basaltic compositions of the studied wells. A) well BD-02, B) well BD-04 and C) well BD-08. Normalization factors from McDonough & Sun (1995). D) Normalized multielement diagram with samples representing the least evolved basaltic compositions in wells BD-02, BD-04 and BD-08. Normalization factors from McDonough & Sun (1995) with Rb, K and P from Thompson (1982).

Table 3: Lithogeochemical data of samples from wells BD-02, BD-04 and BD-08 in Campos Basin. LOI is loss on ignition. Fe2O3t is total iron as ferric iron. Oxides and LOI in wt.% and elements in ppm. bdl is below detection level.

Sequence	3									3			2				2			1
Sample	BD-02 3153,55	BD-02 3153,92	BD-02 3156,25	BD-02 3172,50	BD-02 3173,85	BD-02 3188,82	BD-02 3189,09	BD-02 3190,76	BD-02 3198,49	BD-04 3066,07	BD-04 3069,52	BD-04 3075,22	BD-04 3126,47	BD-04 3130,23	BD-04 3134,7	BD-04 3143,88	BD-08 3149,48	BD-08 3150,59	BD-08 3153,13	BD-08 3165,9
Major elements (wt%)																				
SiO2	48.98	50.26	50.59	50.4	47.55	52.42	52.67	50.17	50.1	50.05	51.04	49.86	46.05	41.79	51.16	47.1	53.23	51.95	51.58	47.7
TiO2	1.154	1.118	1.185	1.18	1.004	1.042	1.028	1.044	0.992	1.05	0.909	1.037	1.572	1.303	1.413	1.51	1.155	1.166	1.172	0.757
Al2O3	15.45	16.29	15.51	15.54	14.8	15.39	15.48	16.67	15.17	15.49	15.56	15.23	13.8	11.51	12.43	13.44	14.23	14.9	14.82	17.08
Fe2O3(T)	10.58	10.34	9.43	10.76	10.63	9.94	9.55	9.68	9.84	10.04	9.15	10.28	14.83	11.32	12.58	13.3	9.88	10.05	9.86	9.8
MnO	0.274	0.186	0.091	0.206	0.203	0.228	0.238	0.166	0.203	0.082	0.126	0.083	0.189	0.156	0.127	0.144	0.147	0.167	0.167	0.126
MgO	5.42	5.65	4.63	5.67	5.64	4.86	5.02	5.53	6.56	5.39	5.4	5.75	6.18	5.33	5.33	5.23	5.6	5.35	5.6	6.04
CaO	7.33	5.02	5.84	6.07	7.3	8.77	8.09	6.73	4.3	4.45	9.41	3.41	8.74	11.85	7.56	5.37	5.87	9.06	9.15	10.61
Na2O	3	3.27	3.54	3.03	2.81	2.62	2.58	2.93	2.54	3.18	2.55	3.46	2.94	3.1	2.52	3.64	4.65	3.46	3.22	2.69
K2O	2.77	3.12	3.21	3.08	3.27	1.71	2.14	2.75	4.89	3.76	1.95	3.7	1.11	1.97	1.21	3.38	2.2	2.04	1.85	1.16
P2O5	0.19	0.18	0.31	0.2	0.18	0.17	0.16	0.17	0.17	0.2	0.09	0.17	0.14	0.1	0.12	0.11	0.2	0.18	0.19	0.08
LOI	4.99	4.95	5.4	4.4	7.02	2.77	3.52	4.78	5.7	5.71	2.56	6.32	4.71	10.16	4.02	5.98	2.86	2.32	2.79	4.12
Total	100.138	100.384	99.736	100.536	100.407	99.92	100.476	100.62	100.465	99.402	98.745	99.3	100.261	98.589	98.47	99.204	100.022	100.643	100.399	100.163
Minor elements (ppm)																				
Ni	60	60	50	60	60	60	60	60	70	70	80	60	70	60	60	60	60	70	70	110
Cr	60	60	50	60	60	80	80	80	90	140	150	150	80	70	70	60	220	220	220	120
Sc	35	34	35	37	34	34	33	35	35	38	35	40	50	39	44	45	44	42	43	35
Co	34	38	32	36	35	33	33	33	36	36	37	36	47	39	43	44	31	36	36	45
V	295	268	262	306	257	274	259	266	257	239	200	264	440	380	419	376	315	310	286	229
Ba	691	773	981	662	674	493	512	543	851	1346	496	1508	272	565	262	810	522	526	519	437
Rb	35	36	36	32	31	26	28	28	47	39	53	37	18	25	28	37	39	35	26	22

Sr	363	296	361	292	334	302	294	315	261	317	316	279	180	172	169	162	196	279	298	243
Y	27.9	23.9	31.4	24.3	22.8	22.9	24.7	19.3	19.6	27.5	20.5	12.7	31.4	27.5	26.1	26.3	21.8	25.8	23.4	18.2
Zr	150	130	150	148	116	133	137	108	127	118	96	112	110	100	99	144	160	132	134	61
Nb	6.8	6.7	7.4	7.1	5.7	6.4	6.5	6.1	6.1	5.4	4.2	5.1	3.8	3.3	3.4	3.6	6.1	6.1	6	2.2
La	28.3	28.1	34.5	29.8	28.7	27.4	27.5	22.3	27.9	27.9	23.3	20.9	8.16	8.37	7.4	8.77	28.2	27.5	27.6	9.75
Ce	61.1	61.5	66.7	62.4	58.2	56.4	61	49	55.4	54.1	46.6	41.6	16.8	17.5	15.7	16	54.9	56.3	56.6	20.7
Pr	7.6	7.48	7.85	7.38	6.86	6.84	7.21	6.02	6.53	6.32	5.5	5.01	2.51	2.43	2.25	2.31	6.59	6.86	6.82	2.64
Nd	29.7	28.8	30.4	29.6	27.3	26.4	27	23.4	25.5	25.5	21.7	19.4	12.1	11.3	11.1	11	25.9	27.8	27	11.1
Sm	5.9	5.53	5.91	5.8	5.12	4.99	5.24	4.63	4.72	5	4.23	3.75	3.98	3.46	3.24	3.3	4.86	5.36	5.38	2.76
Eu	1.69	1.58	1.64	1.61	1.46	1.48	1.49	1.38	1.33	1.68	1.31	1.2	1.46	1.27	1.25	1.25	1.33	1.59	1.62	0.917
Gd	5.25	5.02	5.45	5.16	4.59	4.68	4.87	4.09	4.15	4.94	4.11	3.28	5.06	4.4	4.51	4.55	4.69	5.05	4.91	3.1
Tb	0.85	0.8	0.92	0.82	0.72	0.74	0.77	0.67	0.68	0.82	0.65	0.5	0.96	0.81	0.81	0.79	0.74	0.81	0.79	0.58
Dy	5.34	4.92	5.94	5	4.59	4.58	4.9	4.05	4.14	5.31	3.9	3	6.34	5.36	5.22	4.94	4.43	5.15	4.83	3.53
Ho	1.06	0.97	1.25	0.98	0.92	0.91	0.94	0.8	0.82	1.08	0.78	0.59	1.3	1.09	1.07	1	0.87	1	0.96	0.72
Er	3.23	2.8	3.74	2.89	2.7	2.69	2.86	2.39	2.42	3.36	2.27	1.69	3.98	3.24	3.17	2.94	2.59	3.04	2.83	2.17
Tm	0.47	0.397	0.54	0.405	0.398	0.383	0.383	0.349	0.338	0.472	0.333	0.262	0.579	0.458	0.471	0.416	0.37	0.422	0.412	0.312
Yb	3.03	2.42	3.22	2.63	2.57	2.47	2.56	2.21	2.18	2.97	2.14	1.79	3.91	3.16	3.12	2.8	2.5	2.75	2.74	1.91
Lu	0.454	0.342	0.477	0.402	0.38	0.355	0.382	0.311	0.314	0.41	0.314	0.274	0.607	0.464	0.483	0.425	0.389	0.418	0.419	0.296
Hf	4	3.9	4	4.2	3.7	3.6	3.8	3.5	3.7	3.4	2.4	3.5	2.9	2.5	2.6	2.7	3.5	3.5	3.5	1.8
Th	6.74	4.24	12.2	5.94	4.25	5.12	4.85	2.24	4.94	6.76	3.1	1.84	1.18	0.91	1.14	1.32	4.14	4	3.52	1.87
U	0.18	0.68	4.1	0.59	0.77	0.67	1.4	0.48	0.27	0.87	0.16	1.79	0.37	0.37	0.64	0.44	0.5	0.37	0.31	0.22
Pb	7	9	9	7	6	8	7	7	5									6	6	

4.11 Physical Parameters

4.11.1 Effusion rates

One of the most important controlling parameters of the lava morphology is the effusion rate, along with topography (Hon *et al*., 1994). In this work, the thickness of the lobes was measured between two glassy layers and depth can be taken as a measure of time. Rubbly pahoehoes in tabular-classic geometries, such as those described in Sequence 2 in wells BD-04 and BD-08, are associated with high effusion rates (up to 10^6 m^3/s), preventing the formation of toes and small lobes. New pulses of lava and increasing yield strength may lead to fragmentation of the crust of the flow (Duraiswami *et al*., 2008).

Effusion rates for the compound braided Sequence 1 in well BD-08 and Sequence 3 in wells BD-02 and BD-04 were qualitatively estimated based on the thickness of the lobes (Figure 19). Interpretations did not consider possible topographic controls although the more tabular and inflated flows of Sequence 3 above the rubbly pahoehoe lavas are likely to have travelled over a flat topography similar to extensive ones inflated sheet pahoehoe flows (Hon *et al.*, 1994).

Sequence 1 in well BD-08 comprises classical pahoehoe with small variations (< 1 m) in lobe widths that become greater towards the top where it gets in contact with Sequence 2 (Figure 19C). Sequence 1 in well BD-08 may be related to continuous, low effusion rates which are typically found in classical pahoehoe lavas, leading to quick cooling and stacking of small lobes (Self *et al.*, 1998). A more detailed interpretation is, however, prevented by the thin thickness (~ 8 m) of Sequence 1 in well BD-08.

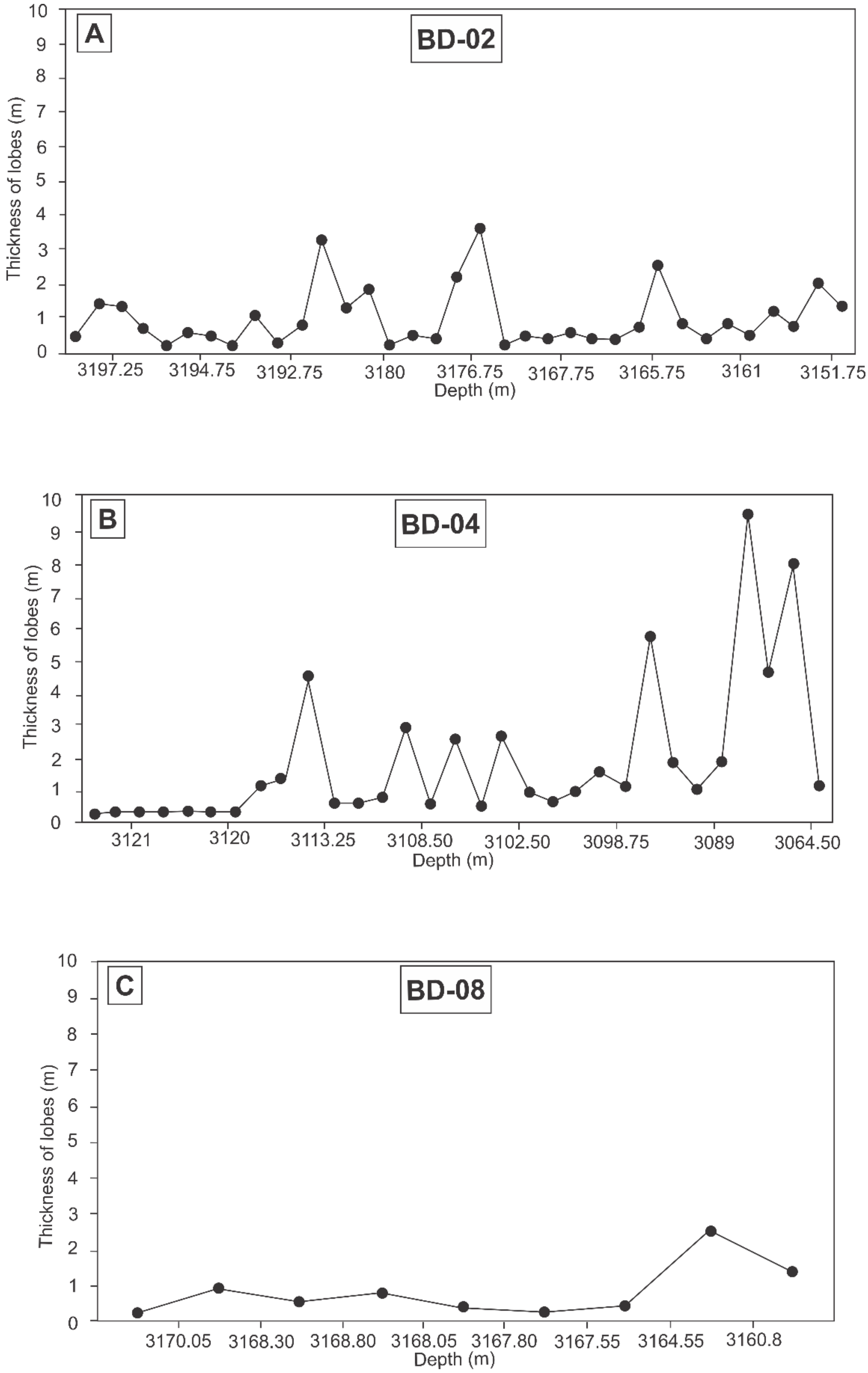

Figure 19: Diagrams depth (m) versus lobe width (m). (A) - Sequence 3 in well BD-02. (B) - Sequence 3 in well BD-04. (C) - Sequence 1 in well BD-08.

Lobe widths in the hummocky pahoehoe in Sequence 3 of well BD-02 are thinner than 1 m but may reach 2.5 m in the interlayered sheet pahoehoes in the central parts of the sequence (Figure 19A). On the other hand, lobes of the hummocky pahoehoes in Sequence 3 of well BD-04 increase topwards and reach 9 m in the sheet pahoehoes at the top of the sequence (Figure 19B). Hummocky pahoehoe lavas are related with inflation and thickening of a vesiculate crust under moderate effusion rates. Inflation is restricted to the tumuli whereas the lava flows continuously through breakouts (Self *et al.*, 1998). The flow may become more tortuous away from the emission centers due to topographic unevenness (Walker, 1991; Hon *et al.* 1994; Duraiswami *et al.*, 2004). On the other hand, the higher effusion rates of the sheet pahoehoe lavas may result in inflation that gives rise to thick lava units (Walker, 1971; Self *et al*., 1997). If high effusion rates are kept constant along time, lava channels will remain open (Self *et al.*, 1998). As such, effusion rates may have been rather low during the formation of the classical pahoehoes at the bottom of Sequence 3 in well BD-04, becoming more variable towards the sheet and hummocky pahoehoes at the top of the sequence (Figure 19). Overall, Sequence 3 seems to be related to an oscillation of supply rates or a discontinuous inflation called as pulsed inflation (Duraiswami, 2009).

4.11.2 Extension of lava flows

The extension of lava flows is dependent of various physical parameters such as viscosity, total volume and effusion rates of the lavas, topographic evenness and the presence of valleys and plains, presence of water pools and climate (Walker, 1973).

The appraisal of the areas covered by the sheet pahoehoe and rubbly lava flows around the studied wells was done on the basis of the aspect ratio correlations (Walker, 1973). No estimative was done for hummocky and classical pahoehoe lavas because these morphologies are characterized by small, short lobes, even in the case of thicker flow units. Two simple equations were obtained for the aspect ratios

50 (y = 20x) and 100 (y = 12.5x), assumed to be the typical interval for low viscosity, basaltic lavas and H values were obtained from them using the values of thickness of the flows (Figure 20). The area covered by the lava flows was calculated considering a circle with a *radius* equal to half of H value. The results are shown on Table 4.

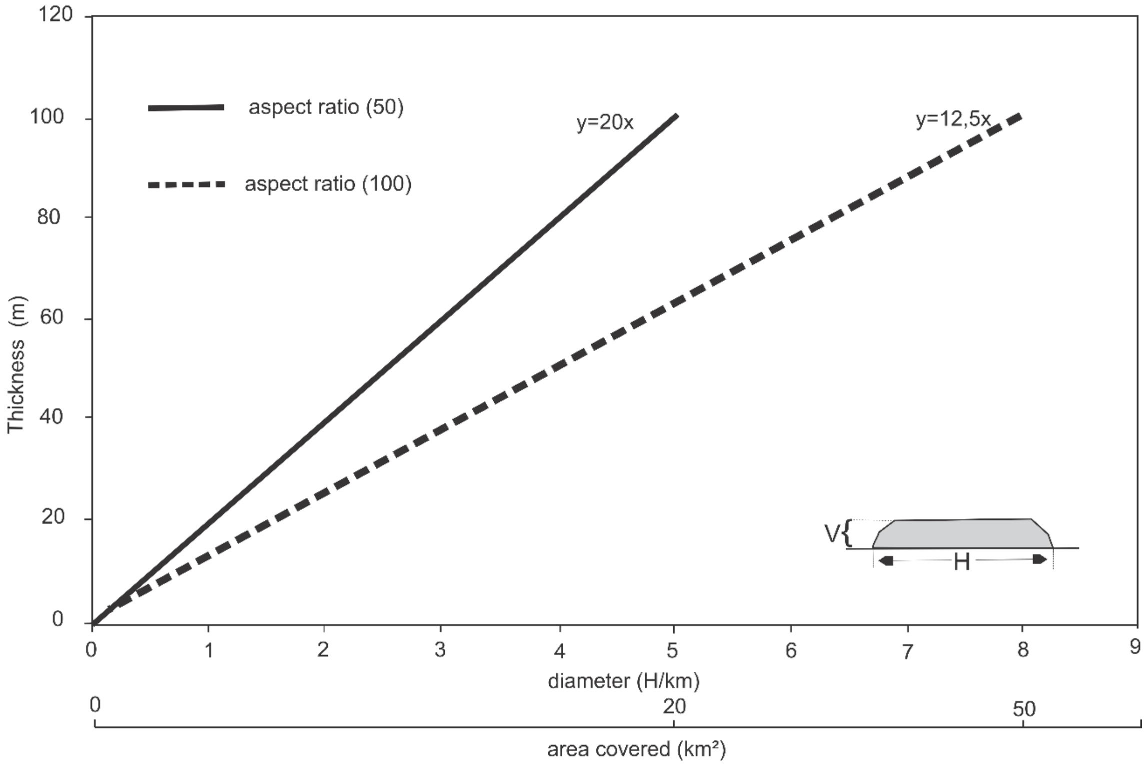

Figure 20: Correlation between thickness and area covered by lavas for aspect ratios 50 and 100 (Walker, 1973). H= ratio of the horizontal extent, V= thickness.

Table 4: Estimative values of surface area covered by rubbly and sheet pahoehoe lavas in wells BD-02, BD-04 and BD-08 in the Badejo field, Campos Basin. The lavas with stars are incomplete.

Well	Litofacies association	Thickness	Aspect ratio (50)		Aspect ratio (100)	
			Diameter (km)	Area covered (Km²)	Diameter (km)	Area covered (km²)
BD-08	Rubbly pahoehoe	20.75*	1.04	0.85	1.66	2.16
BD-04	Rubbly pahoehoe	20.00	1.00	0.79	1.60	2.01
	Sheet pahoehoe	4.50	0.23	0.04	0.36	0.10
		3.00	0.15	0.02	0.24	0.05

		9.75	0.49	0.19	0.78	0.48
		8.00	0.40	0.10	0.64	0.25
		3.50*	0.18	0.02	0.28	0.06
BD-02	Sheet pahoehoe	3.75	0.19	0.03	0.30	0.07
		2.00	0.10	0.01	0.16	0.02

The rubbly pahoehoe lavas in BD-08 and BD-04 wells cover the largest area (0.79 - 2.16 km^2) that may be even greater since the BD-08 well did not sample the vesiculated crust of the flow. Individual pahoehoe lava flows in wells BD-04 and BD-02 cover small areas (< 0.5 km^2). The diameters (H) of the sheet pahoehoe lavas in wells BD-02 and BD-04 are comparable to values measured in Columbia River, where the 9 m-thick lobes of Devils Canyon, the 12 m-thick lobes of FSCS and the 13 m-thick lobes of Jasper Canyon are shorter than 1.0 km (Vye-Brown, 2013). Total extensions of rubbly pahoehoe lavas are more difficult to find in the literature.

4.11.3 Timing

The time (t) related with the accumulation of Kilauea pahoehoe lavas due to inflation can be estimated by $t\ (h) = 164{,}8.H^2$, where H is the thickness of the vesiculated crust (Hon *et al.* 1994). Results are shown in Table 5.

Table 5: Estimative values for time of accumulation of sheet pahoehoe lavas by inflation in wells BD-02 and BD-04 in the Badejo field, Campos Basin.

Well	Litofacies association	Crust thickness	Emplacement duration		
			(hours)	(months)	Sequence 3 (months)
BD-04	*Sheet pahoehoe*	3.00	1483.20	2.06	7.14
		0.75	92.70	0.13	
		3.75	2317.50	3.22	
		2.75	1246.30	1.73	
BD-02	Sheet pahoehoe	3.75	2317.50	3.22	3.28

In well BD-02 well, the minimum emplacement duration is estimated in 3 months for Sequence 3, approximately, despite the fact it records an incomplete lobe. On the other hand, sheet pahoehoe lava flows are well preserved in Sequence 3 of well BD-04. The duration of the eruptive process of lavas of BD-04 is estimated in nearly 7 months. However, the estimated time probably represent a rough approximation to minimum values, since the deposition of the intertrap sedimentary sequences, the formation of volcanic breccias and of the other lithofacies associations were not taken into consideration. Another drawback may be related with the sampling since the measured thickness may be related with flow terminations.

4.11.4 D parameter

The formation of different lava morphologies depends on various parameters, such as viscosity, rate of crust growth and local shear rate. The local shear rate is, in turn, related with lava flow velocity. For instance, classical pahoehoe is typically related with low viscosity, basaltic lava flows with low shear rates (Figure 9). On the other hand, Aa lavas are related with higher viscosities with flows under high shear rates (Gregg, 2017).

The appraisal of strain rates in transitional (classical to slabby pahoehoe) lava flows can be done based on the analysis of vesicle deformation (D parameter) (Duraiswami *et al.*, 2003). The D parameter is expressed by D = (l - b)/(l + b), where b is the vesicle length and l is its width (Taylor, 1934). Five categories of vesicle shapes found in the thin sections of wells BD-02, BD-04 and BD-08 were associated with D parameters from classical and hummocky pahoehoe obtained by the thin sections descriptions were compared with vug porosity values (Figure 8). Interpretations related with the sheet pahoehoe in Sequence 3 must be done with care because the formation of their vesicles are likely to result from the growth and rise of gas bubbles in cooling lavas rather than the result of dynamic conditions such as flow movement or convection (Aubele *et al.* 1988). Besides, strain partitioning within the flow and variation in emplacement can produce very high to medium values of vesicles deformation (Duraiswami *et al.* 2014).

The values of the D parameter for Sequence 1 in well BD-08 are very low or low, rarely intermediate, implying low and constant strain rate for the emplacement of the classical pahoehoe lavas. Values of the D parameter for the classical pahoehoe in Sequence 3 of well BD-04 are also low, but vary greatly in the hummocky pahoehoe interval, implying emplacement under higher strain rates for the latter (Figure 21). In general, D values for hummocky lavas are higher than those for classical pahoehoe lavas. Porosity is minimum for massive basalts. Vuggy porosity and D values tend to increase coherently for hummocky lavas in the three wells. Nevertheless, classical pahoehoe bear high vug porosity values but low D values. Porosities are almost equal for classical and hummocky lithofacies association, but it can be estimated that hummocky pahoehoe may present higher permeability values due to deformation and connection among vesicles.

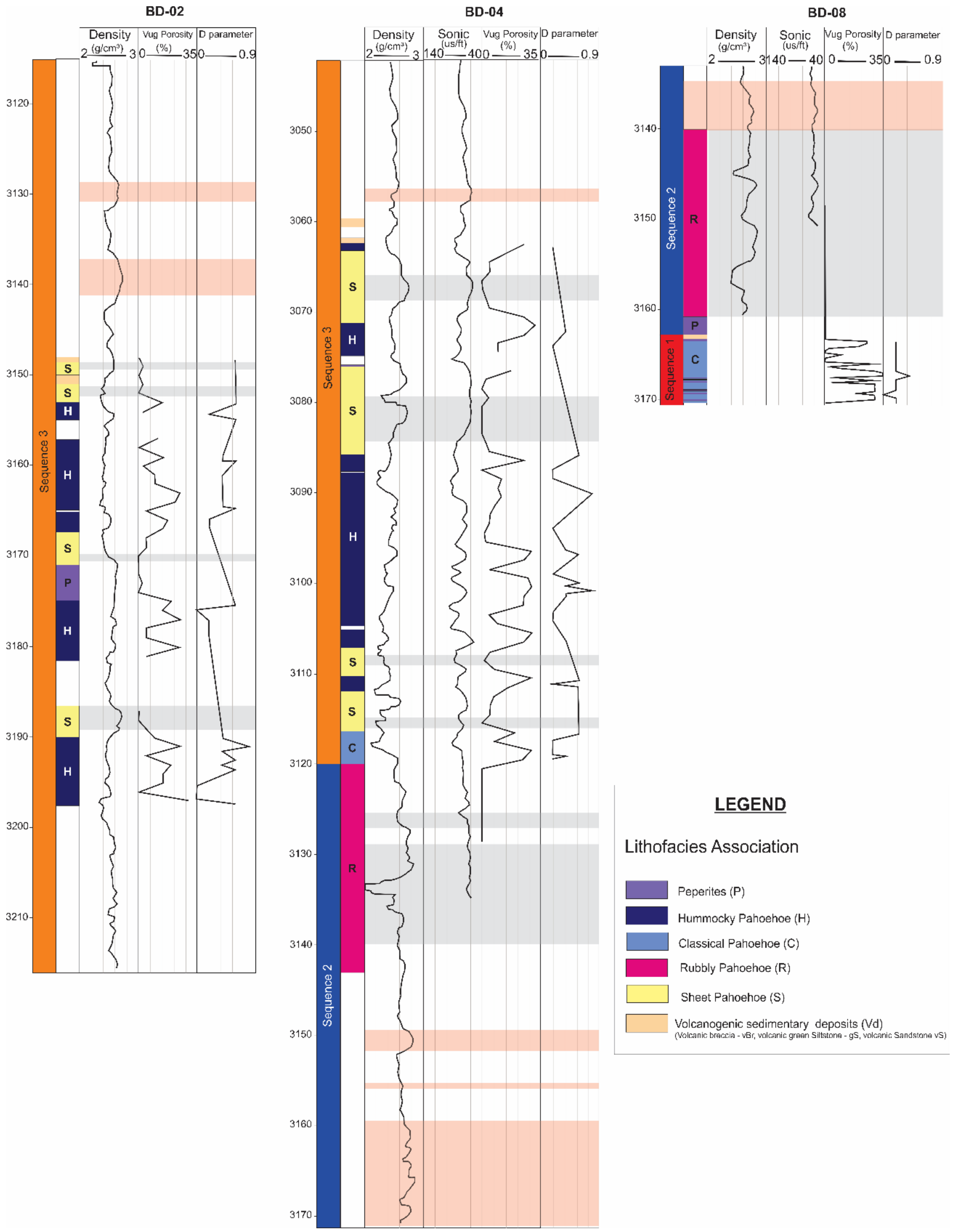

Figure 21: Density log, Sonic log, Vug porosity and D parameter for wells BD-02, BD-04 e BD-08. Greyish areas correspond to massive basalts lithofacies described in the cores and reddish areas correspond to massive basalts lithofacies interpreted using density and sonic logs. The parameter D values founded for the classical and hummocky pahoehoe were extrapolated in the Sequence 1 and 3 core intervals.

4.12 Discussions

4.12.1 Chemical and physical correlations

Higher values of loss on ignition (LOI > 3 wt.%) in samples of massive basalts from lobe core are probably associated with their diktitaxitic texture or alteration. Samples that have relatively low LOI values (< 3 wt.%), such as those in the rubbly pahoehoe in well BD-08, may indicate that degassing occurred either at the vent source (Guilbaud *et al*., 2007) or during propagation across the evolving lava (Self *et al.*, 1998).

Variable trace element ratios and Nb troughs (Figure 17) within continental basalt sequences may be related to either crustal contamination or derivation from distinctive mantle sources. However, basaltic lava flows can travel over long distances and may be related to distinctive subvolcanic magma chambers and complex plumbing systems that have undergone different differentiation processes (Millet *et al.* 2020; Almeida *et al*. 2021). Thus, correlations between geochemical and physical data must be done with great care.

Selected trace element ratios and major element contents of the samples from wells BD-02, BD-04 and BD-08 are rather variable (Figure 18). The most striking correlation between geochemical and physical data can be seen in well BD-08. The MgO and LOI contents of samples vary within a narrow range (5.65 ± 0.29 wt% and 3.02 ± 0.77 wt%, respectively) but the sample from Sequence 1, interpreted as a compound-braided 3D geometry, has lower trace element ratios than those in Sequence 2 (classic-tabular 3D geometry). Intrasequence variation of trace element ratios in Sequence 2 are lower than intersequence variation (*e.g.* Sequence 2 and 3), regardless the lithofacies and morphologies in the former. Similar features apply to well BD-04 where intrasequence variations of trace element ratios are lower than the intersequence ones (Table 6), even considering the anomalous low Y content of sample BD-4-3075.22 (Table 3). Thus, differences in trace element ratios seem to be closely related with the different sequences (or 3D geometries) discriminated in wells BD-04 and BD-08.

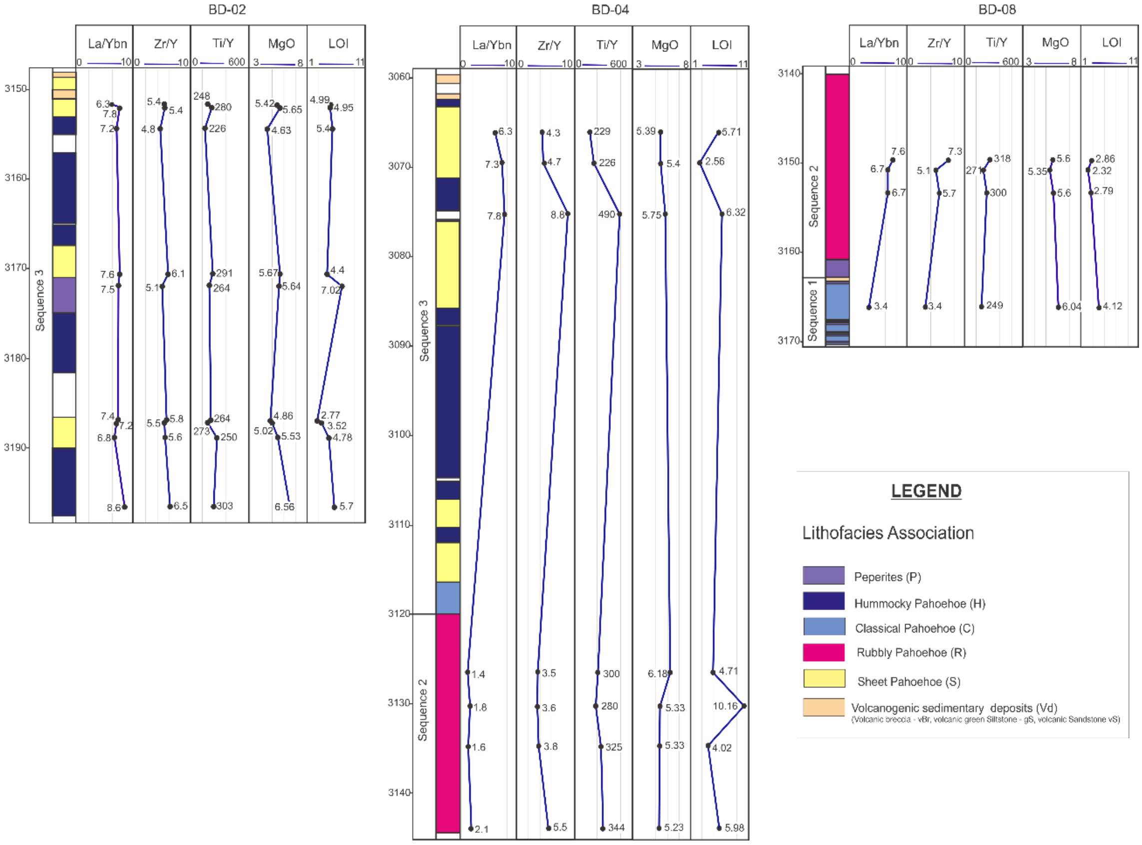

Figure 22: Ranges of selected immobile trace element ratios, MgO and LOI contents (in wt.%) in wells BD-02, BD-04 and BD-08 of the Badejo Field, Campos Basin. Volcanic sequences are indicated. Normalization factors of La/Ybn ratios from McDonough & Sun (1995).

Table 6: Variation of trace element ratios within and between sequences in wells BD-04.

Sequence	Sample	La/Ybn	Zr/Y	Ti/Y
3	3066.07	6.3	4.3	229
	3069.52	7.3	4.7	266
	3075.22	7.8	8.8	490
	Average	7.1	5.9	328
	% variation (intra)	24	106	114
2	3126.47	1.4	3.5	300
	3130.23	1.8	3.6	284
	3134.7	1.6	3.8	325
	3143.88	2.1	5.5	344
	Average	1.7	4.1	313
	% variation (intra)	50	56	15

% variation (inter)	106	87	675

Some authors have used geochemical and paleomagnetic data to infer that even a simple flow unit may be composed of several lobes and also suggested that geochemical changes along time may have contributed to changes in flow morphologies (Duraiswami *et al.*, 2008). More likely, lava flows in those two sequences in wells BD-04 and BD-08 may have travelled long distances from their different emission centers.

Samples from Sequence 3 in well BD-02 present rather invariable La/Ybn ratios (7.4 ± 0.6). The lowermost sample (BD-2, 3198,49) has the highest MgO content (5.70 wt.%) and La/Ybn ratio (8.6) in the sequence and cannot be considered a parental composition for the more evolved samples towards the top of Sequence 3 throught fractional crystallization, with or without concomitant crustal contamination, involving typical fractionating phases of basaltic magmas (*i.e.*, olivine, clinopyroxene and plagioclase). Once more, lava flows in well BD-02 cannot be related with a single subvolcanic magma chamber or simple plumbing systems and may represent lava flows far away from their emission centers. It is worth noting that the average value of La/Ybn ratio (7.4 ± 0.6) of samples from Sequence 3 in well BD-02 is similar to that of samples at the top of Sequence 3 in well BD-04 (7.1 ± 0.8). The same applies for Zr/Y and Ti/Y ratios when sample BD-4-3075,22 in Sequence 3 of well BD-04, when the anomalous low Y content (13 ppm) is not included in calculations. Overall, the lithogeochemical data indicate that Sequence 3 in well BD-02 and Sequence 3 at the top of well BD-04 may be associated with the same emission center.

4.12.2 Petrophysical data and extrapolation of well core data

Wells BD-02, BD-04 and BD-08 were drilled by PETROBRAS between 1976 and 1980. Caliper (in), spontaneous potencial (mV), gamma ray (gAPI), shallow and deep resistivity (ohm.m), compressional sonic (us/ft), density (g/cm^3) and neutron porosity (%) data were obtained for the volcanic sections in the three wells, exception made for sonic data for well BD-02. Top and bottom depths for the volcanic sections in wells BD-02, BD-04 and BD-08 are, respectively 3115-3219 m, 3042-3175 m and 3133-3161.5 m on the basis of the geophysical data, although the volcanic section in well BD-08 was cored down to 3170 m.

Core width tend to be narrower through massive basalt and wider in vesicular and amygdaloidal types. However, sometimes fractured massive basalts can change this expected caliper data (Boldreel *et al.* 2006). Gamma ray data may represent geochemical properties and will not necessarily show similar response within the same lava sequence. Weathering and hydrothermal processes can change the magmatic primary mineralogy that could drastically change gamma ray values inside the flow (Boldreel et. al. 2006). Neutron data are a measure for the hydrogen content and may indicate not only water filled vesicles but also the weathered tops of flows with alteration minerals containing hydrous oxides (Bucker *et al.* 1998). Massive basalts show high values in density and high sonic velocities (low DT values), except where alteration and vesicularity are high (Bucker *et al.* 1998). As such, a reasonable way to discriminate tabular-classic sequences and compound-braided sequences in electric profiles is by the recognition of the inner parts of their lobes (Nelson *et al.*, 2009b).

In wells BD-02, BD-04 and BD-08 the sonic values for the massive basalts in rubbly pahoehoes vary from 51.47 to 76.44 µs/ft, whereas in sheet pahoehoes they vary from 56.458 to 81.61 µs/ft (Figure 23). In general, the values are similar because transit times in sonic logs within the core units seem to be independent of the thickness of the flow (Boldreel *et al.* 2006). Density values for massive basalts in rubbly pahoehoes vary from 2.11 to 2.85 g/cm³ whereas density values are between 2.29 and 2.76 g/cm³ for massive basalts in the sheet pahoehoes (Figure 23). Despite variations in caliper data that may be related to drilling, the cores of the more inflated lobes can be characterized by zones of high porosity and low density, possibly due to the presence of vug and fracture zones. As a result, the massive cores in these inflated lobes present more variable density values within a single lobe, between lobes and between lava lithofacies association. Sonic values below 62.5 µs/ft and density values above 2.65 g/cm³ seem to correspond to massive centers. This massive basalts lithofacies interval were interpreted in the logs (Figure 23). Thus, Sequence 2 may reach 50 m in well BD-04 and 30 m in well BD-08 with the continuity of low compressional sonic and high-density values showing great thickness for interpreted massive basalts. Sequence 3 is 78 m thick in well BD-04 and 101 m thick in well BD-02 with variable density and sonic values showing thin intervals of interpreted massive basalts lithofacies. Overall, the thickness of the compound-braided flows seems to be greater than in the tabular-classical flows, being about 40 m in Sequence 2 and 89.5 m in Sequence 3 (Figure 21).

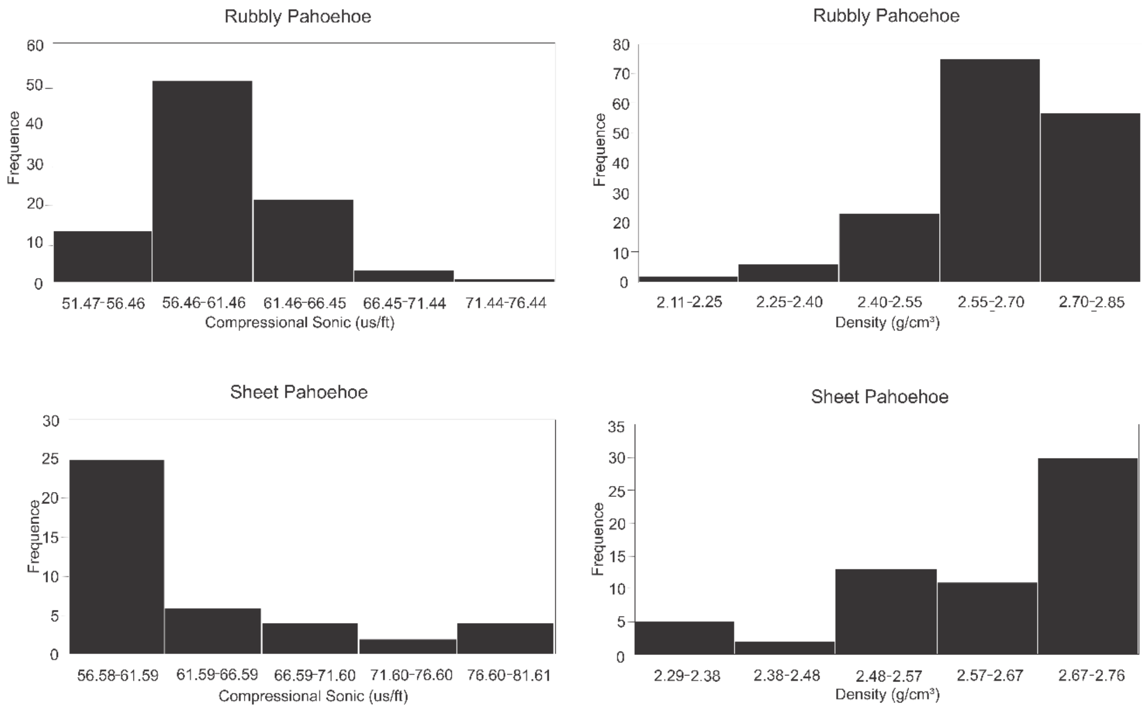

Figure 23: Histograms for density and sonic parameters of massive basalt lithofacies in wells BD-02, BD-04 and BD-08 for rubbly and sheet pahoehoe lithofacies association.

4.12.3 Volcanic paleoenvironment reconstruction

Sequence 1(compound-braided flow) is related to a humid environment (Figure 19A). The low-viscosity, classical pahoehoe lavas were erupted under low effusion and strain rates that made it possible the interaction with wet, unconsolidated sediments. The latter gave rise to thin layers of fluidal, irregular peperite between lobes. Sediments may be derived from either airfall volcanic ash or from *in situ* weathering of the lava flows as proposed elsewhere (Waagstein & Hald 1984). Restricted sedimentation was possible due to the low effusion rates and may have taken place during periods of volcanic quiescence, although not being able to form thick sedimentary sequences. The reddish color of the classical pahoehoe lavas also suggests a long period of subaerial exposition as seen in many CFB provinces (Single & Jerram 2004). At the top of the last lobe a peperite was formed in transition to a reddish volcanic sandstone. The reddish sandstones that end up Sequence 1 may be derived from the alteration of the surrounding basaltic lavas and can be founded in other wells (Marins & Parizek-Silva *et al.*, 2018; Mizusaki *et al.* 1992).

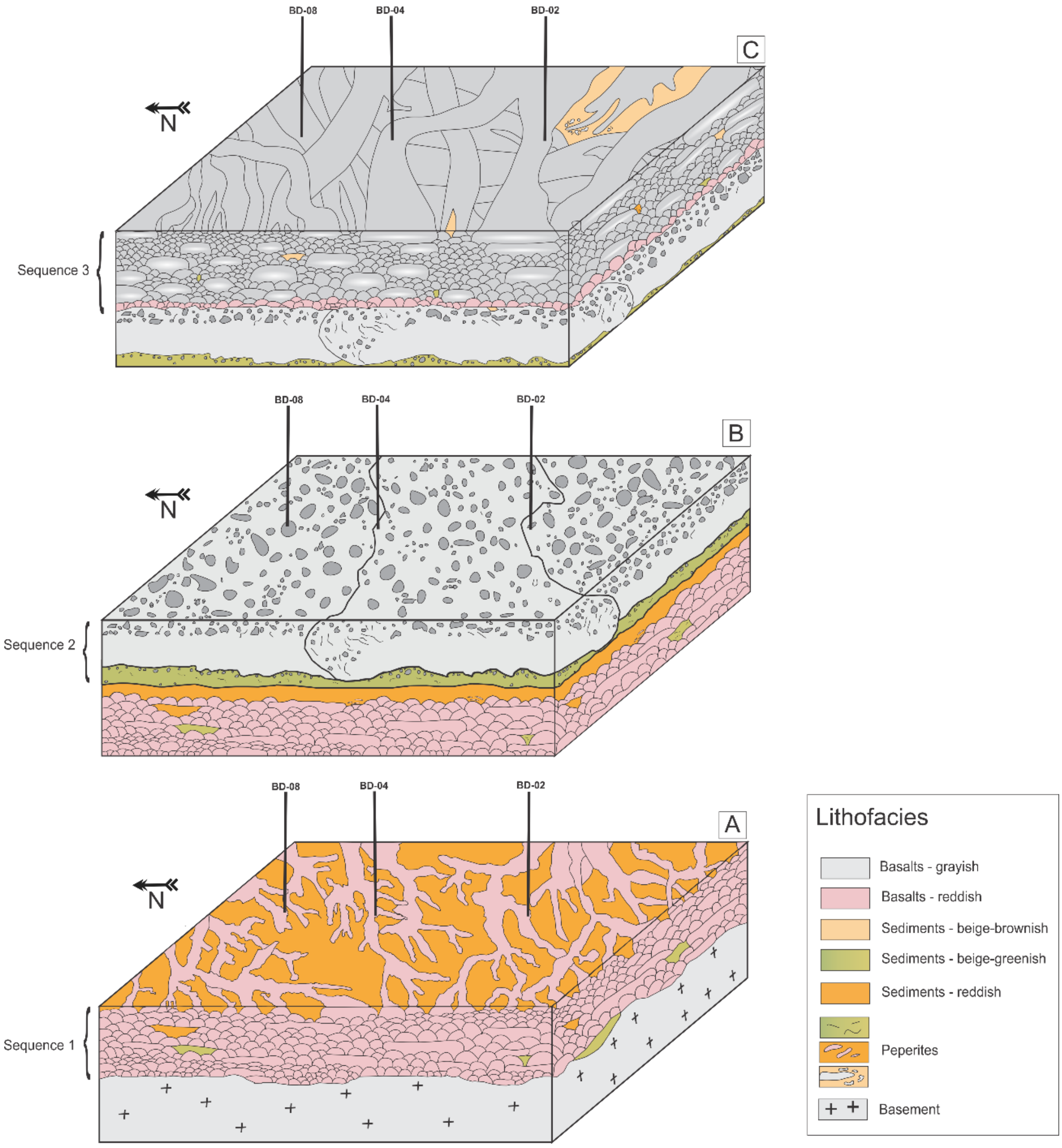

Figure 24: Conceptual models for the volcanic paleoenvironment in the Badejo area. A) Sequence 1: Compound-braided flow. B) Sequence 2: Tabular- Classic flow. C) Sequence 3: Compound-braided flow.

Sequence 2 (Tabular-Classic flow) is associated at the base with small water pods formed during volcanic quiescence (Figure 24B). Wet, siltose unconsolidated sediments interacted with thick rubbly pahoehoe lavas giving rise to a single, 2 m-thick peperite with sheet geometry rather than domic of lenticular ones. The advancing lava flow and the inflation process of the flow and extrusion of new flows did not disturb the peperite. These peperites may be similar to type 2 peperite described in the Paraná CFB (Waichel *et al.,* 2007). The viscous, rubbly pahoehoe lavas were extruded under high and constant effusion rates covering about 2 km^2 with tabular, 40 m thick lava flows. They are probably related with more than one vent or fissure on the basis of their lithogeochemical data in wells BD-04 and BD-08. The autoclastic breccia with basaltic matrix is more abundant than the autoclastic breccia with sedimentary matrix, the latter being formed under subaerial conditions where weathering gives rise to expanding clays that help to break the top portions of the lava flows. Due to the presence of thin layer of autoclastic breccia with sedimentary matrix, was interpreted that more arid conditions may have prevailed at the final stages of lava emplacement. As flow advances, flow-top breccias can fall into flow interior producing others brecciated intervals in the flow front for the same lava unit (Sheth *et al.* 2017). Inflation and coalescence of lobes promoted the flat, smooth upper surface of the lavas at the top of Sequence 2.

Sequence 3 (compound-braided flow), initially, is related with the emplacement of classical pahoehoe lavas formed under low effusion rates over the flat terrain formed by the rubbly pahoehoe lava flows (Figure 24C). The reddish color of the lobes may indicate a longer time of exposition or lower frequence of eruption events, similarly to Sequence 1. There is no interaction between lavas and sediments probably due to longer periods of volcanic quiescence or an arid climate. Subsequently, effusion rates may have become moderate to high, giving rise to hummocky and sheet pahoehoe with an oscillation of supply rates or pulsed inflation. Despite the fact the scale of observation prevented the discrimination of tumulli typically related with hummocky pahoehoe, the variety in size, shape and distribution of vesicles allow a relationship with those types of lavas. Shear rates vary from low to high, possibly to the transitional characteristic of these lavas. The presence of vesicular cores with diktytaxitic texture in most lobes suggests high volatile content in these lavas (Waichel *et al.*, 2006). The sheet pahoehoe may have covered approximately 650 m², with average thickness around 89,5 m. Minimum emplacement time is between 3 to 7 months. Similar trace element ratios of the basalts in Sequence 3 indicate eruption from a single vent or fissure in the final stage. Lava flows are thicker in well BD-04, indicating flow propagation southwards. Nevertheless, thickness may have been controled by the paleorelief, already modified by the emplacement of the previous hummocky lava flows. The presence of blocky peperite in well BD-02 and the predominance of blocky and irregular angular fragments may indicate that quench fragmentation was a major process. The occurrence of vesicles inside the sediments indicates that unconsolidated material and the described pore-water steam explosions may be related to the less viability of forming steam films at the magma/wet sediment interface. It is difficult to explain how vapor films remain stable during the deformation of clasts, but they may have taken advantage of fine grained, well-sorted and loosely packed sandstones in the area as proposed elsewhere (Busby-Spera & White, 1987; Famelli *et al.*, 2021b). Top portions of Sequence 3 may have generated a smooth, bun-like and hummocky surface with a meter-scale relief. Finally, the basalt breccias interbedded with the sheet pahoehoe may be related with a most active phase of the rifting process that formed Campos Basin.

4.13 Conclusions

The 3D arrangement of the volcanic facies of the Cabiúnas Formation within the Badejo field in Campos Basin is represented by three sequences, as such: two compound-braided flows and one Tabular-classic flow. Lava flows includes classical pahoehoe and the transitional types of sheet pahoehoe, hummocky pahoehoe and rubbly pahoehoe. In general, the volcanic paleoenvironment interpretation is predominantly subaerial, as already proposed by previous studies. Nevertheless, interactions between lava flows and humid sediments could be depicted from detailed descriptions of the volcanic facies. Sequence 1 (compound-braided flow) is related to a humid environment. The low-viscosity, classical pahoehoe lavas were erupted under low effusion and strain rates and interacted with wet sediments forming fluidal peperites. The base Sequence 2 (Tabular-Classic flow) is associated with small water pods formed during volcanic quiescence. Predominant rubbly pahoehoe lavas were extruded under high and constant effusion rates. Sequence 3 (compound-braided flow), initially, is related with the emplacement of classical pahoehoe lavas formed under low effusion rates over the flat topography formed by the rubbly pahoehoe lava flows. Subsequently, effusion rates may have become moderate to high, giving rise to hummocky and sheet pahoehoe lithofacies association. The presence of blocky peperite in well BD-02 with predominant blocky and irregular angular fragments may indicate that quench fragmentation was a major process. Differences in trace element ratios seem to be closely related with the different sequences (or 3D geometries) in the BD-04 and BD-08 wells. Sequence 2 in wells BD-02 and BD-08 cannot be correlated on the basis of the distinctive trace element ratios of their samples. However, the lithogeochemical data indicate that Sequence 3 in well BD-02 and Sequence 3 at the top of well BD-04 may be associated with the same emission center. Petrophysical data shows that sonic values below 62.5 µs/ft and density values above 2.65 g/cm³ seem to correspond to massive centers. The extrapolation of well core data with the use of well logs conclude that the thickness of the compound-braided lavas seems to be greater than in the tabular-classical lavas, being about 40 m in Sequence 2 and 89.5 m in Sequence 3. Finally, porosities are almost equal for both compound-braided flows, but the predominance of facies amB/vsB_i and amB_e interbedded with laterally discontinuous massive facies and probably higher permeabilities pointing to best potential hydrocarbon reservoirs for the Sequence 3 in comparison with the two other Sequences.

4.14 Acknowledgments

This work was financially supported by Petrobras (CENPES – Research Center and Exploration) projects. The authors would like to thank also all those who contributed in some way to make this work possible.

4.15 References

Almeida, J., Heilbron, M., Guedes, E., Neubauer, F., Manfred, B., Klausen, M.B., Valeriano, C. de M., Bruno, H., Giro, J.P., McMaster, M., Tetzner, W., 2021. Pre-to-syn-rift tholeiitic magmatism in a transtensive hyperextended continental margin: Onshore and offshore magmatism of the Campos Basin, SE Brazil. Journal of South American Earth Sciences 108, 103218. https://doi.org/10.1016/j.jsames.2021.103218

Alves, D.B., 2005. Sedimentação vulcanoclástica do Cretáceo Superior da Bacia de Campos, Sudeste do Brasil. Boletim de Geociências Petrobras 14, 149–154.

Amorim, N.R., 2013. Caracterização geofísica da dorsal de São Paulo e seu significado evolutivo na Bacia de Santos. Universidade Federal Fluminense, Brazil.

Aubele, J.C., Crumpler, L.S., Elston, W.E., 1988. Vesicle zonation and vertical structure of basalt flows. Journal of Volcanology and Geothermal Research 35, 349–374. https://doi.org/10.1016/0377-0273(88)90028-5

Barreto, C.J.S., de Lima, E.F., Scherer, C.M., Rossetti, L. de M.M., 2014. Lithofacies analysis of basic lava flows of the Paraná igneous province in the south hinge of Torres Syncline, Southern Brazil. Journal of Volcanology and Geothermal Research 285, 81–99. https://doi.org/10.1016/j.jvolgeores.2014.08.008

Bischoff, A.P., Nicol, A., Beggs, M., 2017. Stratigraphy of architectural elements in a buried volcanic system and implications for hydrocarbon exploration. Interpretation 5, SK141–SK159. https://doi.org/10.1190/INT-2016-0201.1

Boldreel, L.O., 2006. Wire-line log-based stratigraphy of flood basalts from the Lopra-1/1A well, Faroe Islands. Geological Survey of Denmark and Greenland Bulletin 9, 7–22.

Bondre, N.R., Duraiswami, R.A., Dole, G., 2004. Morphology and emplacement of flows from the Deccan Volcanic Province, India. Bull Volcanol 66, 29–45. https://doi.org/10.1007/s00445-003-0294-x

Bruhn, C.H.L., Gomes, J.A.T., Del Lucchese Jr., C., Johann, P.R.S., 2003. Campos Basin: Reservoir Characterization and Management – Historical Overview and Future Challenges. Houston, Texas, U.S.A., pp. 1–14.

Busby-Spera, C.J., White, James DL , 1987. Variation in peperite textures associated with differing host-sediment properties. Bull Vulcanol 49, 765–775.

Caddah, L.F.G., Alves , D.B., Mizusaki, A.M.P., 1998. Turbidites associated with bentonites in the Upper Cretaceous of the Campos Basin, offshore Brazil . Sedimentary Geology 115, 175–184.

Caddah, L.F.G., Alves, D. B., Hanashiro, M., Mizusaki, A.M.P., 1994. Characterization and Origin of the “3-dedos” Marker Bed (Santonian) of the Campos Basin. Boletim de Geociências Petrobras 8 (2/4), 315–334.

Cainelli, C., Mohriak, W.U., 1999. Some remarks on the evolution of sedimentary basins along the eastern Brazilian continental margin. Episodes 22, 206–216. https://doi.org/10.18814/epiiugs/1999/v22i3/008

Castro, R.D., Picolini, J.P., 2014. Principais aspectos da geologia regional da Bacia de Campos, in: Geologia e Geomorfologia. Elsevier, Rio de Janeiro, pp. 1–12.

Chang, H.K., Kowsmann, R.O., Figueiredo, A.M.F., Bender, A.A., 1992. Tectonics and stratigraphy of the East Brazil Rift system: an overview. Tectonophysics 213, 97–138. https://doi.org/10.1016/0040-1951(92)90253-3

Costa, J., 2015. Estratigrafia e geoquímica da sequência de Lavas da província magmática do Paraná da região da usina de Itaipu (PR) (Doctoral dissertation). Universidade Federal do Paraná, Brazil.

Dani, A.P.O., Remus, V.D., Lima, E.F., 2017. Basalt magmatism from Alagoas Stage (Campos Basin). Revista do Instituto de Geociências - USP 17, 269–287. https://doi.org/10.11606/issn.2316-9095

Dias, J.L., 2005. Tectonic, stratigraphy and sedimentation during the Aptian along the brasilian eastern margin. Boletim de Geociências Petrobras 13, 7–25.

Duraiswami, R.A., 2009. Pulsed inflation in the hummocky lava flow near Morgaon, western Deccan Volcanic Province and its significance. Current science 97(3), 313–316.

Duraiswami, R.A., Bondre, N.R., Managave, S., 2008. Morphology of rubbly pahoehoe (simple) flows from the Deccan Volcanic Province: Implications for style of emplacement. Journal of Volcanology and Geothermal Research 177, 822–836. https://doi.org/10.1016/j.jvolgeores.2008.01.048

Duraiswami, R.A., Dole, G., Bondre, N., 2003. Slabby pahoehoe from the western Deccan Volcanic Province: evidence for incipient pahoehoe–aa transitions. Journal of Volcanology and Geothermal Research 121, 195–217. https://doi.org/10.1016/S0377-0273(02)00411-0

Duraiswami, R.A., Gadpallu, P., Shaikh, T.N., Cardin, N., 2014. Pahoehoe–a′a transitions in the lava flow fields of the western Deccan Traps, India-implications for emplacement dynamics, flood basalt architecture and volcanic stratigraphy. Journal of Asian Earth Sciences 84, 146–166. https://doi.org/10.1016/j.jseaes.2013.08.025

Dutton, C.E., 1884. Hawaiian volcanoes. U. S. geol. Survey 4th Ann. Rept.

Famelli, N., Lima, E.F., Carmo, I. de O., 2021a. Lithostratigraphy of the Serra Geral Formation in the northern portion of the Paraná-Etendeka Igneous Province: A tool for tracking Early Cretaceous paleoenvironmental changes. Journal of Volcanology and Geothermal Research 410, 107152. https://doi.org/10.1016/j.jvolgeores.2020.107152

Famelli, N., Millett, J.M., Hole, M.J., Lima, E.F., Carmo, I. de O., Jerram, D.A., Jolley, D.W., Pugsley, J.H., Howell, J.A., 2021b. Characterizing the nature and importance of lava-sediment interactions with the aid of field outcrop analogues. Journal of South American Earth Sciences 108, 103108. https://doi.org/10.1016/j.jsames.2020.103108

Fodor, R.V., Vetter , S.K. , 1984. Rift-zone magmatism: Petrology of basaltic rocks transitional from CFB to MORB, southeastern Brazil margin . Contrib Mineral Petrol 88, 307–321.

Fodor, R.V., Mckee, E.H., Asmus, H.E., 1983. K-Ar Ages and the Opening of the South Atlantic Ocean: Basaltic Rock from the Brazilian Margin. Marine Geology 54, M1–M8.

Fornero, S.A., Marins, G.M., Lobo, J.T., Freire, A.F.M., Lima, E.F. de, 2019. Characterization of subaerial volcanic facies using acoustic image logs: Lithofacies and log-facies of a lava-flow deposit in the Brazilian pre-salt, deepwater of Santos Basin. Marine and Petroleum Geology 99, 156–174. https://doi.org/10.1016/j.marpetgeo.2018.09.029

Franke, D., 2013. Rifting, lithosphere breakup and volcanism: Comparison of magma-poor and volcanic rifted margins. Marine and Petroleum Geology 43, 63–87. https://doi.org/dx.doi.org/10.1016/j.marpetgeo.2012.11.003

Gregg, T.K.P., 2017. Patterns and processes: Subaerial lava flow morphologies: A review. Journal of Volcanology and Geothermal Research 352, 3–12. https://doi.org/http://dx.doi.org/10.1016/j.jvolgeores.2017.04.022

Guardado, L.R., Spadini, A.R., Brandão, J.S.L., Mello, M.R., 2000. Petroleum System of the Campos Basin, Brazil. AAPG Memoir 73, 317–324.

Heilbron, M., Mohriak, W.U., Valeriano, C.M., Milani, E.J., Almeida, J., Tupinambá, M., 2000. From Collision to Extension: The Roots of the Southeastern Continental Margin of Brazil . Geophysical Monograph-American Geophysical Union 115, 1–32.

Heine, C., Zoethout, J., Müller, R.D., 2013. Kinematics of the South Atlantic rift. Solid Earth 4, 215–253. https://doi.org/10.5194/se-4-215-2013

Hon, K., Kauahikaua, J., Denlinger, R., Mackay, K., 1994. Emplacement and inflation of pahoehoe sheet flows: Observations and measurements of active lava flows on Kilauea Volcano, Hawaii. Geological Society of America Bulletin 106, 351–370. https://doi.org/10.1130/0016-7606(1994)106<0351:EAIOPS>2.3.CO;2

Jerram, D.A., Single, R.T., Hobbs, R.W., Nelson, C.E., 2009. Understanding the offshore flood basalt sequence using onshore volcanic facies analogues: an example from the Faroe–Shetland basin. Geol. Mag. 146, 353–367. https://doi.org/10.1017/S0016756809005974

Jerram, W.U., 2002. Volcanology and facies architecture of flood basalts, in: Volcanic Rifted Margins. Geological Society of America.

Keszthelyi, L., 2002. 14. Classification of the Mafic Lava Flows from ODP Leg 183, in: Proceedings of the Ocean Drilling Program, Scientific Results.

Kowsmann, R.O., Costa, M.P.A., Boa Hora, M.P., Guimarães, P.P., 1982. Geologia estrutural do platô de São Paulo. Salvador, BA, pp. 1558–1569.

Le Maitre, R., Streckeisen, A., Zanettin, B., Le Bas, M.J., Bonin, B., 2002. Igneous rocks. A Classification and Glossary of Terms: Recommendations of the International Union of Geological Sciences Subcommission on the Systematics of Igneous Rocks, 2002.

Lobo, J.T., Duarte, B.P., Szatmari, P., Valente, S. de C., 2007. Basaltos continentais do Cretáceo Inferior da bacia de Campos, SE do Brasil: compilação de dados e petrogênese. RBG 37, 224–236. https://doi.org/10.25249/0375-7536.2007373224236

Lockwood, J.P., Hazlett, R.W., 2010. Volcanoes: global perspectives. Wiley-Blackwell, Hoboken, NJ.

Macdonald, G.A., 1953. Pahoehoe, aa, and block lava. American Journal of Science 251, 169–191. https://doi.org/10.2475/ajs.251.3.169

MacKenzie, W.S., Donaldson, C.H., Guilford, C., 1991. Atlas of igneous rocks and their textures. Longman scientific and technical J. Wiley and sons, Harlow New York.

Marins, G.M., Parizek-Silva, Y., Millett, J.M., Jerram, D.A., Rossetti, L.M.M., Souza, A. de J. e, Planke, S., Bevilaqua, L.A., Carmo, I. de O., 2022. Characterization of volcanic reservoirs; insights from the Badejo and Linguado oil Field, Campos Basin, Brazil. Marine and Petroleum Geology.

Marins, G.M., Parizek-Silva, Y.M., 2018. Revisitação da sucessão vulcânica basáltica testemunhada de um poço do campo de Badejo, da bacia de Campos. Uma análise vulcano-estratigráfica. Rio de Janeiro.

McDonough, W.F., Sun, S.S., 1995. The composition of the Earth. Chemical Geology 120, 223–253. https://doi.org/10.1016/0009-2541(94)00140-4

McPhie, J., Doyle, M., Allen, R.L., 1993. Volcanic textures: a guide to the interpretation of textures in volcanic rocks. Centre for ore deposit and exploration studies, University of Tasmania, Hobart (Tasmanie).

Millett, J.M., Hole, M.J., Jolley, D.W., Passey, S.R., Rossetti, L., 2020. Transient mantle cooling linked to regional volcanic shut-down and early rifting in the North Atlantic Igneous Province. Bull Volcanol 82, 61. https://doi.org/10.1007/s00445-020-01401-8

Mizusaki, A.M., Thomaz-Filho, A., Roisenberg, A., 2008. Rochas igneo-básicas das bacias sedimentares brasileiras como potenciais reservatórios de hidrocarbonetos. Foz do Iguaçu, PR.

Mizusaki, A.M.P., 1986. Rochas igneo-basicas do Neocomiano da Bacia de Campos-caracterizacao e comportamento como reservatorio do hidrocarbonetos (Doctoral dissertation). Universidade Federal do Rio de Janeiro, Brazil.

Mizusaki, A.M.P., Petrini, R., Bellieni, P., Comin-Chiaramonti, P., Dias, J., De Min, A., Piccirillo, E.M., 1992. Basalt magmatism along the passive continental margin of SE Brazil (Campos basin). Contrib Mineral Petrol 111, 143–160. https://doi.org/10.1007/BF00348948

Mizusaki, A.M.P., Saracchini, F.E., 1992. Catálogo geral de dados geocronologicos da Petrobras (internal). Petrobras/Cenpes/Divex/Setec, Rio de Janeiro, Brazil.

Mizusaki, A.M.P., Thomaz Filho, A., Valença, J., 1988. Volcano-sedimentary sequence of Neocomian age in Campos Basin (Brazil). RBG 18, 247–251. https://doi.org/10.25249/0375-7536.1988247251

Mohriak, W., Nemčok, M., Enciso, G., 2008. South Atlantic divergent margin evolution: rift-border uplift and salt tectonics in the basins of SE Brazil. Geological

Society, London, Special Publications 294, 365–398. https://doi.org/10.1144/SP294.19

Mohriak, W.U., Brown, D.E., Tari, G., 2008. Sedimentary Basins in the Central and South Atlantic Conjugate Margins: Deep Structures and Salt Tectonics. Halifax.

Mohriak, W.U., Palagi, P.R., Mello, M.R., 1998. Tectonic evolution of South Atlantic salt basins. American Association of Petroleum Geologists Bulletin 82 (10), 1945.

Mohriak, W.U., Rosendahl, B.R., Turner, J.P., Valente, S.C., 2002. Crustal architecture of South Atlantic volcanic margins, in: Volcanic Rifted Margins. Geological Society of America. https://doi.org/10.1130/0-8137-2362-0.159

Moraes, L.C., Seer, H.J., 2018. Pillow lavas and fluvio-lacustrine deposits in the northeast of Paraná Continental Magmatic Province, Brazil. Journal of Volcanology and Geothermal Research 355, 78–86. https://doi.org/10.1016/j.jvolgeores.2017.03.024

Moreira, J.L.P., Esteves, C.A., Rodrigues, J.J.G., Vasconcelos, C.S., 2005. Magmatismo, sedimentação e estratigrafia da porção norte da Bacia de Santos. Boletim de Geociências Petrobras 14, 161–170.

Moulin, M., Aslanian, D., Unternehr, P., 2010. A new starting point for the South and Equatorial Atlantic Ocean. Earth-Science Reviews 98, 1–37. https://doi.org/10.1016/j.earscirev.2009.08.001

Nelson, C.E., Jerram, D.A., Hobbs, R.W., 2009b. Flood basalt facies from borehole data: implications for prospectivity and volcanology in volcanic rifted margins. Petroleum Geoscience 15, 313–324. https://doi.org/10.1144/1354-079309-842

Nelson, C.E., Jerram, D.J., Single, R.T., Hobbs, R.W., 2009a. Understanding the facies architecture of flood basalts and volcanic rifted margins. pp. 84–103.

Németh, K., Palmer, J., 2019. Geological mapping of volcanic terrains: Discussion on concepts, facies models, scales, and resolutions from New Zealand perspective. Journal of Volcanology and Geothermal Research 385, 27–45. https://doi.org/10.1016/j.jvolgeores.2018.11.028

Planke, S., Symonds, P.A., Alvestad, E., Skogseid, J., 2000. Seismic volcanostratigraphy of large-volume basaltic extrusive complexes on rifted margins. J. Geophys. Res. 105, 19335–19351. https://doi.org/10.1029/1999JB900005

Rangel, H. D., Martins, F.A.L., Esteves, F.R., Feijó, F.J., 1994. Bacia de Campos. Boletim de Geociências Petrobras 8, 203–217.

Rangel, H.D., 2005. Magmatic occurrences in the southern part of the Campos Basin (Cabo Frio Area) and in the Jequitinhonha Basin. Boletim de Geociências Petrobras 14, 155–160.

Reis, G. dos S., 2013. A formação Serra geral (cretáceo, bacia do Paraná) - como análogo para os reservatórios ígneo-básicos da margem continental brasileira (master´s thesis).

Ren, K., Zhao, J., Liu, Q., Zhao, J., 2020. Hydrocarbons in igneous rock of Brazil: A review. Petroleum Research 5, 265–275. https://doi.org/10.1016/j.ptlrs.2020.06.001

Rossetti, L., Lima, E.F., Waichel, B.L., Hole, M.J., Simões, M.S., Scherer, C.M.S., 2018. Lithostratigraphy and volcanology of the Serra Geral Group, Paraná-Etendeka Igneous Province in Southern Brazil: Towards a formal stratigraphical framework. Journal of Volcanology and Geothermal Research 355, 98–114. https://doi.org/https://doi.org/10.1016/j.jvolgeores.2017.05.008

Rossetti, L.M., Lima, E.F., Waichel, B.L., Scherer, C.M., Barreto, C.J., 2014. Stratigraphical framework of basaltic lavas in Torres Syncline main valley, southern Parana-Etendeka Volcanic Province. Journal of South American Earth Sciences 56, 409–421. https://doi.org/10.1016/j.jsames.2014.09.025

Self, S., Keszthelyi, L., Thordarson, Th., 1998. The importance of pāhoehoe. Annu. Rev. Earth Planet. Sci. 26, 81–110. https://doi.org/10.1146/annurev.earth.26.1.81

Sheth, H., Pal, I., Patel, V., Samant, H., D’Souza, J., 2017. Breccia-cored columnar rosettes in a rubbly pahoehoe lava flow, Elephanta Island, Deccan Traps, and a model for their origin. Geoscience Frontiers 8, 1299–1309. https://doi.org/10.1016/j.gsf.2016.12.004

Single, R.T., Jerram, D.A., 2004. The 3D facies architecture of flood basalt provinces and their internal heterogeneity: examples from the Palaeogene Skye Lava Field. Journal of the Geological Society 161, 911–926.

Stica, J.M., Zalán, P.V., Ferrari, A.L., 2014. The evolution of rifting on the volcanic margin of the Pelotas Basin and the contextualization of the Paraná–Etendeka LIP in the separation of Gondwana in the South Atlantic. Marine and Petroleum Geology 50, 1–21. https://doi.org/10.1016/j.marpetgeo.2013.10.015

Svensen, H.H., Torsvik, T.H., Callegaro, S., Augland, L., Heimdal, T.H., Jerram, D.A., Planke, S., Pereira, E., 2018. Gondwana Large Igneous Provinces: plate reconstructions, volcanic basins and sill volumes. Geological Society, London, Special Publications 463, 17–40. https://doi.org/10.1144/SP463.7

Thomaz Filho, A., Mizusaki, A.M.P., Antonioli, L., 2008. Magmatismo nas bacias sedimentares brasileiras e sua influência na geologia do petróleo. RBG 38, 128–137. https://doi.org/10.25249/0375-7536.2008382S128137

Thomaz Filho, A., Mizusaki, A.M.P., Milani, E.J., Cesero, P.D., 2000. Rifting and magmatism associated with the South America and Africa break up. RBG 30, 017–019. https://doi.org/10.25249/0375-7536.2000301017019Thompson, R.N., 1982. Magmatism of the British Tertiary Volcanic Province. Scottish Journal of Geology 18, 49–107. https://doi.org/10.1144/sjg18010049

Vye-Brown, C., Self, S., Barry, T.L., 2013. Architecture and emplacement of flood basalt flow fields: case studies from the Columbia River Basalt Group, NW USA. Bull Volcanol 75, 697. https://doi.org/10.1007/s00445-013-0697-2

Waagstein, R., Hald, N., 1984. Structure and petrography of a 660 m lava sequence from the Vestmanna-1 drillhole, lower and middle basalt series, Faeroe Islands 39–70.

Waichel, B.L., de Lima, E.F., Lubachesky, R., Sommer, C.A., 2006. Pahoehoe flows from the central Paraná Continental Flood Basalts. Bull Volcanol 68, 599–610. https://doi.org/10.1007/s00445-005-0034-5

Waichel, B.L., de Lima, E.F., Sommer, C.A., Lubachesky, R., 2007. Peperite formed by lava flows over sediments: An example from the central Paraná Continental Flood Basalts, Brazil. Journal of Volcanology and Geothermal Research 159, 343–354. https://doi.org/10.1016/j.jvolgeores.2006.07.009

Waichel, B.L., de Lima, E.F., Viana, A.R., Scherer, C.M., Bueno, G.V., Dutra, G., 2012. Stratigraphy and volcanic facies architecture of the Torres Syncline, Southern Brazil, and its role in understanding the Paraná–Etendeka Continental Flood Basalt Province. Journal of Volcanology and Geothermal Research 215–216, 74–82. https://doi.org/10.1016/j.jvolgeores.2011.12.004

Walker, G.P.L., 1991. Structure, and origin by injection of lava under surface crust, of tumuli, "lava rises," "lava-rise pits," and "lava-inflation clefts" in Hawaii. Bull Volcanol 53, 546–558. https://doi.org/10.1007/BF00298155

Walker, G.P.L., 1973. Mount Etna and the 1971 eruption - Lengths of lava flows. Phil. Trans. R. Soc. Lond. A 274, 107–118. https://doi.org/10.1098/rsta.1973.0030

Walker, G.P.L., 1971. Compound and simple lava flows and flood basalts. Bull Volcanol 35, 579–590. https://doi.org/10.1007/BF02596829

Wilmoth, R.A., Walker, G.P.L., 1993. P-type and S-type pahoehoe: a study of vesicle distribution patterns in Hawaiian lava flows. Journal of Volcanology and Geothermal Research 55, 129–142. https://doi.org/10.1016/0377-0273(93)90094-8

Winchester, J.A., Floyd, P.A., 1977. Geochemical discrimination of different magma series and their differentiation products using immobile elements. Chemical Geology 20, 325–343. https://doi.org/10.1016/0009-2541(77)90057-2

Winter, W.R., Jahnert, R.J., França, A.B., 2007. Bacia de Campos. Boletim de Geociências Petrobras 15 (2), 511–529.

Zhang, G., Qu, H., Chen, G., Zhao, C., Zhang, F., Yang, H., Zhao, Z., Ma, M., 2019. Giant discoveries of oil and gas fields in global deepwaters in the past 40 years and the prospect of exploration. Journal of Natural Gas Geoscience 4, 1–28. https://doi.org/10.1016/j.jnggs.2019.03.002

5 APLICAÇÃO DA METODOLOGIA EM ÁREAS SEM TESTEMUNHO

O intervalo dos basaltos da formação Cabiúnas no campo de Badejo contribuiu para produção de óleo na bacia de Campos. A reserva de óleo para os basaltos de Badejo é estimada em 36.6 MM bbl com óleo entre 28 to 32° API (Bruhn *et al.*, 2003; Ren *et al.* 2020). Os poços BD-1 (Figura 4, 5), BD-11, BD-14 e RJS-258 foram poços produtores enquanto os poços BD-02, BD-03 e BD-04 são sub-comerciais devido as permeabilidades muito baixas (Mizusaki, 1986). O A migração e o acúmulo do óleo em Badejo de deu devido a existência de falhas com grande rejeito que colocaram os basaltos da formação Cabiúnas em contato lateral com os folhelhos geradores do grupo Lagoa Feia (Mizusaki *et al.*, 2008).

Com o objetivo de constatar as zonas identificadas em regiões sem testemunho e com produção de hidrocarbonetos, foi feita a análise dos perfis elétricos de densidade e sônico do poço BD-01. Este poço foi o descobrir de hidrocarbonetos na formação Cabiúnas apresenta uma coluna com mais de 150 metros de óleo. O poço com óleo de 33° API, foi testado até o contato óleo/água com vazões de 216 de metros cúbicos (1356 bb) por dia (Tigre *et al.*, 1983). Em perfil, as características do poço são bastante similares aos poços estudados apresentando as três sequências bem desenvolvidas. Análise dos perfis possibilita a separação destas lavas em unidades de fluxo (Walker, 1971). Para isso foi utilizado os valores de corte abaixo de 62,5 us/ft para o sônico compressional e acima de 2,65 g/cm³ densidade para identificar os basaltos maciços que correspondem, de forma simplificada, a parte central das lavas *pahoehoe* simples. Nos locais com valores mais baixos de densidade, mais alto de sônico e padrão serrilhado corresponderiam aos basaltos vesiculares/amigadoloidais que forma as lavas do tipo *pahoehoe* composta (Figura 25).

A Sequência 3 apresenta 65 metros de um padrão serrilhado onde 3 basaltos maciços delgados foram identificados pelas duas ferramentas, podendo ser estes relacionados ao núcleo das *sheet pahoehoe*. A Sequência 2 apresenta 35 metros de espessura, nos dois perfis foram interpretados espessos basaltos maciços que podem ser correlacionados ao núcleo das *Rubbly pahoehoe*. A Sequência 1 apresenta um padrão serrilhado com 127 metros de espessura onde 3 intervalos delgados de basaltos maciço, provavelmente no contexto do núcleo das *sheet pahoehoe*, foram interpretados em ambos os perfis. A presença de centros maciços mais desenvolvido na Sequência 1 indica que houve momentos com taxas de efusão mais elevadas, o que não pode ser constatado pelos poços estudados. As espessuras encontradas para as Sequências 2 e 3 são muito parecidas com as médias vistas nos poços com testemunho. A Sequência 1 parece ter sido a de maior duração para formação dos basaltos da Formação Cabiúnas devido a sua espessura e ao tipo de das lavas predominantemente compostas (*Hummocky ou classical pahoehoe*) com menores taxa de efusão.

As rochas do BD-01 podem ser classificadas com basaltos, andesitos e andesitos-dacitos que se apresentam-se preservados em parte da Sequência 2, alterados ou com zona de transição na Sequência 1 e bastante fraturados/brechados na Sequência 3 e parte da Sequência 1. A classificação do tipo de rocha por perfil para os poços BD-08 e BD-04 é coerente com diagramas de classificação que indicam composição basáltica e andesítica (Figura 17). A Sequência 2 é a que mostra a melhor preservação. A maior parte dos dados caem no campo das *transicional zone* e *breccia*, sendo que a Sequência 3 inteira está nestes dois campos. Comparando os dois gráficos, percebe-se que a Sequência 3 dos poços BD-08 e BD-04 apresenta um maior grau de alteração e no poço BD-01 predomina as brechas/fraturas. A Sequência 2 apresenta resultado bastante similares com rochas preservadas e a Sequência 1, apenas no BD-01, apresenta um grau elevado de alteração e composição mais próxima da dacítica.

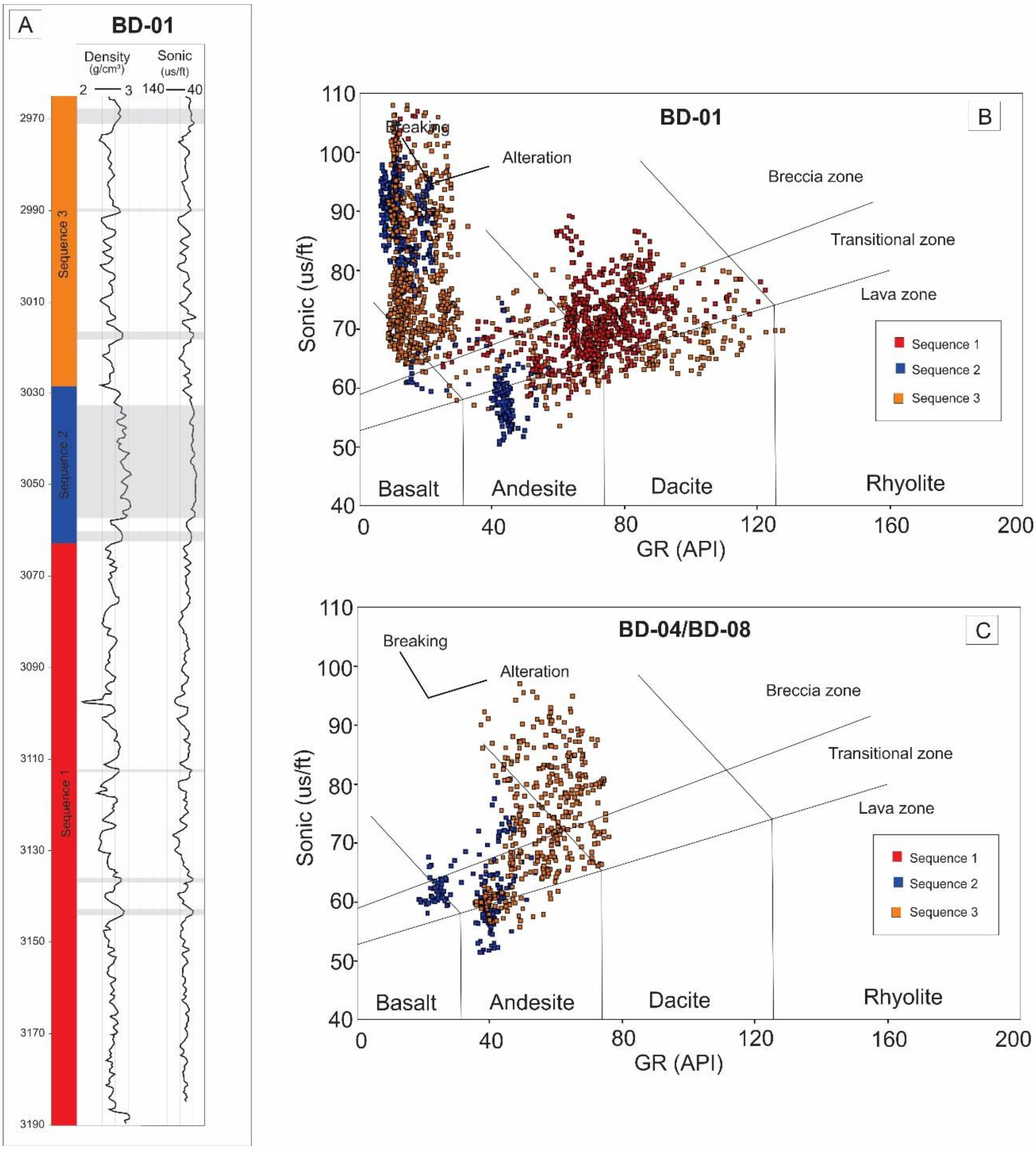

Figura 25: Análise da resposta dos perfis do poço BD-01 em comparação com os poços BD-04 e BD-08. A) Perfis de densidade e sônico para o poço BD-01. Os intervalos em cinza correspondem as litofacies basalto maciço interpretadas. B e C) Gráfico de identificação de rochas vulcânicas e grau de alteração. Modificado de Zou et al. 2013. B) Raio gama versus sônico compressional para o poço BD-01 e as Sequências estimadas. C) Raio gama versus sônico compressional para o poço BD-04 e BD-08 com as Sequências identificadas.

6 CONCLUSÃO GERAL E TRABALHOS FUTUROS

Esta dissertação de mestrado abordou os processos envolvidos na colocação das rochas vulcânicas dos poços BD-02, BD-04 e BD-08 e as possíveis correlações de sequências vulcânicas discriminadas entre os poços. Foi feita uma caracterização de três grandes sequências (geometrias 3D) para a Formação Cabiúnas amostrada pelos três poços no campo de Badejo, Bacia de Campos. O estudo das rochas vulcânicas, a partir da óptica da arquitetura de fácies e da vulcanologia física, possibilitou compreender a relevância das feições identificadas dentro de escalas de observação diferentes. Por exemplo, a litofácies basalto maciço é muito importante no contexto das *rubbly pahoehoe* (associação de litofácies). Porém, em relação à Formação Cabiúnas como um todo, a sua relevância é muito pequena (considerando os poços estudados).

Dois fluxos compostos entrelaçados (Sequência 1 e Sequência 3) e um fluxo tabular clássico (Sequência 2) foram identificados a partir deste estudo. Morfologias ou associações de litofácies incluem lavas do tipo clássico, *hummocky*, tabular e *rubbly pahoehoe*. Foram encontradas litofácies coerentes, brechados e peperitos e intertrapas. Taxas de efusão, estimadas a partir da espessura dos lóbulos, indicaram que inflação por pulsos foi o processo predominante na Sequência 3. A duração mínima de colocação dos fluxos foi estimada em 3 meses e 7 meses para os poços BD-02 e BD-04, respectivamente. Estimativas de valores D para as lavas *hummocky* são maiores que para as lavas *pahoehoe* clássicas, indicando porosidades e permeabilidades potencialmente boas para *plays* exploratórios. Os dados litogeoquímicos mostraram boa correlação na parte superior da Sequência 3, indicativo de emissão a partir do mesmo conduto. A Sequência 2, do tipo composto entrelaçado, pode ter alcançado até 89,5 m, sendo bem mais espessa que os 40 m estimados para as lavas tabulares clássicas na Sequência 3. O paleoambiente vulcânico era predominantemente subaéreo e úmido em todas as sequências. A análise integrada do poço BD-01, sem testemunho, com os resultados obtidos dos testemunhos dos poços BD-02, BD-04 e BD-08 deixam claro que as características permo-porosas da Sequência 3 são mais favoráveis do que as demais Sequências. A predominância das *facies Amygdaloidal basalt with interconnecting vesicles* (amB/vsB_i) e *basalts with enlongated amygdales within a glassy crust* (amB_e) e a descontinuidade dos lobos, com intervalos maciços pouco contínuos lateralmente, típico dos *compounded-braided flows*, seriam os fatores mais relevante provenientes da análise dos testemunhos. Já no poço BD-01, a presença de um perfil com características mais brechadas e nem tão alterada e menor porcentagem de rocha maciça sã corroboram com a proposta. Os resultados do estudo destes três poços poderão servir à caracterização de reservatórios vulcânicos potenciais em outras partes da Bacia de Campos e em bacias sedimentares do SE do Brasil associadas à fragmentação do Gondwana.

Os resultados obtidos nesta dissertação de mestrado não exaurem o tema. Trabalhos futuros podem explorar a construção de modelo geológico 3D e simulações de fluxos visando a comparação com os resultados de produção, a identificação das sequências discriminadas em perfis sísmicos e a correlação de rocha e perfil com outros poços da Formação Cabiúnas dentro e fora campo de Badejo.

7 REFERÊNCIAS BIBLIOGRÁFICAS DA DISSERTAÇÃO DE MESTRADO

Blaich, O.A., Faleide, J.I., Tsikalas, F., Gordon, A.C., Mohriak, W., 2013. Crustal-scale architecture and segmentation of the South Atlantic volcanic margin. Geological Society, London, Special Publications 369, 167–183. https://doi.org/10.1144/SP369.22

Bueno, G.V., Zacharias, A.A., Orebro, S.G., Supertino, J.A., Falkenhein, F.U.H., Martins-Neto, A.M., 2007. Bacia de Pelotas. Boletim de Geociências da Petrobras 15(2), 551–559.

França, R.L., Del Rey, A.C., Tagliari, C.V., Brandão, J.R., Fontanelli, P.R., 2007. Bacia do Espirito Santo. Boletim de Geociências Petrobras 15(2), 501–509.

Fornero, S.A., 2018. Caracterização faciológica de rochas vulcânicas e vulcanoclásticas por meio de perfis de imagem microresistiva e acústica: estudo de caso no pré-sal, Bacia de Santos (dissertação de mestrado). Universidade Federal Fluminense, Brasil.

Mizusaki, A.M.P., 1986. Rochas igneo-basicas do Neocomiano da Bacia de Campos-caracterização e comportamento como reservatorio do hidrocarbonetos (Tese de doutorado). Universidade Federal do Rio de Janeiro, Brasil.

Mizusaki, A.M.P., 1987. Datação radiometrica de rochas igneas basicas do pogo 3-bd-15-RJS. (internal). Petrobras/Cenpes/Segel, Rio de Janeiro, Brazil.

Moreira, J.L.P., Madeira, C.V., Gil, J.A., Machado, M.A.P., 2007. Bacia de Santos. Boletim de Geociências da Petrobras 15(2), 531–549.

Ren, K., Zhao, J., Liu, Q., Zhao, J., 2020. Hydrocarbons in igneous rock of Brazil: A review. Petroleum Research 5, 265–275. https://doi.org/10.1016/j.ptlrs.2020.06.001

Rossetti, L., Lima, E.F., Waichel, B.L., Hole, M.J., Simões, M.S., Scherer, C.M.S., 2018.

Tigre, C.A., Schaller, H.A., Del Lucchese, C., Possato, S.A., 1983. Pampo, Linguado, and Badejo Fields: Their Discoveries,Appraisals, and Early Production Systems, in: All Days. Presented at the Offshore Technology Conference, OTC, Houston, Texas, p. OTC-4627-MS. https://doi.org/10.4043/4627-MS

Zou, C., 2013. Volcanic reservoirs in petroleum exploration, First edition. ed. Elsevier, Amsterdam.